NAVAL POSTGRADUATE SCHOOL

MONTEREY, CALIFORNIA

THESIS

OPERATIONAL ASSESSMENT OF TARGET ACQUISITIONS WEAPONS SOFTWARE (TAWS) PREDICTION PERFORMANCE AT NELLIS AFB NV

by

Jerome H. Hernandez

March 2006

Thesis Advisor:	Kenneth L. Davidson
Thesis Co-Advisor:	Andreas K. Goroch

Approved for public release, distribution is unlimited

THIS PAGE INTENTIONALLY LEFT BLANK

REPORT DOCUMENTATION PAGE			Form Approved OMB No. 0704-0188
Public reporting burden for this collection of information is estimated to average 1 hour per response, including the time for reviewing instruction, searching existing data sources, gathering and maintaining the data needed, and completing and reviewing the collection of information. Send comments regarding this burden estimate or any other aspect of this collection of information, including suggestions for reducing this burden, to Washington headquarters Services, Directorate for Information Operations and Reports, 1215 Jefferson Davis Highway, Suite 1204, Arlington, VA 22202-4302, and to the Office of Management and Budget, Paperwork Reduction Project (0704-0188) Washington DC 20503.			
1. AGENCY USE ONLY ***(Leave blank)***	**2. REPORT DATE** March 2006	**3. REPORT TYPE AND DATES COVERED** Master's Thesis	
4. TITLE AND SUBTITLE: Operational Assessment of Target Acquisition Weapons Software (TAWS) Prediction Performance at Nellis AFB, NV			**5. FUNDING NUMBERS**
6. AUTHOR(S) Jerome H Hernandez			
7. PERFORMING ORGANIZATION NAME(S) AND ADDRESS(ES) Naval Postgraduate School Monterey, CA 93943-5000			**8. PERFORMING ORGANIZATION REPORT NUMBER**
9. SPONSORING /MONITORING AGENCY NAME(S) AND ADDRESS(ES) N/A			**10. SPONSORING/MONITORING AGENCY REPORT NUMBER**
11. SUPPLEMENTARY NOTES The views expressed in this thesis are those of the author and do not reflect the official policy or position of the Department of Defense or the U.S. Government.			
12a. DISTRIBUTION / AVAILABILITY STATEMENT Approved for public release, distribution is unlimited			**12b. DISTRIBUTION CODE**

13. ABSTRACT (maximum 200 words)

Target Acquisition Weapons Software (TAWS) Version 3.4 is a joint Tactical Decision Aid (TDA) used to predict performance of electro-optic and electro-magnetic (EM/EO) munitions and navigation systems. TAWS is the USAF and USN mission-planning standard for laser-guided, infrared, and TV munitions and navigation systems TDAs. As TAWS continues to deploy through the mission planning community there is a need to establish a systematic approach to assessing TAWS accuracy. This study was an operational assessment of TAWS Infrared (IR) model performance and consisted of two parts: a comparison of model predictions to pilot observations of IR detection range of a static tank target and an assessment of physical temperature predictions. Limiting factors of this project are similar to those encountered in real world utilization of TAWS mission planning TDAs. This evaluation found TAWS predicted detection ranges and target scene model output were representative forecasts of observed values. The TDA provided a good description of background thermal behavior and highlighted the necessity of careful evaluation of the target scene because of component facet complexity and the geometry of facets exposed to the sensor view. The resulting component analysis illuminated the benefit of focusing new TAWS development on improving the target physical model.

14. SUBJECT TERMS Target Acquisition Weapons Software, TAWS, Tactical Decision Aids, TDA, weather impacts, physical meteorology, Electro-Optical Tactical Decision Aids, EOTDA			**15. NUMBER OF PAGES** 95
			16. PRICE CODE
17. SECURITY CLASSIFICATION OF REPORT Unclassified	**18. SECURITY CLASSIFICATION OF THIS PAGE** Unclassified	**19. SECURITY CLASSIFICATION OF ABSTRACT** Unclassified	**20. LIMITATION OF ABSTRACT** UL

NSN 7540-01-280-5500 Standard Form 298 (Rev. 2-89)
Prescribed by ANSI Std. 239-18

THIS PAGE INTENTIONALLY LEFT BLANK

Approved for public release; distribution is unlimited.

OPERATIONAL ASSESSMENT OF TARGET ACQUISITIONS WEAPONS SOFTWARE (TAWS) PREDICTION PERFORMANCE AT NELLIS AFB NV

Jerome H. Hernandez
Captain, United States Air Force
B.S., Texas A&M University, 1999

Submitted in partial fulfillment of the
requirements for the degree of

MASTER OF SCIENCE IN METEOROLOGY

from the

NAVAL POSTGRADUATE SCHOOL
March 2006

Author: Jerome H. Hernandez

Approved by: Kenneth L. Davidson
Thesis Advisor

Andreas K. Goroch
Co-Advisor

Philip A. Durkee
Chairman, Department of Meteorology

THIS PAGE INTENTIONALLY LEFT BLANK

ABSTRACT

Target Acquisition Weapons Software (TAWS) Version 3.4 is a joint Tactical Decision Aid (TDA) to predict performance of electro-optic and electro-magnetic (EM/EO) munitions and navigation systems for specific mission scenarios. TAWS uses sensor system, mission and environmental parameters to predict the thermal environment which is then used to provide target detection range predictions. TAWS is the USAF and USN mission-planning standard for laser guided, infrared, and TV munitions and navigation systems TDAs. As TAWS continues to be deployed through the mission planning community there is a need to establish a systematic approach to assessing TAWS product accuracy. This study is an operational assessment of TAWS Infrared (IR) model performance. The study consists of two parts: a comparison of model predictions to actual pilot observations of IR detection range oaf a static tank target and an assessment of the physical temperatures predicted. The limiting factors of this project are similar to those encountered in real world utilization of TAWS mission planning tactical decision aid. This evaluation found TAWS predicted detection ranges and target scene model output were a representative forecast of observed values. The TDA provided a good description of background thermal behavior and highlighted the necessity of careful evaluation of the target scene because of the complexity of component facets and the geometry of facets seen by the sensor. The resulting component analysis illuminated the benefit of focusing new TAWS development on improving the target physical model. The methodology of the study provides guidance for systematic evaluation of TDA and sensor performance at the Combat Weather Team (CWT) level.

THIS PAGE INTENTIONALLY LEFT BLANK

TABLE OF CONTENTS

I. INTRODUCTION 1
A. OVERVIEW 1
B. MOTIVATION 1
1. How Accurate are TAWS Predictions of Detection Range? 1
2. How Accurate are TAWS Predictions of Target Scene Temperatures? 2
C. INTRODUCTION TO TAWS 2
1. TAWS Input 2
2. TAWS Model Components 3
a. Illumination Model 3
b. Target Scene Contrast Model 3
c. Transmittance Model 4
d. Sensor Model 6
3. TAWS Component Interaction 6
4. TAWS Output 8

II. METHODS 9
A. PART #1, EVALUATING DETECTION RANGE PREDICTIONS 9
1. Target 10
2. Airborne Measurements 11
3. TAWS Procedures 12
4. Comparative Analysis Procedures 12
B. PART #2, EVALUATING TARGET SCENE TEMPERATURE PREDICTIONS 13
1. Target 14
2. Target Sensor Suite 14
a. Apogee IR Temperature Sensor (1) 14
b. Everest Interscience IR Temperature Sensor (2) 14
c. Adhesive Thermocouples (10) 15
d. Air Temperature Sensor (1) 15
e. Relative Humidity Sensor (1) 15
f. Short-Wave (SW) Radiance (1) 15
g. Soil Temperature (1) 15
h. Atmospheric Pressure (1) 15
i. Solar Panel (1) 15
j. Data Logger (1) 16
3. TAWS Procedures 16
4. Comparative Analysis Procedures 16

III. RESULTS 19
A. PART #1, DETECTION RANGE COLLECTIONS 19
1. 18 Nov 2004 20

a. Weather *20*
b. Predicted and Measured Detection Ranges *20*
2. 19 Nov 2004 ..... **21**
a. Weather *21*
b. Predicted and Measured Detection Ranges *21*
3. 22 Nov 2004 ..... **22**
a. Weather *22*
b. Predicted and Measured Detection Ranges *22*
4. 23 Nov 2004 ..... **23**
a. Weather *23*
b. Predicted and Measured Detection Ranges *23*
5. 29 Nov 2004 ..... **24**
a. Weather *24*
b. Predicted and Measured Detection Ranges *24*
6. 30 Nov 2004 ..... **25**
a. Weather *25*
b. Predicted and Measured Detection Ranges *25*
7. 01 Dec 2004 ..... **26**
a. Weather *26*
b. Predicted and Measured Detection Ranges *26*
8. 02 Dec 2004 ..... **27**
a. Weather *27*
b. Predicted and Measured Detection Ranges *27*
9. 04 Dec 2004 ..... **28**
a. Weather *28*
b. Predicted and Measured Detection Ranges *28*
10. 06 Dec 2004 ..... **29**
a. Weather *29*
b. Predicted and Measured Detection Ranges *29*
11. 07 Dec 2004 ..... **30**
a. Weather *30*
b. Predicted and Measured Detection Ranges *30*
12. 08 Dec 2004 ..... **31**
a. Weather *31*
b. Predicted and Measured Detection Ranges *31*
13. 09 Dec 2004 ..... **32**
a. Weather *32*
b. Predicted and Measured Detection Ranges *32*
14. 13 Dec 2004 ..... **33**
a. Weather *33*
b. Predicted and Measured Detection Ranges *33*
15. 14 Dec 2004 ..... **34**
a. Weather *34*
b. Predicted and Measured Detection Ranges *34*
16. 15 Dec 2004 ..... **35**

a. Weather *35*
b. Predicted and Measured Detection Ranges *35*
B. PART #1, RESULTS OF THE DETECTION RANGE COLLECTIONS **36**
1. Potential Bias **36**
2. Discrepancy **37**
3. Part #1 Remarks **37**
C. PART #2, TARGET SCENE TEMPERATURE COLLECTIONS **38**
1. 17 Jan 2005 (View Direction 360) **39**
a. Weather *39*
b. Temperature Discrepancies *39*
2. 18 Jan 2005 (View Direction 360) **40**
a. Weather *40*
b. Temperature Discrepancies *40*
3. 19 Jan 2005 (View Direction 360) **41**
a. Weather *41*
b. Temperature Discrepancies *41*
4. 20 Jan 2005 (View Direction 360) **42**
a. Weather *42*
b. Temperature Discrepancies *42*
5. 21 Jan 2005 (View Direction 360) **43**
a. Weather *43*
b. Temperature Discrepancies *43*
6. 22 Jan 2005 (View Direction 360) **44**
a. Weather *44*
b. Temperature Discrepancies *44*
7. 17 Jan 2005 (View Direction 180) **45**
a. Weather *45*
b. Temperature Discrepancies *45*
8. 18 Jan 2005 (View Direction 180) **46**
a. Weather *46*
b. Temperature Discrepancies *46*
9. 19 Jan 2005 (View Direction 180) **47**
a. Weather *47*
b. Temperature Discrepancies *47*
10. 20 Jan 2005 (View Direction 180) **48**
a. Weather *48*
b. Temperature Discrepancies *48*
11. 21 Jan 2005 (View Direction 180) **49**
a. Weather *49*
b. Temperature Discrepancies *49*
12. 22 Jan 2005 (View Direction 180) **50**
a. Weather *50*
b. Temperature Discrepancies *50*

D. PART #2, RESULTS OF THE SCENE TEMPERATURE COLLECTIONS 51
1. Potential Bias 51
2. Discrepancies 51
3. Part #2 Remarks 52

IV. CONCLUSION 55
A. STUDY CONCLUSIONS 55
B. RECOMMENDATIONS 55

APPENDIX A - SCREEN CAPTURES OF TAWS INPUTS 57

APPENDIX B - SAMPLE TABULAR OUTPUT OF TAWS TEMPERATURE ANALYSIS 59

APPENDIX C - NELLIS APPROACH PLATE 61

APPENDIX D - T-62 TANK IMAGES 63

APPENDIX E - SENSOR INSTALLATION PLAN AND SCHEMATIC 65

APPENDIX F - PART #2 STATISTICAL WORKSHEET, TAWS PREDICTIONS AND HOURLY MEASUREMENTS 67

APPENDIX G – STUDY LIMITATIONS 71
A. PART #1 DETECTION RANGE COLLECTION 71
1. Assumption A: Aircraft Targeting System Ranges are “Truth” 71
2. Assumption B: KLSV Weather Most Representative of Target Conditions 71
3. Limfac A: Trees in Target Scene 71
4. Limfac B: Background not Specifically Modeled in TAWS 72
5. Limfac C: Descending Aircraft Flight Level 72
6 Limfac D: Sample Size and Weather Variability 72
7. Limfac E: Range Determination from Graphical Product 72
B. PART #2 TARGET SCENE TEMPERATURE COLLECTIONS 72
1. Limfac A: Scientific Sensor not Specifically Modeled in TAWS 72
2. Limfac B: Scientific Sensor to Target Geometry 73
3. Limfac C: Two Types of Scientific Sensors Used 73
4. Limfac D: Background not Specifically Modeled in TAWS 73

LIST OF REFERENCES 75

INITIAL DISTRIBUTION LIST 77

LIST OF FIGURES

Figure 1. Beers Law. Aircraft is positioned at the boundary of the surface layer in this simplified two-layer depiction 5
Figure 2. TAWS Component Interactions....8
Figure 3. WFOV/NFOV Conceptual Scenario....10
Figure 4. T-62 Target scene (Heading 030), Nellis AFB....11
Figure 5. Sensor Lay Out 14
Figure 6. Explanation of Detection Range Charts....19
Figure 7. 18 Nov 04, TAWS Analysis by time vs. A/C measured ranges 20
Figure 8. Same as Fig. 7 for 19 Nov 04. 21
Figure 9. Same as Fig. 7 for 22 Nov 04 22
Figure 10. Same as Fig. 7 for 23 Nov 04 23
Figure 11. Same as Fig. 7 for 29 Nov 04 24
Figure 12. Same as Fig. 7 for 30 Nov 04 25
Figure 13. Same as Fig. 7 for 01 Dec 04....26
Figure 14. Same as Fig. 7 for 02 Dec 04....27
Figure 15. Same as Fig. 7 for 04 Dec 04....28
Figure 16. Same as Fig. 7 for 06 Dec 04....29
Figure 17. Same as Fig. 7 for 07 Dec 04....30
Figure 18. Same as Fig. 7 for 08 Dec 04....31
Figure 19. Same as Fig. 7 for 09 Dec 04....32
Figure 20. Same as Fig. 7 for 13 Dec 04....33
Figure 21. Same as Fig. 7 for 14 Dec 04....34
Figure 22. Same as Fig. 7 for 15 Dec 04....35
Figure 23. WFOV Detection Predictions and Measurements 36
Figure 24. NFOV Detection Predictions and Measurements....37
Figure 25. Sample Target Scene Temperature Collection Plot. 38
Figure 26. 17 Jan 05, 360. Predicted and Measured Diurnal Temperature Curves....39
Figure 27. Same as Figure 26 for 18 Jan 05, 360. 40
Figure 28. Same as Figure 26 for 19 Jan 05, 360. 41
Figure 29. Same as Figure 26 for 20 Jan 05, 360. 42
Figure 30. Same as Figure 26 for 21 Jan 05, 360. 43
Figure 31. Same as Figure 26 for 22 Jan 05, 360. 44
Figure 32. Same as Figure 26 for 17 Jan 05, 180. 45
Figure 33. Same as Figure 26 for 18 Jan 05, 180. 46
Figure 34. Same as Figure 26 for 19 Jan 05, 180. 47
Figure 35. Same as Figure 26 for 20 Jan 05, 180. 48
Figure 36. Same as Figure 26 for 21 Jan 05, 180. 49
Figure 37. Same as Figure 26 for 22 Jan 05, 180. 50
Figure 38. Graphs of Delta-T, Correlation Coefficient and Chi-square test for independence. Dashed lines are dark hour delta-Ts, all other lines are associated with day hours. 52

THIS PAGE INTENTIONALLY LEFT BLANK

LIST OF TABLES

Table 1. Common TAWS Input Parameters 3
Table 2. Target Scene Model Comparison 4
Table 3. Extinction Components 6
Table 4. 17 Jan 05, 360. Temperature differences by period. "IR" indicates a comparison to IR apparent and "Th" indicates a comparison to inherent temperatures. Background temperatures considered independent of view direction, only analyzed for 360. 39
Table 5. Same as Table 4 for 18 Jan 05, 360. 40
Table 6. Same as Table 4 for 19 Jan 05, 360. 41
Table 7. Same as Table 4 for 20 Jan 05, 360. 42
Table 8. Same as Table 4 for 21 Jan 05, 360. 43
Table 9. Same as Table 4 for 22 Jan 05, 360. 44
Table 10. Same as Table 4 for 17 Jan 05, 180. 45
Table 11. Same as Table 4 for 18 Jan 05, 180. 46
Table 12. Same as Table 4 for 19 Jan 05, 180. 47
Table 13. Same as Table 4 for 20 Jan 05, 180. 48
Table 14. Same as Table 4 for 21 Jan 05, 180. 49
Table 15. Same as Table 4 for 22 Jan 05, 180 50
Table 16. Temperature differences between observed and predicted target temperatures by period (ΔT = predicted – measured). Background temperatures considered independent of view direction, only analyzed for 360. 51

THIS PAGE INTENTIONALLY LEFT BLANK

ACKNOWLEDGMENTS

While I am listed as the author of this thesis, it is truly a culmination of the efforts many. To my thesis co-advisors, Professor Kenneth L. Davidson and Dr. Andreas K. Goroch, thank you both for your patience and unwavering support through this process. I will always remember and appreciate your trust and friendship. I also thank Richard Lind for his outstanding equipment support and help overcoming technical challenges. Mr. Lind, you've spoiled me for life. Capt. David Moeller, USAF Weapons School, thank you so much for taking time to collect data for this project, it couldn't have happened without you. I also extend my thanks to the members of the Nellis Threat Training Facility for allowing me to instrument one of their tanks. Finally, words fail me when trying to express my humble appreciation and gratitude the Command Staffs of the Naval Postgraduate School, the Air Force Institute of Technology, and the Air Force Operational Test & Evaluation Center. Thank you all for allowing me this opportunity.

THIS PAGE INTENTIONALLY LEFT BLANK

I. INTRODUCTION

A. OVERVIEW

Target Acquisition Weapons Software 3.4 (TAWS) is a joint tactical decision aid (TDA) for performance predictions of electro-magnetic and electro-optic (EM/EO) munitions and navigation systems for specific mission scenarios. It is the USAF and USN mission-planning standard for laser guided, infrared, and TV munitions and navigation systems TDAs. This study is an assessment of TAWS performance in an operational environment. The study consists of two parts: The comparison of target and background temperatures predicted by the model to the measured temperatures of a tank target at NELLIS AFB; and the comparison of predicted detection range of the Nellis tank to F-16 FLIR observations. Evaluations of TAWS predicted detection ranges and modeled output of the thermal target scene were accomplished. The limiting factors of this project are not uncommon to those encountered in real world applications.

B. MOTIVATION

As TAWS continues to proliferate through the mission planning community, there was a need to establish a systematic approach to assessing its performance at various operating locations. The first part of this study explores such an approach. The intent was to demonstrate a simple method for evaluating total TAWS performance as a part of the recurring aircrew debriefing cycle. The second part investigated the performance of the target scene contrast model. This was a more rigorous scientific approach applied to an operational setting. Each study was motivated by one of two base questions.

1. How Accurate are TAWS Predictions of Detection Range?

Anecdotal evidence from aircrew debriefings indicate TAWS predictions are often representative but there are no recent quantitative studies to support or debunk this notion. Could a methodic approach find a prediction bias? Could users replicate the study to determine TAWS performance for local aircraft configurations and environments?

2. How Accurate are TAWS Predictions of Target Scene Temperatures?

Accurate predictions of target and background temperatures are essential to producing representative detection ranges (Elrick, 1987). Could precise measurements of target scene thermometric and radiometric temperatures be used to assess TAWS predictions of the same? Could such a process isolate TAWS model component strengths and weaknesses and enable developers to focus on the most cost beneficial improvements?

C. INTRODUCTION TO TAWS

TAWS was originally developed by the Air Force Research Laboratory and has evolved into a joint program with help from each services premiere research facilities. TAWS version 1, a successor to Electro-Optic Tactical Decision Aid (EOTDA, v1 1982 - v3.1 1994), was originally released in 1998. Most physical models have seen few updates since 1994 (AFRL, 2004). The exception was a target scene model improvement for selected high-resolution targets with Multi-Service Electro-optics Signature (MuSES, TAWS v2). Program developments have since been focused on graphical user interface, expansion of sensor/target database, reach-back capability and integration with other mission planning systems.

1. TAWS Input

Table 1 [table should go after first reference to it] shows a common list of important input variables required for a standard single point based IR detection or temperature analysis (Reference Appendix A for screen captures of TAWS Inputs). TAWS v3.4 requires manual input of target and sortie information. TAWS can estimate the background characteristics and elevation data for the provided location from a low-resolution database. It is beneficial to confirm this information with satellite imagery and adjust as needed. Elevation estimates can be acquired from National Geospatial-Intelligence Agency (NGA) Digital Terrain and Elevation Data (DTED) discs or network server. Model weather data can be acquired from remote servers, but is most accurate when forecasters ensure input is representative for the particular scenario. The deliberate

grouping of input variables into three main data categories attests to the original design concept of ensuring each analysis was a collaborative product of three military agencies; intelligence, aircrew and weather.

Table 1. Common TAWS Input Parameters

Target	Sortie	Weather
Latitude	Sortie Vehicle Type	Temperature
Longitude	Sortie Vehicle Altitude	Dew Point (or Relative Humidity)
Background Properties (example below, Soil)	Sensor View Driection	Sea Surface Temperature
Background Type	Sensor Type	Wind Direction/Speed
Surface Moisture	Date (Time over Target)	Visibility
Depth Moisture	Time over Target	Precipitation Type/Rate
Slope		Surface Aerosol
Albedo		Battlefield Induced Contaminants
Clutter		Surface Layer Depth
Target Type		High Level Clouds
Target Altitude		Mid Level Clouds
Target Heading		Low Level Clouds
Target Operating State		U/L Layer Temperatures
Target Speed		U/L Layer Visibility
Target Slope Orientation		U/L Layer Aerosol

2. TAWS Model Components

TAWS uses information from three sources to produce predictions. Models used in TAWS are associated with each of three agency functions. Since this is an infrared (IR) study, discussions will be limited to the IR portions of the TAWS models. This section contains a brief discussion of each model and the responsibility for each input.

a. Illumination Model

Inputs for this component are obtained from scenario specifications made in the target and sortie sections used in an acquisition or temperature analysis. The TAWS illumination model uses the U.S. Naval Observatory Solar-Lunar Almanac Code Version 1.1 (AFRL, 2004) to determine the solar/lunar positions and illumination that impact solar loading on a target scene. The output from this model directly contributes to the target scene contrast model.

b. Target Scene Contrast Model

Intel (military intelligence) is responsible for providing accurate target and background information. TAWS uses this data in either the Target Contrast Model 2 (TCM2) or Multi-Service Electro-optics Signature (MuSES) (AFRL, 2004) model to

produce the thermal contrast scene that is the foundation of scenario specific IR detection capabilities. Model determination is based on the selection of targets in the scene. High-resolution targets use the MuSES model and low-resolution targets use TCM. There is no indication of the model selection in final user output. Users must refer to the TAWS target list within the help file to determine if the target is high or low resolution. Some target model differences are listed in Table 2. There are obvious advantages to using the MuSES model but it is also apparent, MuSES performs many more calculations than TCM and therefore requires more time to produce an analysis. There are also differences in how each model handles long and short wave radiation, solar loading, sky and earth emissions, wind convection, and precipitation. These models develop the IR temperature difference between the target and background, target scene contrast, within the selected sensor's operative band (this study, 8-12 μm). This zero-range contrast signature is the maximum signal strength for the scenario.

Table 2. Target Scene Model Comparison.

TCM2	MuSES
Developed with FORTRAN	Developed with C++
Solves 1D – conduction through thickness of material	Solves 3D – conduction and lateral transfer though material
Multiple facets comprise node, nodes are isothermal portions of target	Mesh of elements make a part, parts have common thermal properties, targets are composite of parts
Limited to 70 nodes	Unlimited elements – common targets have less than 100 parts and 1000-2000 elements
Develops solution at node level	Develops solution at element level
Low Resolution Target (T-62) 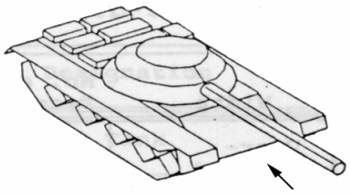	High Resolution Target (T-72) 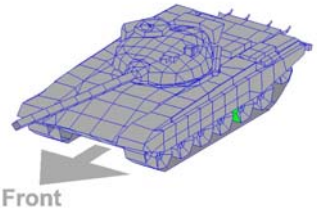

c. Transmittance Model

The military weather team provides meteorological data for TAWS calculations. Weather data spans 24 hours, 18 hours before time over target and 6 hours post. This data impacts both target scene contrast and IR atmospheric transmission

model. TAWS uses the Low Resolution Transmission Model 6 (LOWTRAN 6) to compute the atmospheric extinction coefficient for 3-5 or 8-12 μm (AFRL, 2004). The atmospheric attenuation model reduces the maximum signal strength (range = 0) over the sensor view path to provide the environmentally affected thermal contrast signature (Figure 1). This signal reduction is wavelength dependent and most simply described by Beers Law as seen in Figure 1.

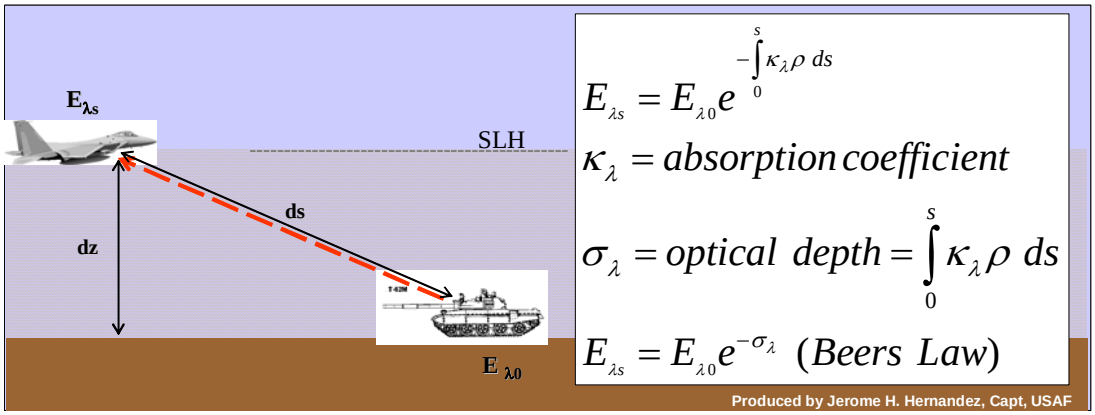

Figure 1. Beers Law. Aircraft is positioned at the boundary of the surface layer in this simplified two-layer depiction

While LOWTRAN 6 is capable of multiple layers, TAWS limits calculations to two layers to conform to computer hardware limitations at the time of original development. The layers are separated at the location of a sharp thermal gradient, moisture gradient or zone of wind shear (Goroch, 2005). The transmittance model sums the contributions of the 4 extinction components (Table 3) to determine the signal reduction along the path through the surface layer. These are "clear air" calculations. An additional extinction factor is applied in the vicinity of cloud base heights with the Army Vertical Structure Algorithm.

Table 3. Extinction Components

Component	Influential input factors
Molecular	Air temperature & dew point (i.e. water vapor content)
Aerosol	Rural, urban, maritime, tropospheric - visibility & RH
	Desert aerosol - wind speed
	Snow, fog, smokes - visibility.
Precipitation	Rain rate
Battlefield Induced Contaminants	Small particle dust & smoke - "averaged" value

The upper layer adjustment is done mostly through atmospheric transmissivity (Kneizys, 1988). In simple terms, the Surface Layer Height (SLH) distinguishes the "dirty" high extinction lower layer from the "clean" high transmissivity upper layer. In the infrared, the dominant extinction mechanism is gaseous water vapor and precipitation, with aerosols generally playing a small part.

d. Sensor Model

Finally, aircrews are responsible for providing sortie information that determines sensor performance model parameters. As aircrews select a sensor ID, TAWS references a sensor library to obtain system specifications; fields of view (FOV), instantaneous field of view (IFOV), spatial frequency, SNR threshold, etc. The IR sensor performance model is governed by numerous system and scenario specific parameters and equations. The major parameters include: the angle subtended by the target for the given range, system signal to noise ratio, noise equivalent temperature difference, detector angular subtense, detector area, detector quantity, spectral band, user perception parameters, etc. The complexity of this program component puts it beyond the scope of this paper. An excellent source for detailed information about IR system calculations is the Infrared and Electro-Optical Systems Handbook Volumes 1-8.

3. TAWS Component Interaction

TAWS model solutions depend on interactions between the model components. As an example, the illumination model provides a first guess of incident short wave radiance and weather inputs adjust this first guess to provide the impact to solar loading in the TCM model. The general relationship of these interactions can be seen in Figure 2.

It is easy to recognize the role of each model component when considering a simplified target detection scenario and performance prediction method. Consider the following operational scenario #1.

Operational Scenario #1: An older generation Surface to Air Missile (SAM) launch vehicle with a well known effective range is to be targeted. The last known position of the target is suspect. Naturally, the aircrew wants to detect the target with their IR system while outside the effective range of the SAM. Since the mission is still in the planning phase, the Weapons Systems Officer (WSO) wants to know what time of day is best for target detection from just outside the range of the SAM.

Know consider the following solution to the aforementioned operational problem. The desired detection range and target dimensions are known. Adapting J.D. Howes' approach (Howe, 1993), first determine the geometry. Calculate the solid angle subtended by target from outside the effective range of the SAM, range R (*Target Scene contrast Model, TSCM*). Predict the zero-range target scene temperatures of the target and background (*TSCM and illumination model*). Estimate the apparent thermal contrast signal, as affected by atmospheric transmission along the path, at range R (*transmittance model*). Now calculate the MDT difference (*TSCM, transmittance and Sensor Models*). MDT difference is inversely related to the target area. Since target area can be obtained by the angle subtended by the target at range R, the MDT difference for target detection from range R can be found. The best time of day for detection from range R can be found by looking up the required MDT difference on the predicted diurnal thermal contrast profiles.

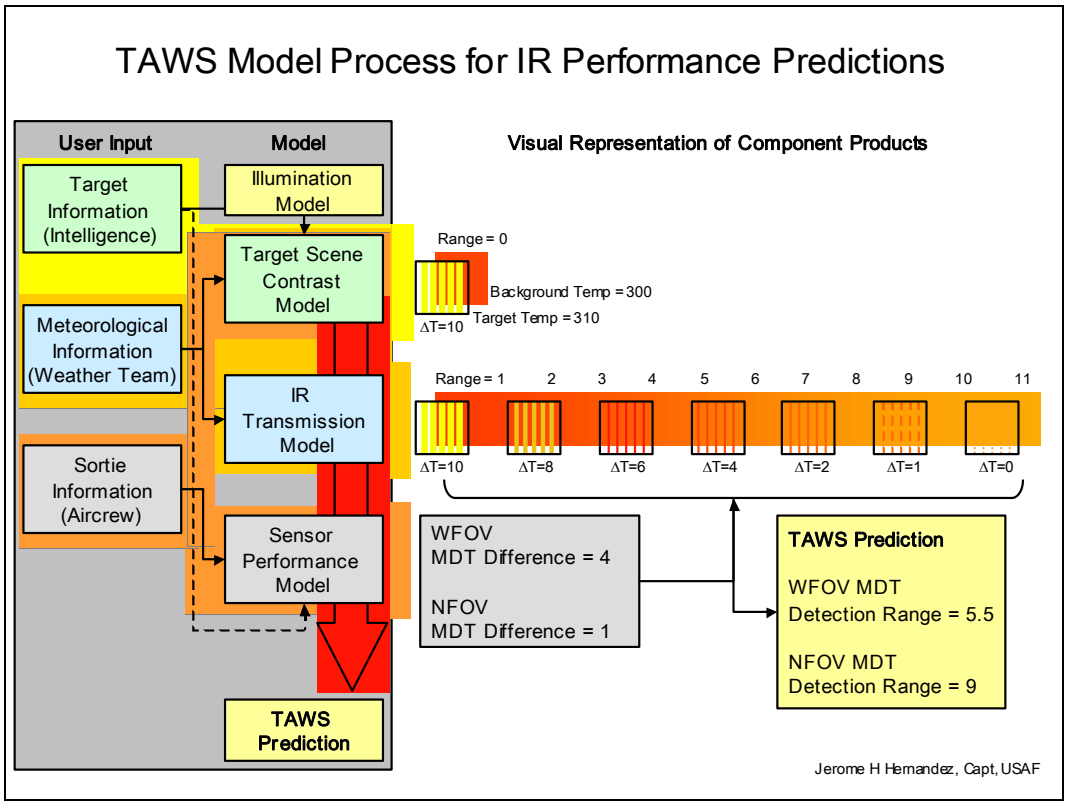

Figure 2. TAWS Component Interactions

4. TAWS Output

Output can be presented in graphic or tabular formats (See Appendix B). Analysis can be plotted as a function of temperature or detection/lock-on ranges over view direction or over time. Tables provide only the greater of Minimum Detectable Temperature (MDT) difference or Minimum Resolvable Temperature (MRT) difference detection ranges. This can be a limiting factor when providing support to aircrews. All detection range/lock-on and temperature combinations are available via graphic plots. Knowledge of each flying squadron's target (or navigation) sensing strategies is essential to providing the correct TAWS analysis.

II. METHODS

A. PART #1, EVALUATING DETECTION RANGE PREDICTIONS

Detection (and lock-on) range predictions are the result of all TAWS model component interactions. Thoughtful combinations of detection modes (MDT, MRT) and fields of view (Wide FOV, Narrow FOV) are critical in developing aircrew situational awareness. Minimum Detectable Temperature (MDT) difference describes the thermal contrast threshold at which a system can distinguish between a hot (cold) spot and a cooler (warmer) environment. Minimum Resolvable Temperature (MRT) difference describes the threshold when target shape, as provided by thermal contrast of the scene, can be resolved. Target detection and scene interrogation can be enhanced with systems that offer multiple fields of view. Two fields of view, wide and narrow, are the most common configuration. WFOV is used for target detection and tracking while NFOV is used for target selection and lock-on. WFOV applies the energy from a large scene (3-6°) to the IR sensor array. NFOV applies the energy from a much smaller portion of the scene (1-3°) to the same IR sensor array. Using the same detection mode (both MDT or both MRT), the high-resolution NFOV detection range will be greater than WFOV detection range. However, with differing detection modes (one MDT and one MRT), WFOV detection range can be greater than NFOV. Considering these system mode and FOV combinations, this study was built around the following operational scenario #2.

Operational Scenario #2: A combat aircraft Weapons System Officer (WSO) is provided the last known position of a vehicular target. The WSO needs to provide a performance prediction for operations using both wide and narrow field of view settings.

Consider the following common solution to operational scenario #2. The WSO loads the coordinates into the targeting system and selects WFOV MDT. WFOV enables a larger view area and increases the opportunity for target detection when target location is questionable. Once target is acquired, WSO will switch to NFOV MRT to resolve the target (target discrimination) and lock-on to destroy the target. Figure 3 illustrates this solution.

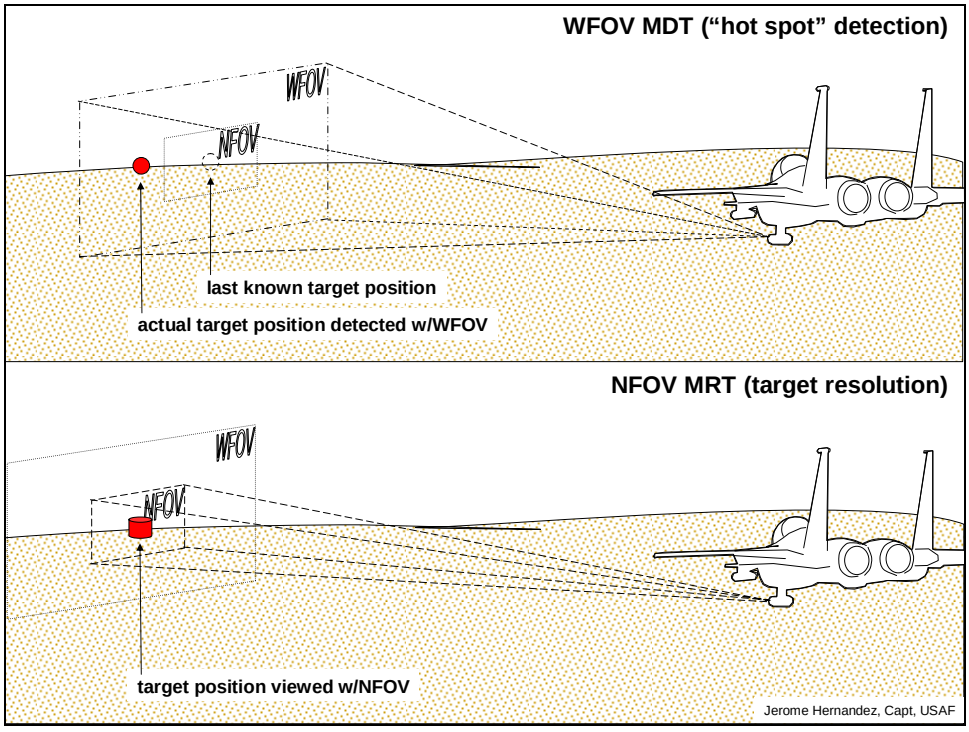

Figure 3. WFOV/NFOV Conceptual Scenario

The data acquisition for this program was conducted by collecting WFOV MDT and NFOV MRT detection range observations. Lock-on ranges were not collected. Measurements were compared to TAWS predictions. TAWS predictions were generated after the mission using observed weather data. Any unit using TAWS can repeat the procedures in this study with help from a cooperative flying element.

1. Target

The target used for the both parts of this study was a Russian built T-62 Main Battle Tank. The tank was measured and corresponded to the TCM T-62 Version C within TAWS. The target was located on Nellis AFB (NAFB, See Appendix C) at N13° 13' W115° 03' as measured by mil-spec handheld Garmin Global Positioning unit. Tank heading was 165° at an elevation of 1847ft. The target sat on a 10-15 cm thick layer of 2-5 cm diameter pumice stone over a sandy-loam soil base. Trees, 4-6 m tall, were widely spaced in a rectangle configuration around the target. The tree-tank separation distance was not measured. Shadows of the trees were observed passing over the southeast quadrant of the tank during early morning hours only. Impact to solar loading on the tank

was negligible, but could "cool" the background scene as viewed by the aircraft IR sensors. This target was the only spatially separated ground vehicle on NAFB that is also modeled in TAWS and was chosen to maximize collection opportunities as aircraft approached NAFB. The location allowed for detection range collections with each final approach to either NAFB runway heading (See Appendices D & E).

Figure 4. T-62 Target scene (Heading 030), Nellis AFB

2. Airborne Measurements

Captain David Moeller (USAF/WS WSO Instructor) used one IR targeting system to measure all detection ranges in this study. Capt Moeller carried a data collection worksheet on training missions. Each worksheet listed the target location and prompts to record: date, detection time, runway (sensor heading), flight level, flight level winds, flight level temperature, WFOV (MDT) detection range, and NFOV (MRT) detection range. Training missions were flown over the NAFB range complex north of Las Vegas, NV and aircraft returned to base upon completion of each training mission. During each final approach to NAFB, the WSO entered the target location in the targeting system and recorded detection ranges for WFOV MDT and then for NFOV MRT on the worksheet. Standard instrument glide slope angle for NAFB is 3°, heading magnetic 207 for runway 21 and 027 for runway 03. The glide slope put all incoming aircraft below 5000 ft MSL (3130 ft AGL) during detection range measurements. Collections started on 18 Nov 04 and continued until 15 Dec 04, 16 separate measurement pairs were made.

3. TAWS Procedures

TAWS sortie information was taken from the recovered aircrew worksheets. Time of detection for WFOV MDT and associated flight level were used as the time over target and sensor height for each TAWS run. NAFB METAR observations (KLSV), Dessert Rock (KDRA) upper air soundings, and ETA upper air analysis products were used to build TAWS weather input. Target background information was only adjusted for changes in surface moisture as estimated by METAR observations. One view direction was prescribed by each recorded heading. A TAWS time series prediction was calculated for each sortie. TAWS tabular outputs provide only the greater range for each FOV with no indication of detection mode. This limited the study to the use of graphic plots to match predetermined sensor mode and FOV combinations. Sixteen plots of four possible mode and FOV combinations were produced.

4. Comparative Analysis Procedures

Each TAWS detection range plot was scrutinized to obtain TAWS predicted values for WFOV MDT and NFOV MRT detections for the time over target prescribed by the aircraft measurements. The aircraft measured range for each associated plot was added to each graph in the form of a standard crosshair or rotated crosshair. Each discrepancy between the measured and predicted value was recorded. This provided three arrays of data: predicted, measured, and discrepancy. Aircraft measured ranges were considered most accurate and therefore used as the standard. A simple plot of the discrepancy values was used to identify any potential model bias. To further explore the similarities between the two series, a Chi squared test (Utts, 1999) for independence was calculated. The null hypothesis for the Chi-square test(Chi-square = 0) states the series are independent. Chi-square values closer to unity, indicate a strong relationship between the two series. A qualitative analysis of differences between predicted and calculated ranges was accomplished with a standard percent error formula using measured range as the reference value. Resultant values were used to develop the average discrepancy in terms of percent error, ***Percent Error = [(Predicted – Measure) / Measured] × 100%.***

B. PART #2, EVALUATING TARGET SCENE TEMPERATURE PREDICTIONS

The goal of this part of the study was to assess TAWS ability to accurately represent the diurnal thermal characteristics of a target scene. Part #2 was built upon the following conceptual model.

Over an extended period, record accurate radiometric and thermometric temperatures of a target and background for two view directions. Using meteorological data collected at the target location, produce TAWS model estimates of the target and background radiometric temperatures for same measured period. Complete a statistical analysis to identify any system bias.

The same view directions were used for each calibrated radiometric sensor and TAWS modeled IR sensor. It should be noted, TAWS predicts the inherent physical temperature of the background and target. TAWS then converts the inherent temperature to apparent IR temperature as the final output product. Radiometric temperatures describe the emitted thermal radiation from a surface (R, W/m^2). It is related to the inherent temperature (T, K) and emissivity (ε) by the Stefan-Boltzmann equation (Lloyd, 1975) as

$$\mathbf{R = \varepsilon \sigma T^4}$$

where $\sigma = 5.670 \times 10^{-8}$ W/m^2K^4 is the Boltzmann constant and ε is the emissivity of the surface.

TAWS targets and land-based backgrounds are not perfect blackbodies ($\varepsilon = 1$) so normally the apparent IR temperatures are less than the thermometric temperature. The non-linear response of the Stefan-Boltzmann equation makes it difficult to find a compensating factor for this reduction (SBIR, 2005). Since both predictions and IR measurements were in radiometric temperature units, a direct comparison was accomplished. The design of this assessment was such that it could be completed independent of aircraft participation.

1. Target

This analysis used the same target described in study #1. The orientation of the background viewing IR sensor, discussed in next section, eliminated the influence of tree shading in this target scene scenario. The target location on NAFB improved sensor suite security and reduced cost by eliminating the need for radio transmission from NAFB range complex to a remote data collection source.

2. Target Sensor Suite

The deployed measurement system consisted of 19 sensors, one solar panel, and one data logger. Measurements were collected from 20:13 UTC 16 Jan to 21:28 UTC 23 Jan. This section provides a brief description of the sensor instrumentation and installation.

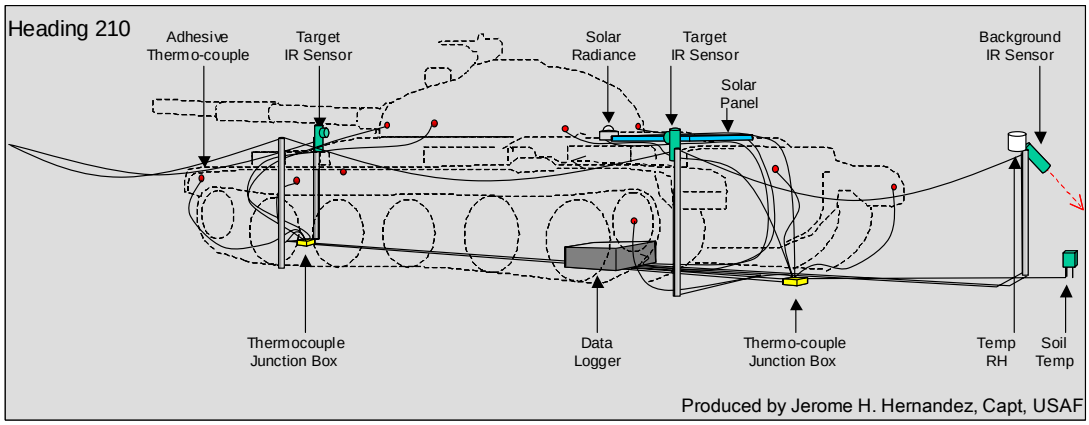

Figure 5. Sensor Lay Out

a. Apogee IR Temperature Sensor (1)

The 8-14 μm wide-angle (3:1 FOV) apogee radiometric sensor was installed at a height of 48 cm heading 330 with a depression of 40° from horizontal. This orientation kept the FOV unaffected by shadows from nearby trees and ensured an accurate measure of the effective background temperature.

b. Everest Interscience IR Temperature Sensor (2)

These 8-14 μm 4° FOV radiometric sensors were installed horizontally 53 cm (Heading 180) and 55 cm (Heading 360) above the ground. The sensor-to-turret distance was approximately 144 cm for sensor view direction 180° and 184 cm for sensor view direction 360°. The visual footprint of each sensor was centered on the lower half

of the tank turret. This is a partial footprint with respect to TAWS modeled aircraft view of the entire target. Consider that at 144 cm from the target, the 4° FOV Everest sensor spans a 10 cm horizontal width while the TAWS modeled IR sensor IFOV spans 55 cm horizontally from 3 nm away.

c. Adhesive Thermocouples (10)

Small patches of the tank surface were cleaned prior to attaching the adhesive thermocouples. Thermocouples were divided into two groups of five. Each group was installed to optimize facet variety among visible surfaces from target IR sensor positions. Averaged measurements within a group provided an estimate of the area averaged surface thermometric temperature for a particular sensor heading.

d. Air Temperature Sensor (1)

Air temperature was measured 48 cm above the ground and approximately 46 cm from the closest tank surface. This was not an aspirated sensor.

e. Relative Humidity Sensor (1)

Unit was co-located with air temperature sensor.

f. Short-Wave (SW) Radiance (1)

The SW radiance sensor was installed on the horizontal tank facet immediately aft of the turret. SW measurements provided a description of solar loading characteristics incident on the target and background.

g. Soil Temperature (1)

Soil temperature was measured 10 cm below the top of the pumice stone layer at the boundary between pumice stone layer and underlying soil. The sensor was placed 140 cm from the tank in a location unaffected by tank and tree shadows.

h. Atmospheric Pressure (1)

Sensor was in the data logger box. Not directly utilized in this analysis.

i. Solar Panel (1)

Power from the solar panel replenished battery voltage levels depleted during night hours. Panel was installed over the engine compartment aft of the turret. Positioning over a vented surface reduced the impact to solar loading on the facet.

j. Data Logger (1)

The CR5000 Campbell Scientific data logger was programmed to continuously collect instantaneous one-minute (i.e. not averaged) samples from the 18 individual sensors. Data arrays were stored on a PCMCIA card and transferred to a PC for analysis.

3. TAWS Procedures

The TAWS weather file was built from in-situ measurements, KLSV, KDRA, and Eta analysis data. In-situ temperature and humidity measurements were compared with NAFB CWT measurements as a quality control measure. KLSV observations provided wind, visibility and sky condition. Sensor ID and target information remained the same as previous study. Sortie flight level was set to 10ft and sensor view direction matched installed IR sensors. Time over target was set to 2000 UTC (12:00 PST) for each run. An analysis-over-time was accomplished for each view direction over six 24-hour periods for a total of 12 runs. TAWS tabular output of temperature estimates were imported into a separate program for further analysis.

4. Comparative Analysis Procedures

Data from the logger were imported into a spreadsheet and filtered to present instantaneous measurements collected on the hour. Measured temperatures were converted to Kelvin and temporally corresponding TAWS temperatures were imported into the same spreadsheet. All statistical analysis assumed measured values as the standard. Background and target temperature pairs were individually analyzed. Night and day hours were analyzed separately since solar loading invokes model components not used in night situations. Dark hours were split to investigate the difference between a more strongly radiating target, after sunset, and a more weakly radiating target, before sunrise. Background temperatures were independent of view direction therefore only produced for one heading. WFOV and NFOV MDT temperatures (radiometric) were compared to the average thermocouple temperatures (thermometric) and IR (radiometric) measurements within the associated field of view. Recall, TAWS converts inherent temperatures into IR apparent temperatures. Since the tank is not a perfect blackbody, TAWS IR apparent temperatures can be expected to be cooler than inherent temperatures, but the basic curve characteristics will be similar since the emissivity is constant. Direct

comparisons of predicted and measured radiometric temperatures were used to indicate the presence of a positive or negative temperature prediction bias. Since arrays represent a time series, a Chi squared test for independence and correlation coefficient was calculated for each comparison to assess the strength of the relationship between the two arrays. Finally, average temperature differences (ΔT = predicted - measured) were explored.

THIS PAGE INTENTIONALLY LEFT BLANK

III. RESULTS

A. PART #1, DETECTION RANGE COLLECTIONS

Comparisons of predicted and measured values were made. Related pairs are indicated with gold boxes at the bottom of Figures 7-22. Figure 6 explains the information on each graph. Each figure shows a TAWS analysis over time for the detection of the T-62 tank on a particular date. The lines represent the TAWS predictions of detection ranges for our sensor. The crosshair icons on the chart indicate the actual detection range measured by the aircraft sensor. The table in the upper right corner provides the numerical values of each predicted and measured sample. METAR weather observations are included in the discussions of each chart. For comprehensive help in decoding METAR observations, refer to National Oceanic and Atmospheric Agency (NOAA) METAR website (http://metar.noaa.gov).

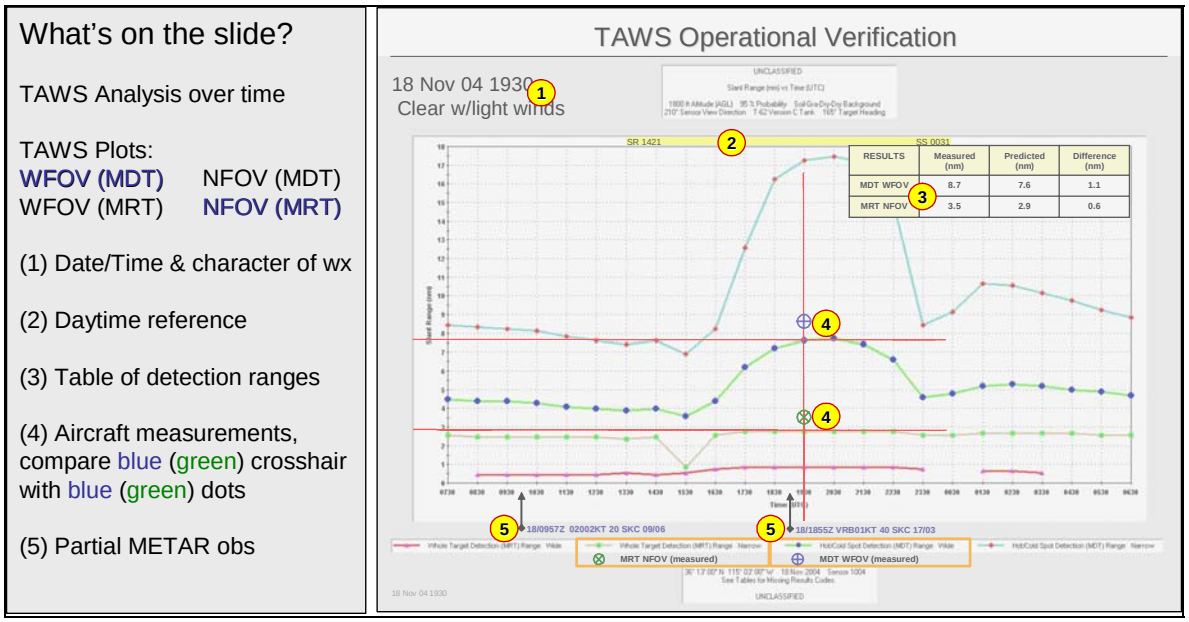

Figure 6. Explanation of Detection Range Charts

1. 18 Nov 2004

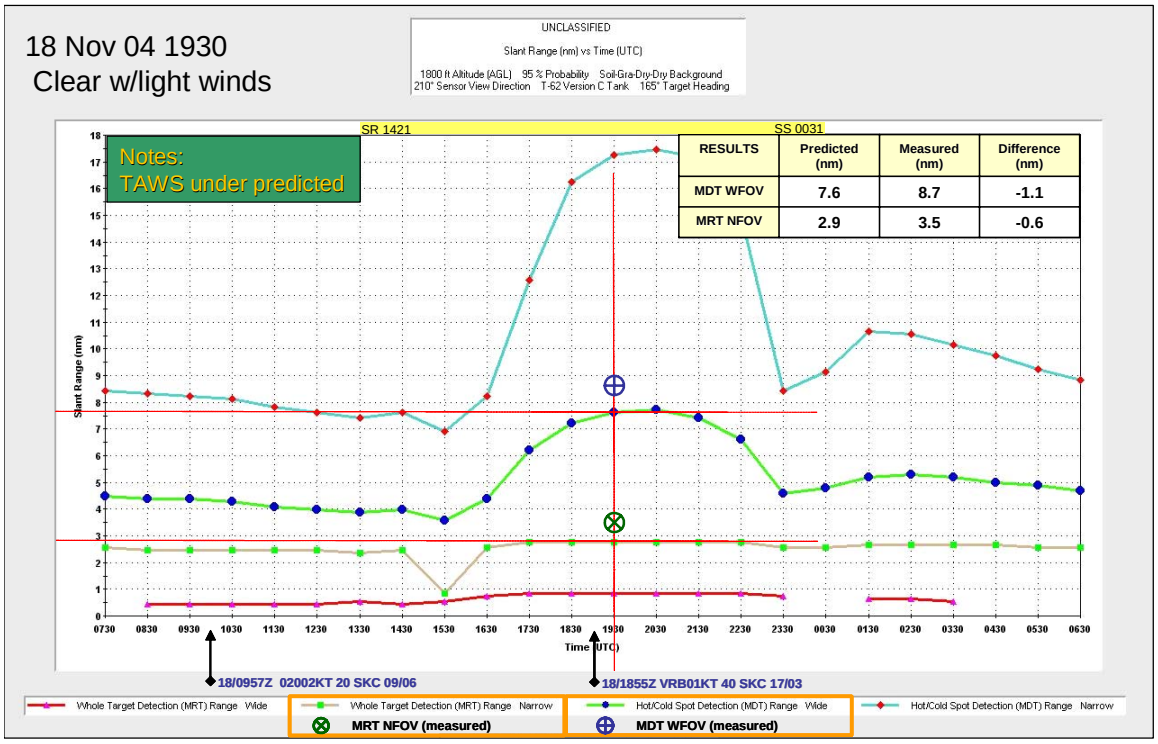

Figure 7. 18 Nov 04, TAWS Analysis by time vs. A/C measured ranges

a. Weather

Skies were clear with unrestricted visibility and light winds. Minimum temperature (T_{min}), 6 °C, was recorded at 1359 UTC and maximum temperature (T_{max}), 21 °C, at 2157 UTC. Dewpoints (T_{dpt}) varied from 2 to 5 °C. Weather report valid at Time Over Target (TOT): METAR KLSV 181855Z VRB01KT 40SM SKC 17/03 A3020 RMK SLP221 WND DATA ESTMD

b. Predicted and Measured Detection Ranges

TAWS predicted ranges were MDT WFOV 8.7 nm/MRT NFOV 3.5 nm and aircraft collected detection ranges were MDT WFOV 7.6 nm/MRT NFOV 2.9 nm. Range prediction discrepancies were MDT WFOV -1.1 nm (-12.6 % Error) and MRT NFOV -0.6 nm (-17.1 % Error).

2. 19 Nov 2004

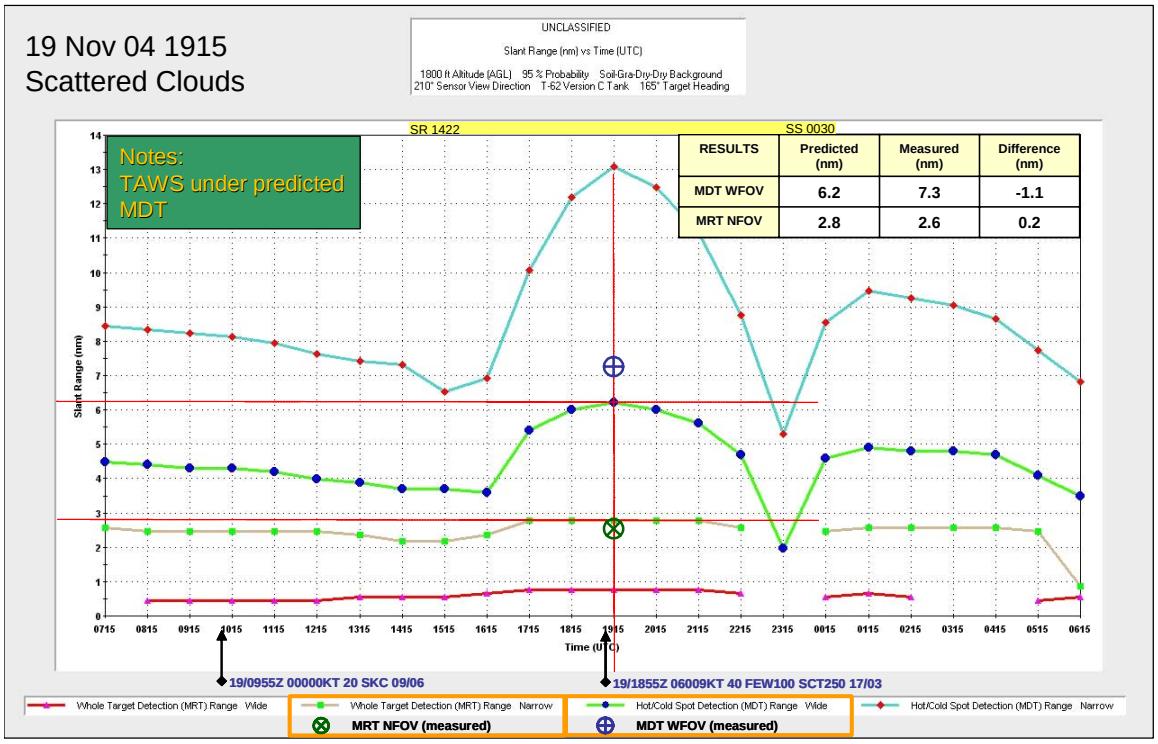

Figure 8. Same as Fig. 7 for 19 Nov 04.

a. Weather

Scattered mid-level clouds and occasionally broken high-level clouds. Visibility was unrestricted. Morning winds were light and variable then increased to NE 8-12 kt by 1900 UTC. T_{min}, 7 °C, was recorded at 1258 UTC and T_{max}, 20 °C, at 2155 UTC. T_{dpt} varied from 4 to 6 °C. Weather report valid at TOT: METAR KLSV 191855Z 07009KT 030V090 40SM FEW100 SCT250 17/03 A3003 RMK SLP161 WND DATA ESTMD

b. Predicted and Measured Detection Ranges

TAWS predicted ranges were MDT WFOV 6.2 nm/MRT NFOV 2.8 nm and aircraft collected detection ranges were MDT WFOV 7.3 nm/MRT NFOV 2.6 nm. Range prediction discrepancies were MDT WFOV -1.1 nm (-15.1 % Error) and MRT NFOV 0.2 nm (7.7 % Error).

3. 22 Nov 2004

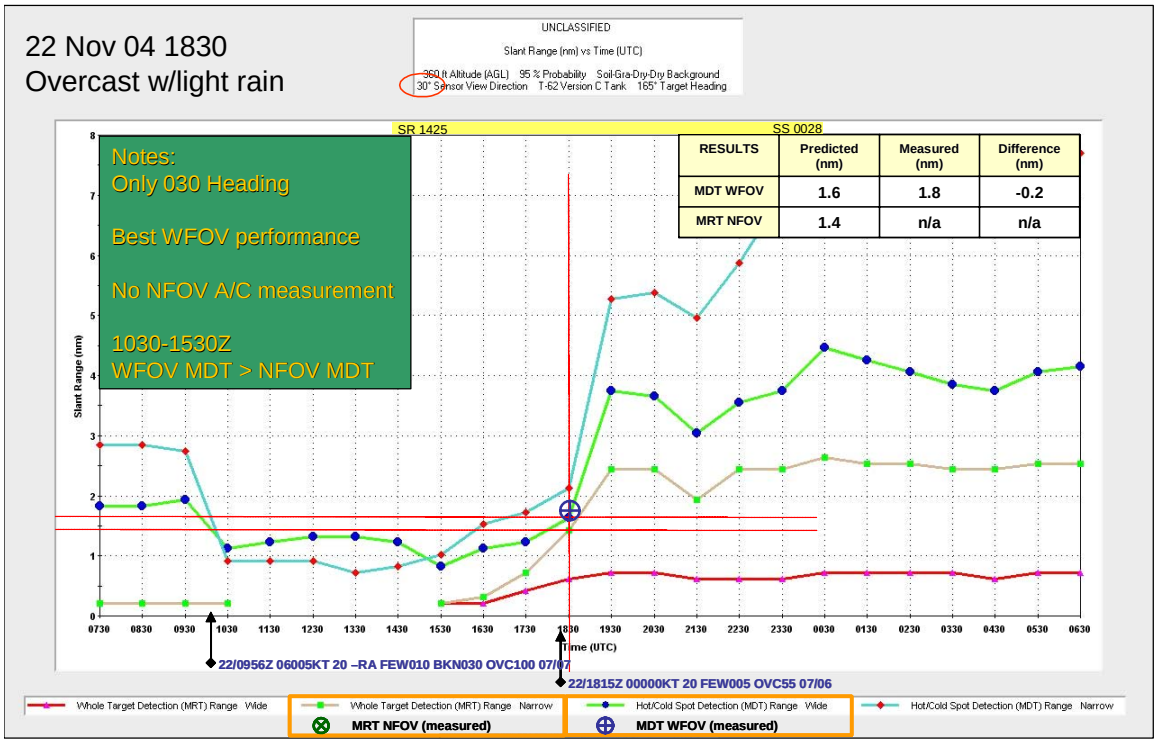

Figure 9. Same as Fig. 7 for 22 Nov 04

a. Weather

Strong cold air advection occurred at the surface. Maximum temperature dropped 10 degrees. Generally, cloudy and rainy with light winds. Ceilings were 3000-5000 ft (AGL) and visibility remained greater than 5 nm. Rain stopped at 1815 UTC. T_{min}, 6 °C, was recorded at 1058 UTC and T_{max}, 10 °C, at 2155 UTC. T_{dpt} varied from 6 to 7 °C. Weather report valid at TOT: SPECI KLSV 221815Z 00000KT 20SM FEW005 SCT020 OVC055 07/06 A3001 RMK WND DATA ESTMD WR//

b. Predicted and Measured Detection Ranges

TAWS predicted ranges were MDT WFOV 1.6 nm/MRT NFOV 1.4 nm and aircraft collected detection ranges were MDT WFOV 1.8 nm/MRT NFOV n/a. Range prediction discrepancies were MDT WFOV -0.2 nm (-11.1 % Error) and MRT NFOV n/a.

4. 23 Nov 2004

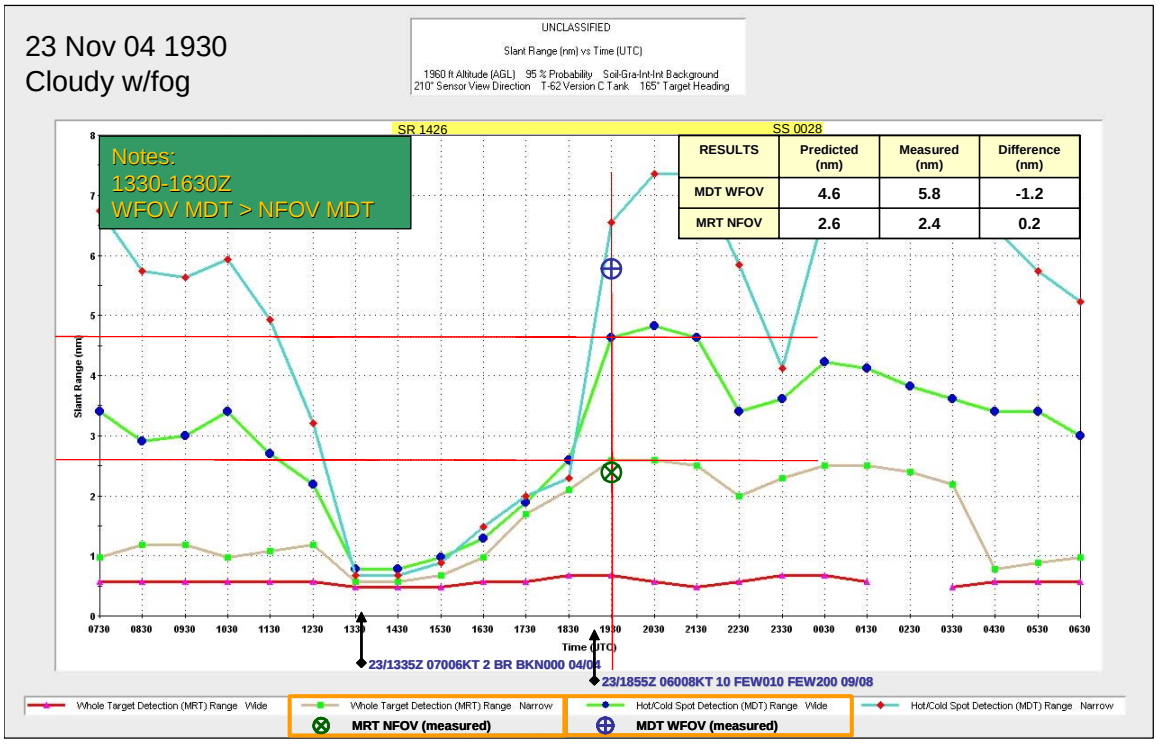

Figure 10. Same as Fig. 7 for 23 Nov 04

a. Weather

Residual moisture and stable conditions led to development of radiation fog. Morning fog and surface based obscuration lifted into scattered low clouds by 1700 UTC. Visibility was 1 to 2 sm [nm?] until 1500 UTC, then, gradually increased until unrestricted at 1900 UTC. Winds were less than 10 kt from NE. T_{min}, 4 °C, was recorded at 1055 UTC and T_{max}, 13 °C, at 2155 UTC. T_{dpt} varied from 3 to 9 °C. Weather report valid at TOT: METAR KLSV 231855Z 06008KT 10SM FEW010 FEW200 09/08 A3004 RMK SLP175 WND DATA ESTMD

b. Predicted and Measured Detection Ranges

TAWS predicted ranges were MDT WFOV 4.6 nm/MRT NFOV 2.6 nm and aircraft collected detection ranges were MDT WFOV 5.8 nm/MRT NFOV 2.4 nm. Range prediction discrepancies were MDT WFOV -1.2 nm (-20.7 % Error) and MRT NFOV 0.2 nm (8.3 % Error).

5. 29 Nov 2004

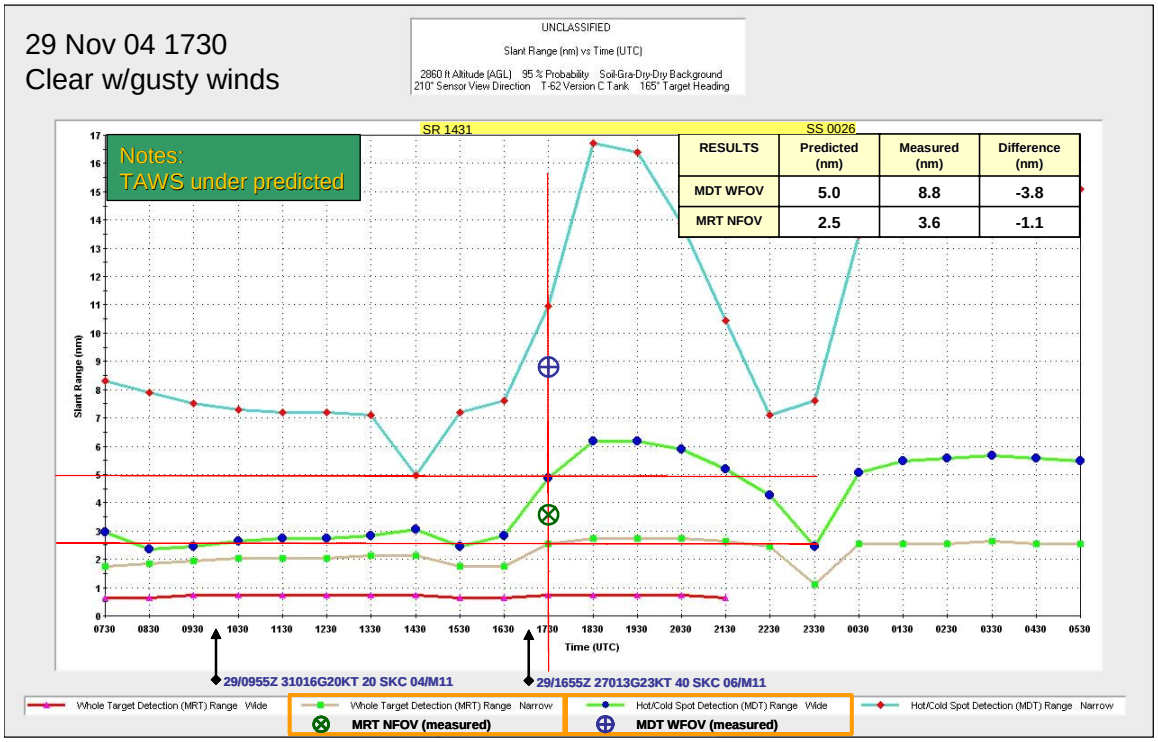

Figure 11. Same as Fig. 7 for 29 Nov 04

a. Weather

Generally, clear skies and gusty winds. Visibility was unrestricted. Sustained winds were from the NW-N 10-17 kt with gusts 20-29 kt until 1800 UTC. After 1900 UTC, winds decreased to 8-12 kt and shifted from NE. T_{min}, 3 °C, was recorded at 1355 UTC and T_{max}, 10 °C, at 2155 UTC. T_{dpt} varied from -9 to -11 °C. Weather report valid at TOT: METAR KLSV 291655Z 27013G23KT 40SM SKC 06/M11 A3042 RMK SLP307 WND DATA ESTMD

b. Predicted and Measured Detection Ranges

TAWS predicted ranges were MDT WFOV 5.0 nm/MRT NFOV 2.5 nm and aircraft collected detection ranges were MDT WFOV 8.8 nm/MRT NFOV 3.6 nm. Range prediction discrepancies were MDT WFOV -3.8 nm (-43.2 % Error) and MRT NFOV -1.1 nm (-30.6 % Error).

6. 30 Nov 2004

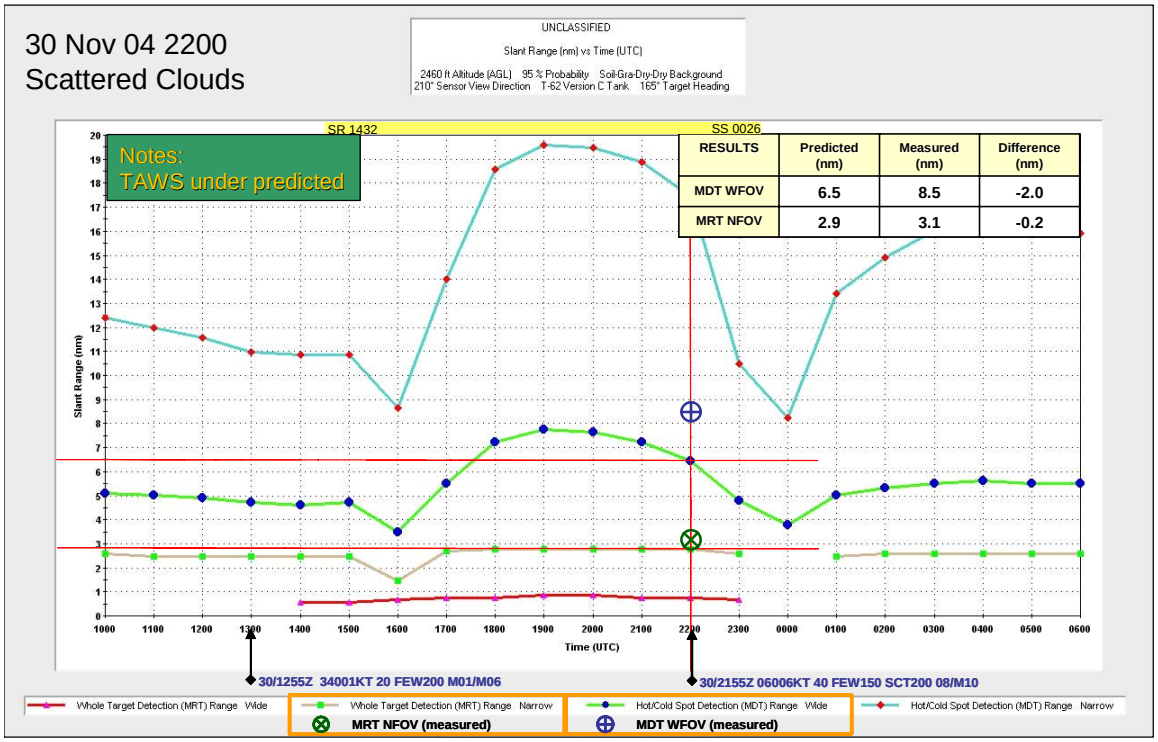

Figure 12. Same as Fig. 7 for 30 Nov 04

a. Weather

Scattered high level clouds, unrestricted visibility and light winds. T_{min}, -2°C, was recorded at 1455 UTC and T_{max}, 8 °C, at 2155 UTC. T_{dpt} varied from -5 to -6 °C. Weather report valid at TOT: METAR KLSV 302155Z 06006KT 40SM FEW150 SCT200 08/M10 A3032 RMK SLP275 WND DATA ESTMD [make sure units are correct and there is not a break between the number and the units]

b. Predicted and Measured Detection Ranges

TAWS predicted ranges were MDT WFOV 6.5 nm/MRT NFOV 2.9 nm and aircraft collected detection ranges were MDT WFOV 8.5 nm/MRT NFOV 3.1 nm. Range prediction discrepancies were MDT WFOV -2.0 nm (-23.5 % Error) and MRT NFOV -0.2 nm (-6.5 % Error).

7. 01 Dec 2004

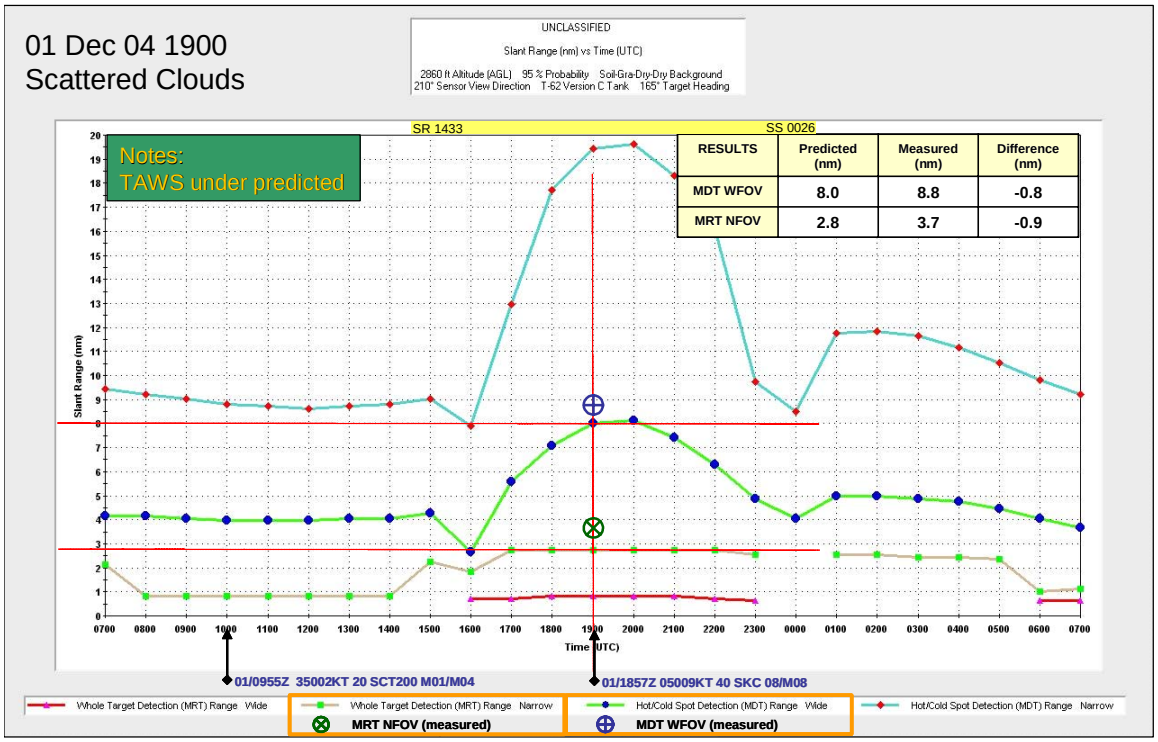

Figure 13. Same as Fig. 7 for 01 Dec 04

a. Weather

Few high clouds, light winds and unrestricted visibility. T_{min}, -1 °C, was recorded at 0955 UTC and T_{max}, 11 °C, at 2259 UTC. T_{dpt} varied from -4 to -9 °C. Weather report valid at TOT: METAR KLSV 011857Z 05009KT 40SM SKC 08/M08 A3024 RMK SLP243 WND DATA ESTMD

b. Predicted and Measured Detection Ranges

TAWS predicted ranges were MDT WFOV 8.0 nm/MRT NFOV 2.8 nm and aircraft collected detection ranges were MDT WFOV 8.8 nm/MRT NFOV 3.7 nm. Range prediction discrepancies were MDT WFOV -0.8 nm (-9.1 % Error) and MRT NFOV -0.9 nm (-27.3 % Error).

8. 02 Dec 2004

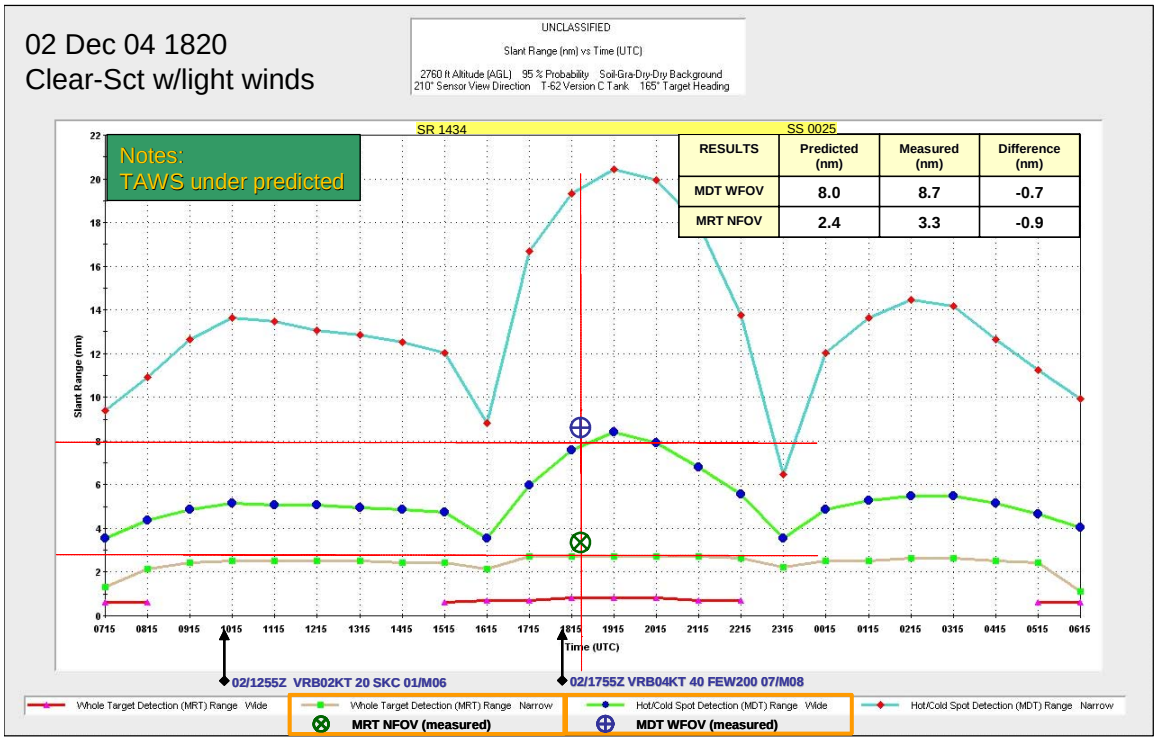

Figure 14. Same as Fig. 7 for 02 Dec 04

a. Weather

Few high clouds, light winds and unrestricted visibility. T_{min}, 1 °C, was recorded at 1155 UTC and T_{max}, 12 °C, at 2158 UTC. T_{dpt} varied from -6 to -1 °C. Weather report valid at TOT: METAR KLSV 021755Z VRB04KT 40SM FEW200 07/M08 A3029 RMK SLP258 WND DATA ESTMD CONTRAILS 51012

b. Predicted and Measured Detection Ranges

TAWS predicted ranges were MDT WFOV 8.0 nm/MRT NFOV 2.4 nm and aircraft collected detection ranges were MDT WFOV 8.7 nm/MRT NFOV 3.3 nm. Range prediction discrepancies were MDT WFOV -0.7 nm (-8.0 % Error) and MRT NFOV -0.9 nm (-27.3 % Error).

9. 04 Dec 2004

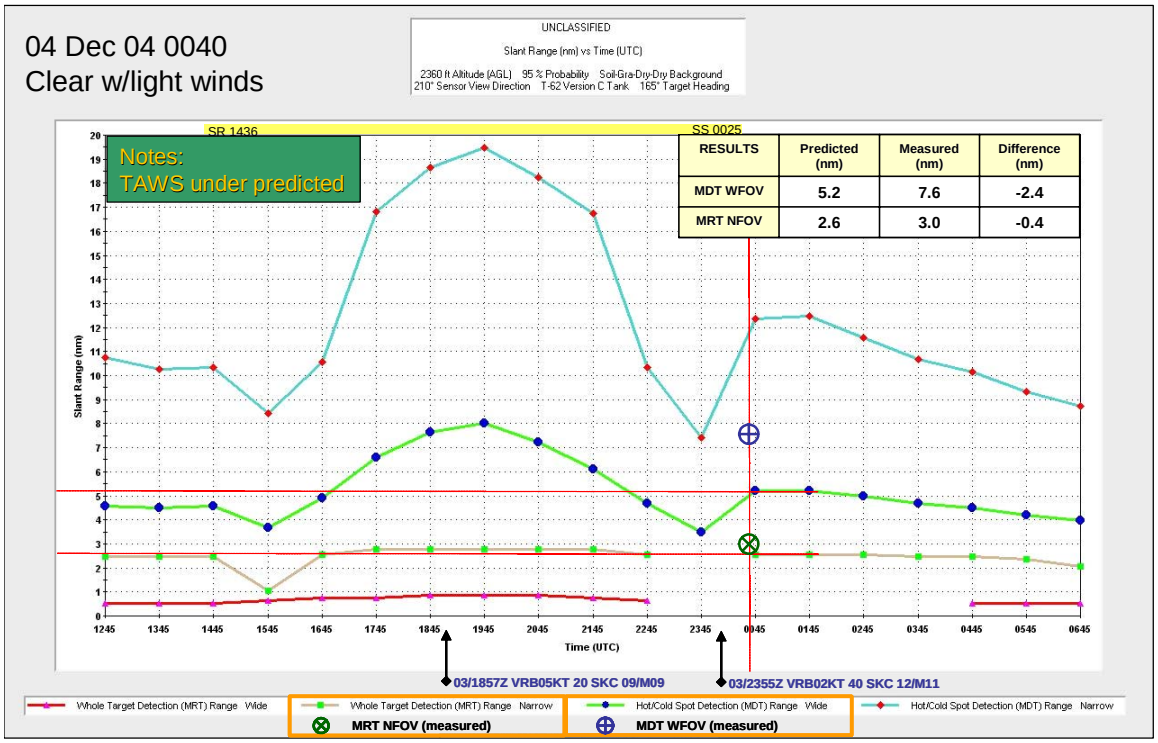

Figure 15. Same as Fig. 7 for 04 Dec 04

a. Weather

Skies held few mid-level clouds, broken high-level clouds, and unrestricted visibility. Winds were light until 2100 UTC, thne increased to 10-15 kt from NE. T_{min}, -2 °C, was recorded at 1455 UTC and T_{max}, 12 °C, at 2159 UTC. T_{dpt} varied from -4 to -8 °C. Weather report valid at TOT: METAR KLSV 042355Z 07005KT 40SM FEW150 BKN200 11/M08 A2976 RMK SLP078 WND DATA ESTMD 56022

b. Predicted and Measured Detection Ranges

TAWS predicted ranges were MDT WFOV 5.2 nm/MRT NFOV 2.6 nm and aircraft collected detection ranges were MDT WFOV 7.6 nm/MRT NFOV 3.0 nm. Range prediction discrepancies were MDT WFOV -2.4 nm (-31.6 % Error) and MRT NFOV -0.4 nm (-13.3 % Error).

10. 06 Dec 2004

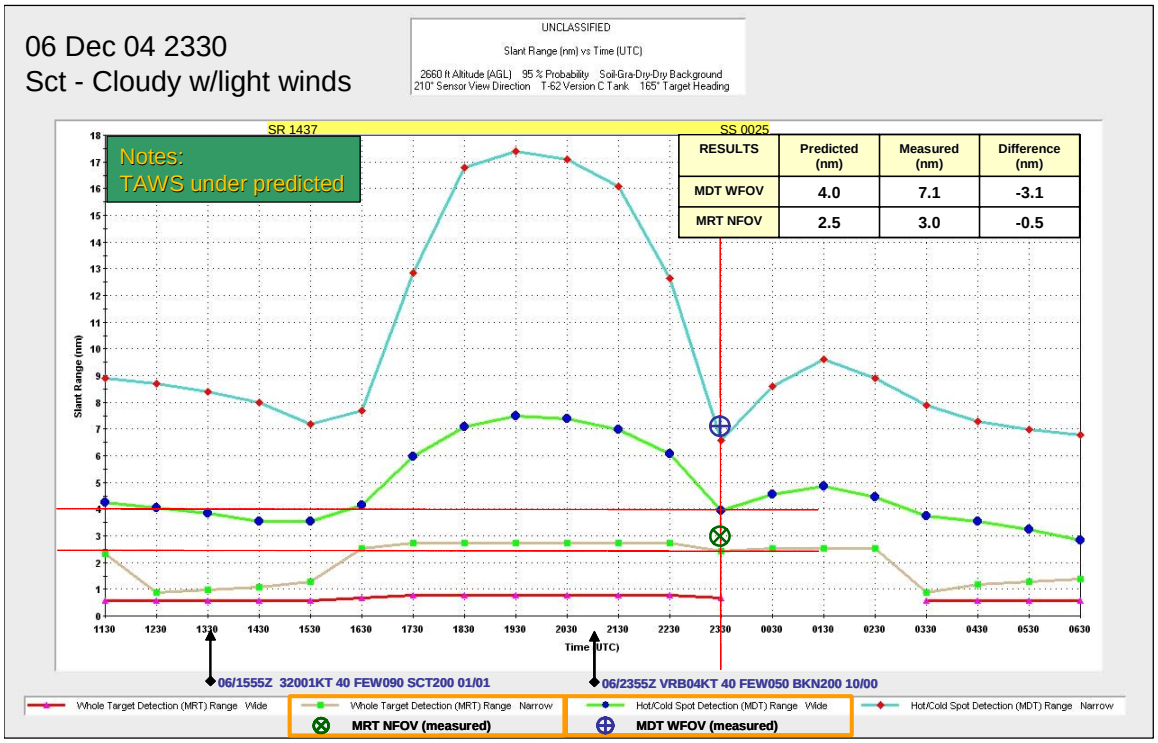

Figure 16. Same as Fig. 7 for 06 Dec 04

a. Weather

Generally, scattered mid-level clouds, broken high-level clouds after 2100 UTC, and light winds. Visibility was unrestricted. T_{min}, 0 °C, was recorded at 1259 UTC and T_{max}, 11 °C, at 2155 UTC. T_{dpt} varied from -1 to 2 °C. Weather report valid at TOT: METAR KLSV 062255Z 05006KT 40SM FEW050 BKN200 11/M01 A2998 RMK SLP155 WND DATA ESTMD

b. Predicted and Measured Detection Ranges

TAWS predicted ranges were MDT WFOV 4.0 nm/MRT NFOV 2.5 nm and aircraft collected detection ranges were MDT WFOV 7.1 nm/MRT NFOV 3.0 nm. Range prediction discrepancies were MDT WFOV -3.1 nm (-43.7 % Error) and MRT NFOV -0.5 nm (-16.7 % Error).

11. 07 Dec 2004

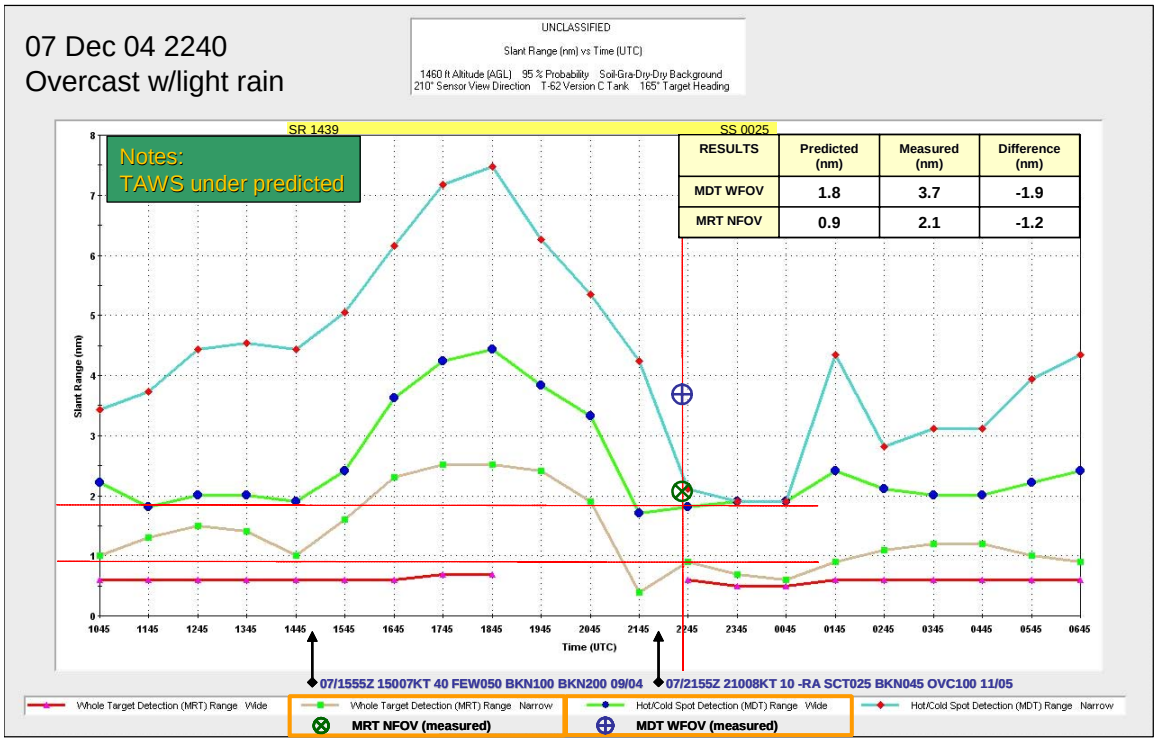

Figure 17. Same as Fig. 7 for 07 Dec 04

a. Weather

Warm air advection and wind shift indicated approaching warm front. Skies were cloudy with unrestricted visibility and light rain from 2100 to 2200 UTC. Winds were 10-15 kt from SE. T_{min}, 8 °C, was recorded at 0955 UTC and T_{max}, 12 °C, at 1757 UTC. T_{dpt} varied from 3 to 5 °C. Weather report valid at TOT: METAR KLSV 072155Z 21008KT 10SM -RA SCT025 BKN045 OVC100 11/05 A2996 RMK VIS N 6 SLP142 WND DATA ESTMD WR//

b. Predicted and Measured Detection Ranges

TAWS predicted ranges were MDT WFOV 1.8 nm/MRT NFOV 0.9 nm and aircraft collected detection ranges were MDT WFOV 3.7 nm/MRT NFOV 2.1 nm. Range prediction discrepancies were MDT WFOV -1.9 nm (-51.4 % Error) and MRT NFOV -1.2 nm (-57.1 % Error).

12. 08 Dec 2004

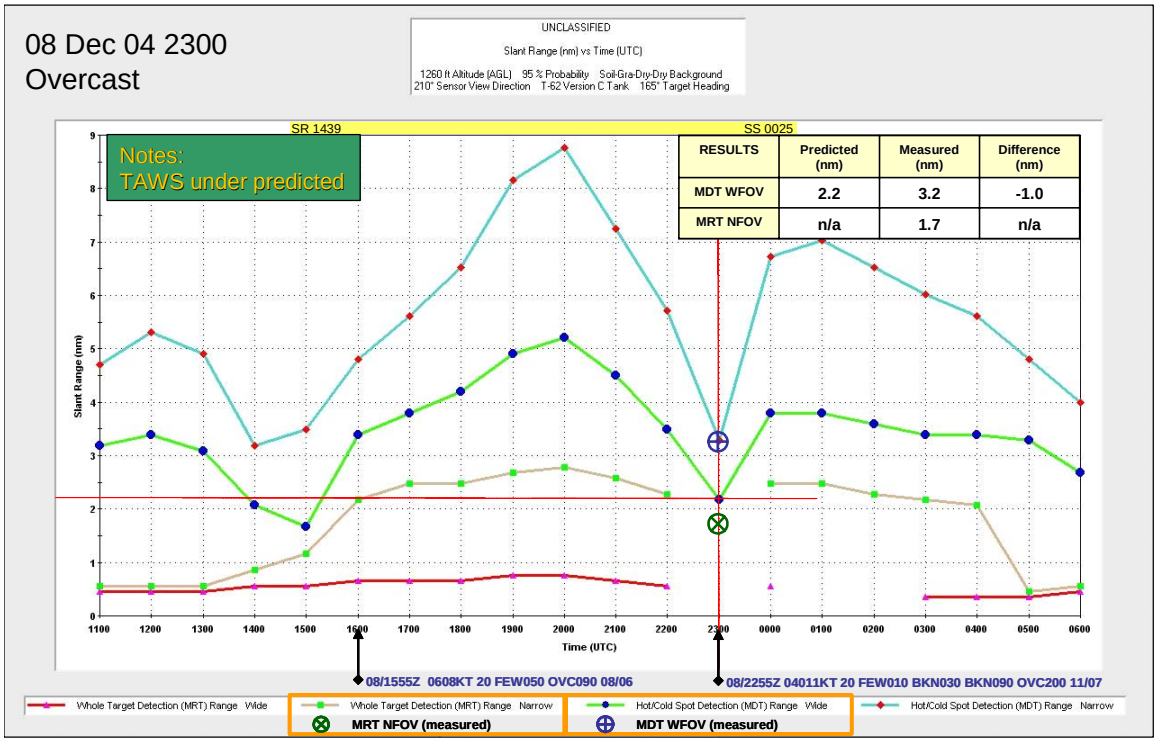

Figure 18. Same as Fig. 7 for 08 Dec 04

a. Weather

Scattered, occasionally broken, low clouds and broken to overcast mid-level clouds. Visibility was unrestricted. Winds were less than 10 kt from the ENE. T_{min}, 5 °C, was recorded at 1257 UTC and T_{max}, 12 °C, at 2056 UTC. T_{dpt} varied from 4 to 7 °C. Weather report valid at TOT: METAR KLSV 082256Z 04011KT 20SM FEW010 BKN030 BKN090 OVC200 11/07 A3008 RMK SLP186 WND DATA ESTMD

b. Predicted and Measured Detection Ranges

TAWS predicted ranges were MDT WFOV 2.2 nm/MRT NFOV n/a and aircraft collected detection ranges were MDT WFOV 3.2 nm/MRT NFOV 1.7 nm. Range prediction discrepancies were MDT WFOV -1.0 nm (-31.3 % Error) and MRT NFOV n/a.

13. 09 Dec 2004

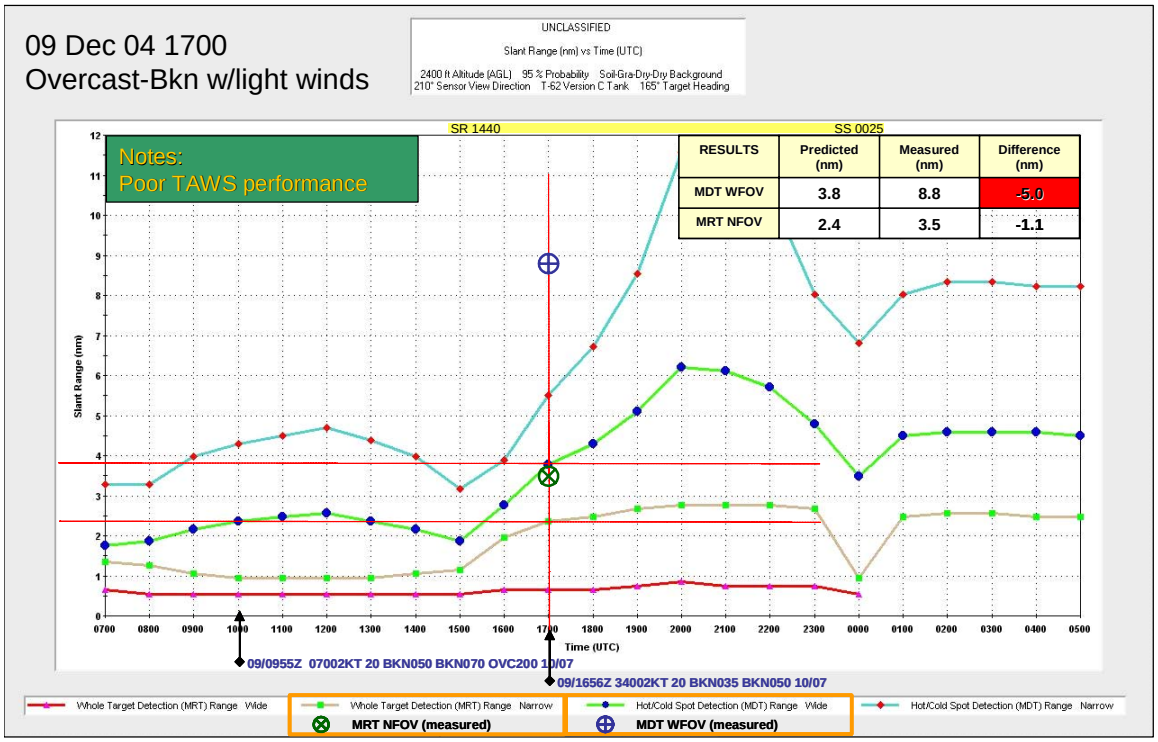

Figure 19. Same as Fig. 7 for 09 Dec 04

a. Weather

Low level clouds were broken to overcast until 1800 UTC, scattered after. Visibility was unrestricted. Winds were light and variable. T_{min}, 9 °C, was recorded at 1255 UTC and T_{max}, 15 °C, at 2155 UTC. T_{dpt} varied from 5 to 7 °C. Weather report valid at TOT: METAR KLSV 081655Z 06007KT 20SM FEW050 OVC090 09/06 A3010 RMK SLP192 WND DATA ESTMD WR//

b. Predicted and Measured Detection Ranges

TAWS predicted ranges were MDT WFOV 3.8 nm/MRT NFOV 2.4 nm and aircraft collected detection ranges were MDT WFOV 8.8 nm/MRT NFOV 3.5 nm. Range prediction discrepancies were MDT WFOV -5.0 nm (-56.8 % Error) and MRT NFOV -1.1 nm (-31.4 % Error).

14. 13 Dec 2004

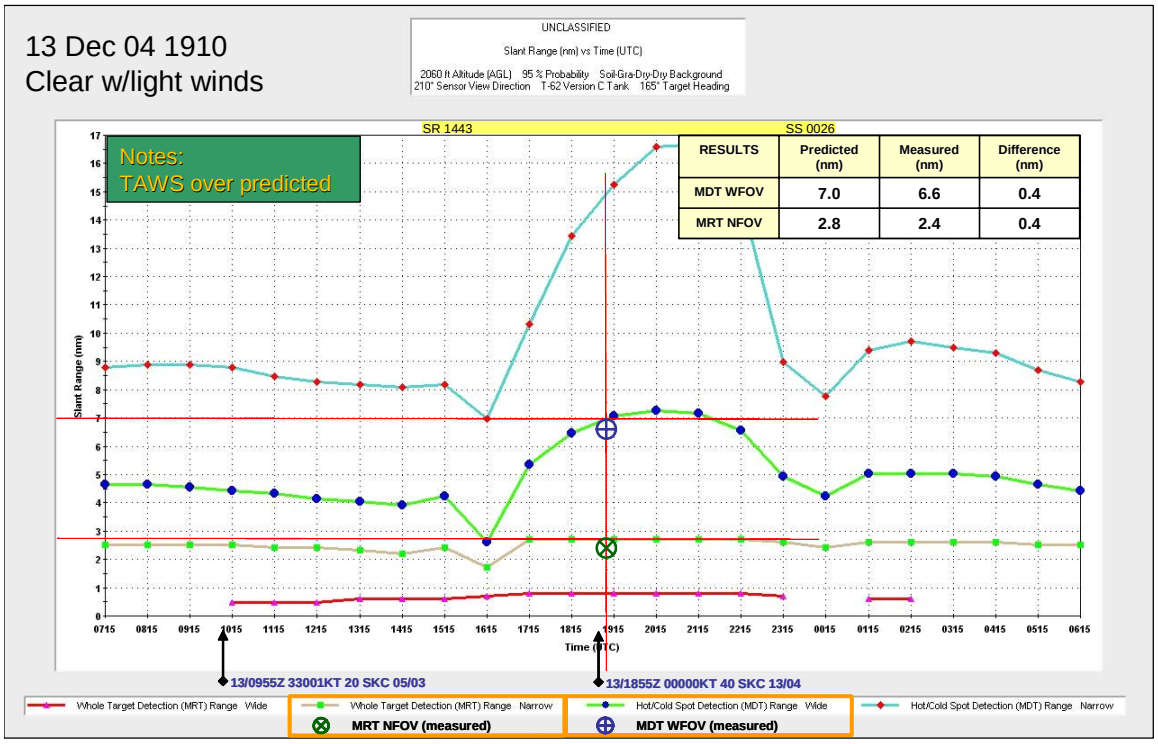

Figure 20. Same as Fig. 7 for 13 Dec 04

a. Weather

Generally, clear skies and unrestricted visibility. Winds were light and variable. T_{min}, 3 °C, was recorded at 1356 UTC and T_{max}, 18 °C, at 2255 UTC. T_{dpt} varied from 2 to 5 °C. Weather report valid at TOT: METAR KLSV 131855Z 00000KT 40SM SKC 13/04 A3028 RMK SLP251 WND DATA ESTMD

b. Predicted and Measured Detection Ranges

TAWS predicted ranges were MDT WFOV 7.0 nm/MRT NFOV 2.8 nm and aircraft collected detection ranges were MDT WFOV 6.6 nm/MRT NFOV 2.4 nm. Range prediction discrepancies were MDT WFOV 0.4 nm (6.1 % Error) and MRT NFOV 0.4 nm (16.7 % Error).

15. 14 Dec 2004

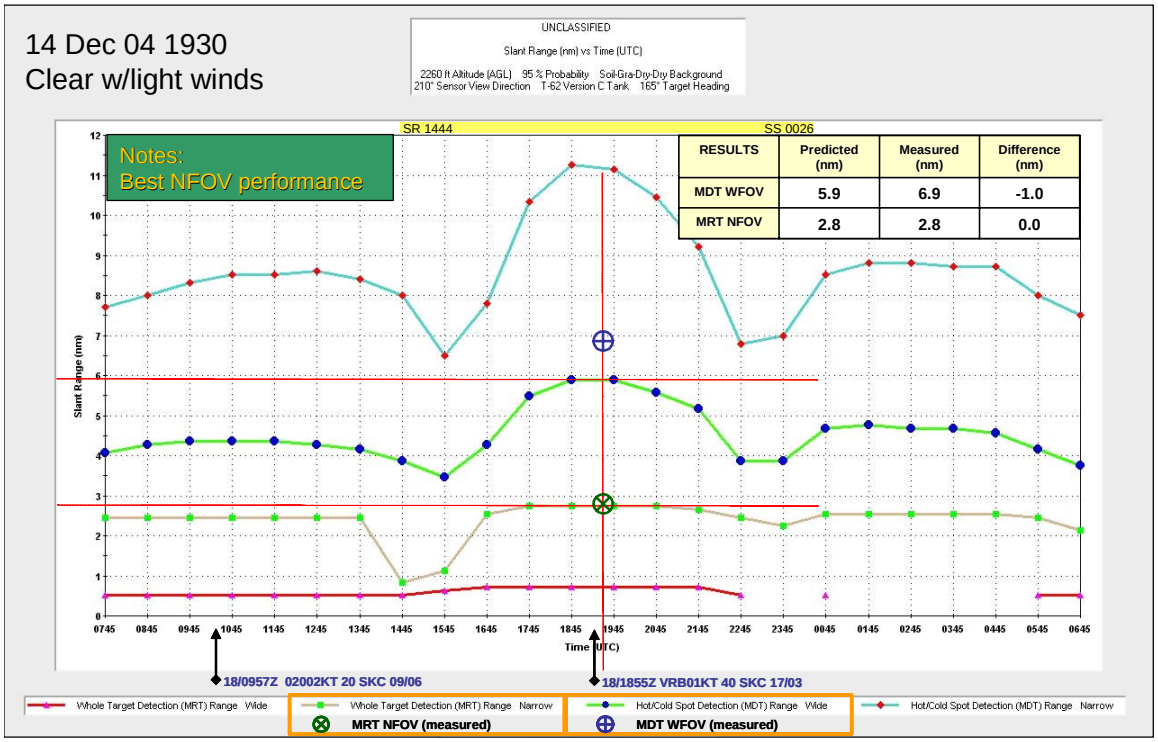

Figure 21. Same as Fig. 7 for 14 Dec 04

a. Weather

High-level clouds were scattered and visibility was unrestricted. Winds were light and variable. T_{min}, 3 °C, was recorded at 1155 UTC and T_{max}, 18 °C, at 2155 UTC. T_{dpt} varied from 2 to 4 °C. Weather report valid at TOT: METAR KLSV 141855Z 00000KT 40SM FEW200 13/02 A3036 RMK SLP278 WND DATA ESTMD CONTRAILS

b. Predicted and Measured Detection Ranges

TAWS predicted ranges were MDT WFOV 5.9 nm/MRT NFOV 2.8 nm and aircraft collected detection ranges were MDT WFOV 6.9 nm/MRT NFOV 2.8 nm. Range prediction discrepancies were MDT WFOV -1.0 nm (-14.5 % Error) and MRT NFOV 0.0 nm (0 % Error).

16. 15 Dec 2004

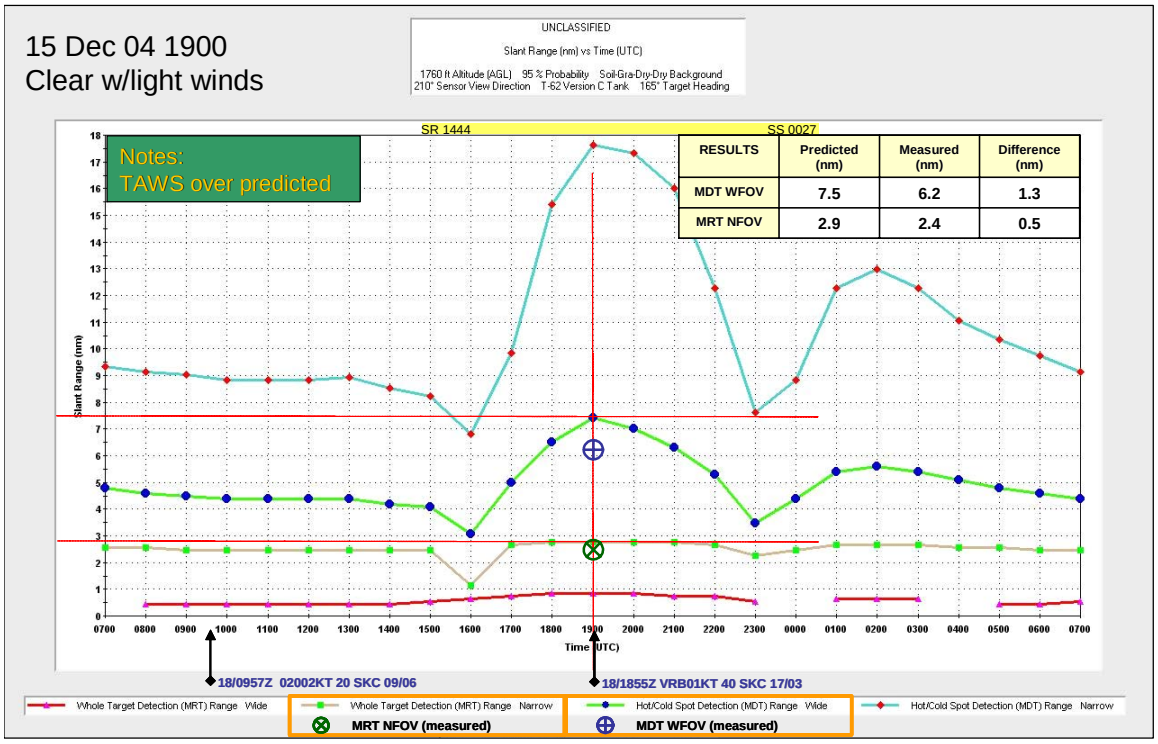

Figure 22. Same as Fig. 7 for 15 Dec 04

a. Weather

High-level clouds were scattered to broken and visibility was unrestricted. Winds were light and variable. T_{min}, 4 °C, was recorded at 1055 UTC and T_{max}, 18 °C, at 2055 UTC. Relative humidity decreased and T_{dpt} varied from 3 to -3 °C. Weather report valid at TOT: METAR KLSV 151856Z VRB03KT 40SM BKN200 14/M01 A3032 RMK SLP267 WND DATA ESTMD CONTRAILS

b. Predicted and Measured Detection Ranges

TAWS predicted ranges were MDT WFOV 7.5 nm/MRT NFOV 2.9 nm and aircraft collected detection ranges were MDT WFOV 6.2 nm/MRT NFOV 2.4 nm. Range prediction discrepancies were MDT WFOV 1.3 nm (21.0 % Error) and MRT NFOV 0.5 nm (20.8 % Error).

B. PART #1, RESULTS OF THE DETECTION RANGE COLLECTIONS

1. Potential Bias

To determine the presence of positive or negative bias in the TAWS calculations, graphs of predicted and measured ranges were created (Figures 23 & 24. TAWS ranges predictions for MDT WFOV were less than aircraft measurements in 88 % of the samples. TAWS range predictions for MRT NFOV were less than measured values in 64% of the samples. The graphs illustrate a tendency for TAWS to underestimate detection ranges in WFOV and NFOV predictions compared to aircraft measurements. Correlation coefficients for this study indicated a good relation between predicted and measured MDT WFOV, 0.94, and a weaker relationship between those for MRT NFOV, 0.72.

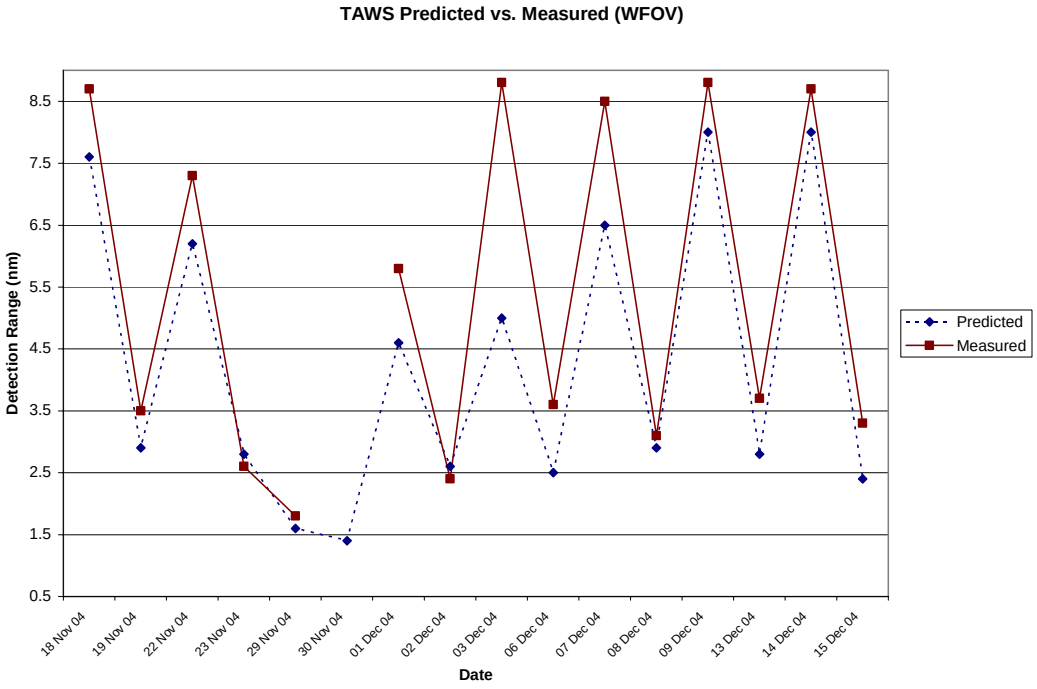

Figure 23. WFOV Detection Predictions and Measurements

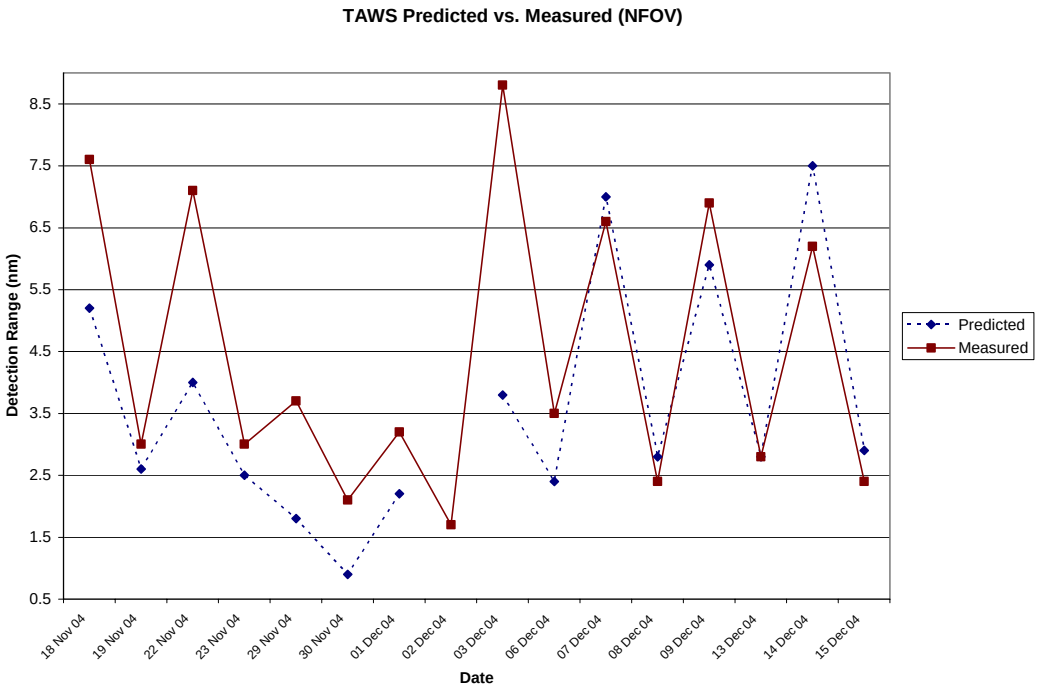

Figure 24. NFOV Detection Predictions and Measurements

2. Discrepancy

A Chi-square test for the two MDT WFOV series, predicted and measured, indicated a strong probability, 0.98, that the two arrays were significantly similar. This, as well as the correlation coefficients, supports the statistical significance of a direct comparison of the series. In terms of percent error, the average discrepancy of TAWS predictions of MDT WFOV detection range was determined to be –21.6%. A Chi-square test for MRT NFOV arrays indicated a lesser probability, 0.42, that variances of the two series were similar. In terms of percent error, the average discrepancy of TAWS MRT NFOV detection range predictions, were determined to be –12.2%.

3. Part #1 Remarks

In this part of the study, TAWS MRT NFOV predictions showed an average error (-12.2%) that was less than the error (-21.6%) for TAWS MDT WFOV. However, the strong correlation between predicted and measured values of MDT WFOV indicated the discrepancy was systematic and therefore easier to anticipate than the smaller percent error associated with MRT NFOV. It should be noted, the sample population for this study was collected during a highly variable weather period at Nellis AFB NV.

C. PART #2, TARGET SCENE TEMPERATURE COLLECTIONS

Comparisons of predicted and measured temperatures were made graphically and numerically. Figure 25 is an example of the graphic comparison product. In this figure, the top grouping of lines represent temperatures. The lower grouping of lines displays the delta-T and RH. The single solid line on bottom marks time of incoming shortwave radiation. Figures 26-37 show the comparisons of predicted values and measured values from two view directions over the period from 17-22 Jan 06.

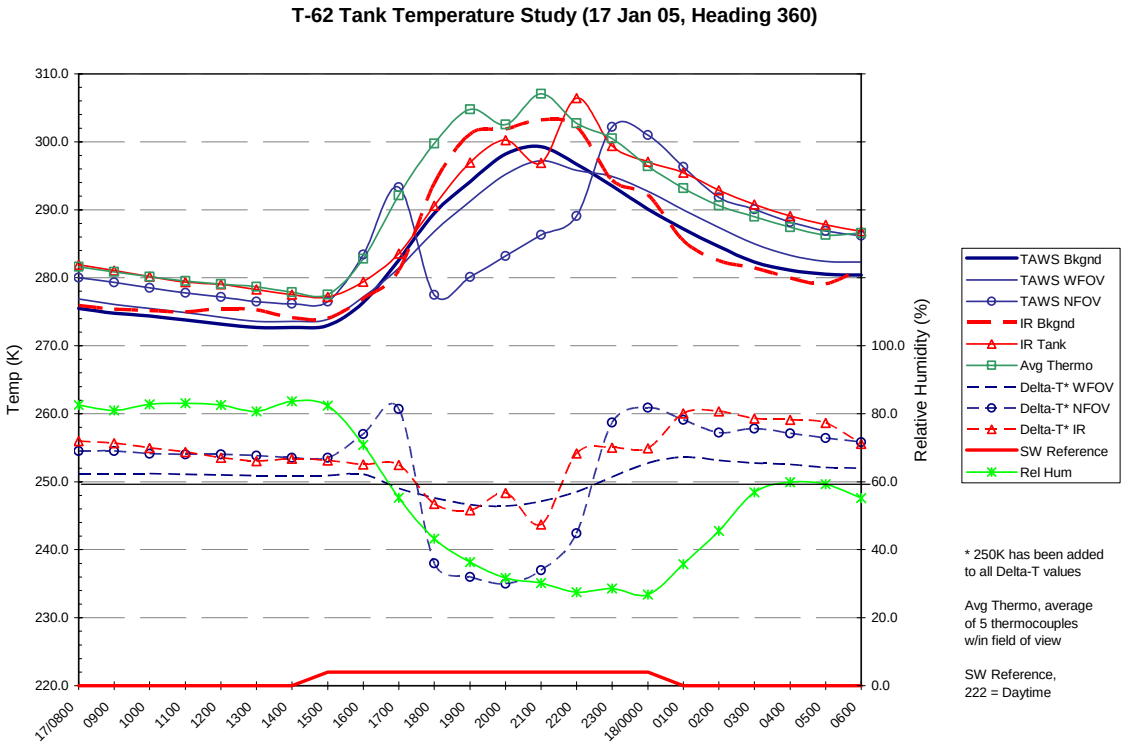

Figure 25. Sample Target Scene Temperature Collection Plot.

A summary of each daily temperature discrepancy statistical analysis is provided in Tables 4-15. Special attention should be given to the differences of the correlation strengths between the day and night measurements. This relationship illustrates the complexity of the physical model when dealing with the solar loading component upon multiple facets of the target.

1. 17 Jan 2005 (View Direction 360)

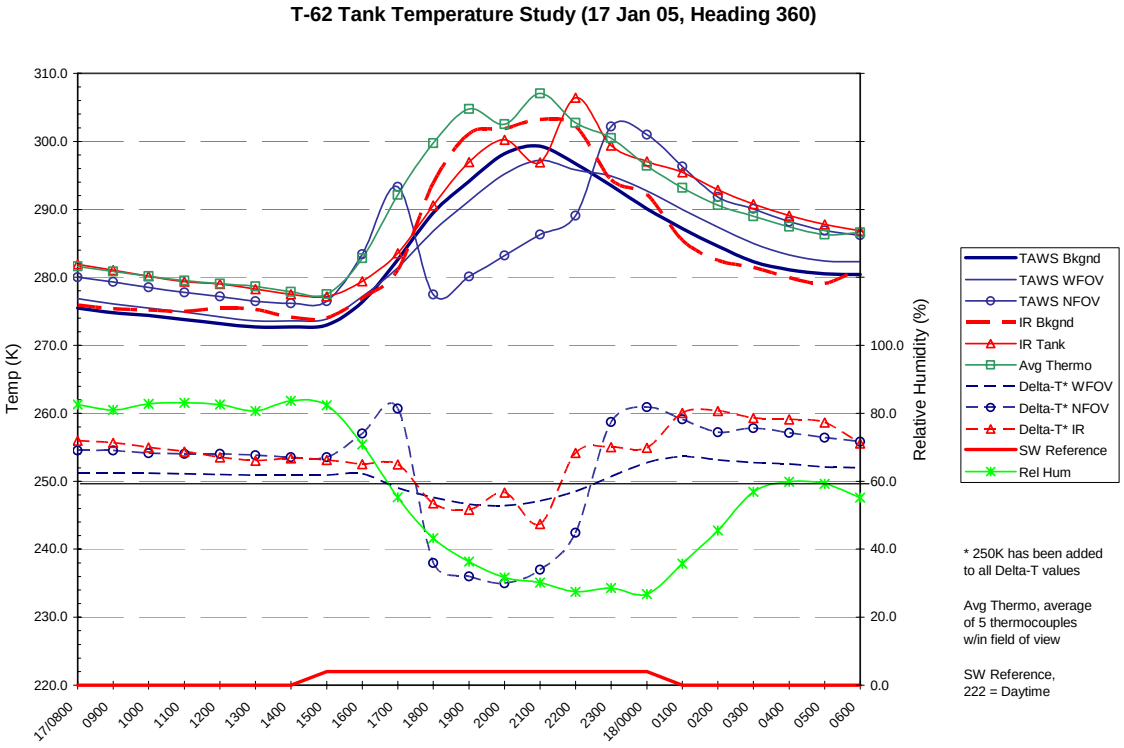

Figure 26. 17 Jan 05, 360. Predicted and Measured Diurnal Temperature Curves.

a. Weather

Skies were predominantly clear, occasionally scattered high-clouds were present. Visibility was unrestricted and winds were light and variable. T_{min}, 4 °C, was recorded at 1155 UTC and T_{max}, 20 °C, at 2255 UTC. T_{dpt} varied from 1 to 5 °C.

b. Temperature Discrepancies

Table 4. 17 Jan 05, 360. Temperature differences by period. "IR" indicates a comparison to IR apparent and "Th" indicates a comparison to inherent temperatures. Background temperatures considered independent of view direction, only analyzed for 360.

View Dir 360	Bkgnd			WFOV			NFOV		
	AM Dark	Day	PM Dark	AM Dark	Day	PM Dark	AM Dark	Day	PM Dark
Chi-test	1.00	1.00	1.00	1.00	1.00	0.99	1.00	0.87	1.00
Correlation	**0.65**	0.98	0.93	0.98	0.96	0.99	0.99	**0.38**	0.99
Avg Δ T (IR)	**-1.3**	**-2.7**	**1.0**	**-4.6**	**-4.1**	**-5.4**	**-1.7**	**-5.5**	**-0.5**
Chi-test				1.00	0.98	1.00	1.00	**0.58**	1.00
Correlation				0.98	0.93	1.00	0.99	**0.22**	0.99
Avg Δ T (Th)				**-4.7**	**-8.0**	**-3.8**	**-1.8**	**-9.4**	**1.1**

2. 18 Jan 2005 (View Direction 360)

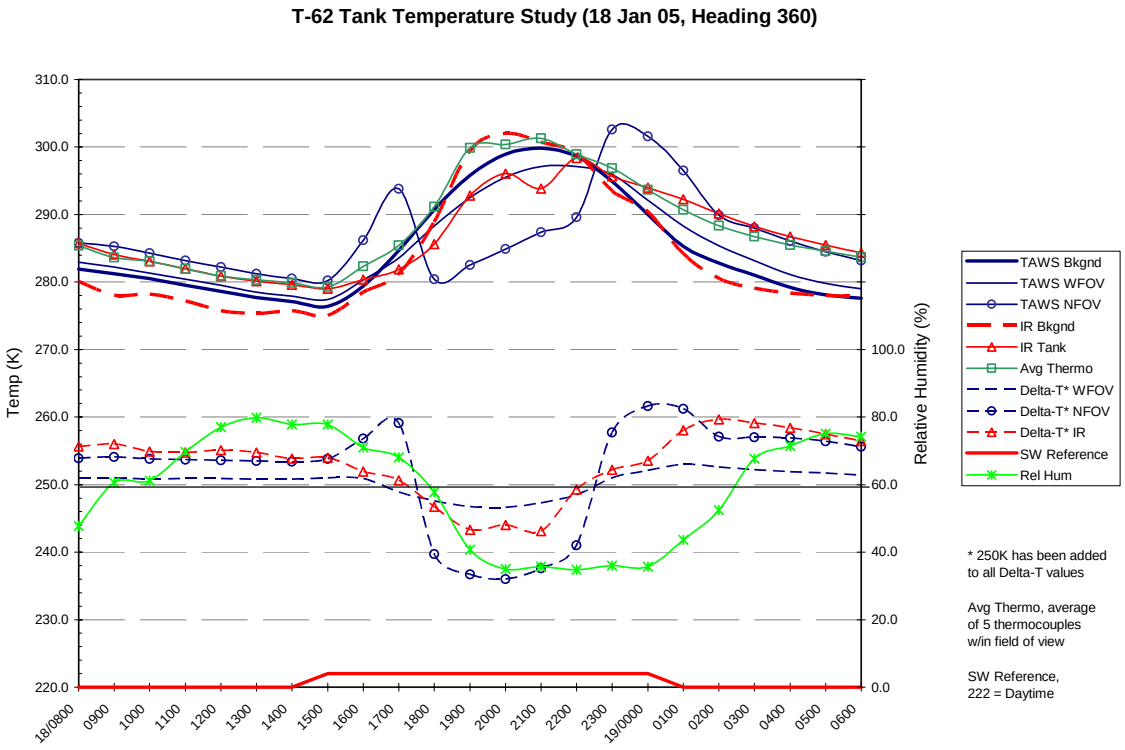

Figure 27. Same as Figure 26 for 18 Jan 05, 360.

a. Weather

Scattered to broken high-level clouds, unrestricted visibility and light variable winds. T_{min}, 6 °C, was recorded at 1456 UTC and T_{max}, 18 °C, at 2255 UTC. Relative humidity decreased and T_{dpt} varied from 2 to 7 °C.

b. Temperature Discrepancies

Table 5. Same as Table 4 for 18 Jan 05, 360.

View Dir 360	Bkgnd			WFOV			NFOV		
	AM Dark	Day	PM Dark	AM Dark	Day	PM Dark	AM Dark	Day	PM Dark
Chi-test	1.00	1.00	1.00	1.00	1.00	0.99	1.00	0.99	1.00
Correlation	0.94	0.98	0.95	0.99	0.97	1.00	0.98	**0.39**	0.97
Avg Δ T (IR)	**2.3**	**0.0**	**1.0**	**-1.8**	**0.2**	**-5.1**	**1.0**	**-0.8**	**0.2**
Chi-test				1.00	1.00	1.00	1.00	0.92	1.00
Correlation				0.98	0.97	1.00	0.98	**0.18**	0.99
Avg Δ T (Th)				**-1.8**	**-2.9**	**-3.8**	**1.1**	**-4.0**	**1.4**

3. 19 Jan 2005 (View Direction 360)

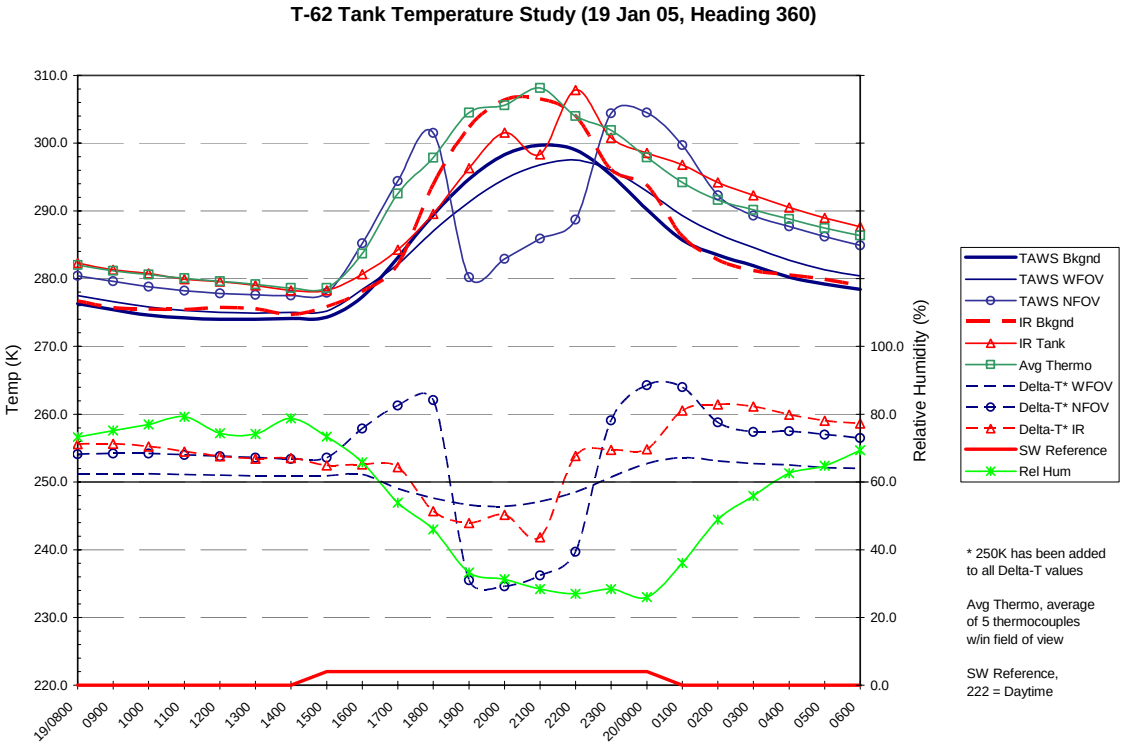

Figure 28. Same as Figure 26 for 19 Jan 05, 360.

a. Weather

There were scattered high-level clouds, unrestricted visibility and light variable winds. T_{min}, 4 °C, was recorded at 1355 UTC and T_{max}, 19 °C, at 2255 UTC. Relative humidity decreased and T_{dpt} varied from 2 to 4 °C.

b. Temperature Discrepancies

Table 6. Same as Table 4 for 19 Jan 05, 360.

View Dir 360	Bkgnd			WFOV			NFOV		
	AM Dark	Day	PM Dark	AM Dark	Day	PM Dark	AM Dark	Day	PM Dark
Chi-test	1.00	1.00	1.00	1.00	1.00	0.94	1.00	0.83	1.00
Correlation	0.77	0.98	0.97	0.94	0.97	1.00	0.97	**0.24**	0.96
Avg Δ T (IR)	**-1.0**	**-3.8**	**-0.1**	**-4.4**	**-4.4**	**-7.6**	**-1.6**	**-3.1**	**-1.7**
Chi-test				1.00	0.97	0.98	1.00	**0.67**	1.00
Correlation				0.94	0.95	1.00	0.97	**0.19**	0.97
Avg Δ T (Th)				**-4.5**	**-8.3**	**-5.6**	**-1.6**	**-6.9**	**0.2**

4. 20 Jan 2005 (View Direction 360)

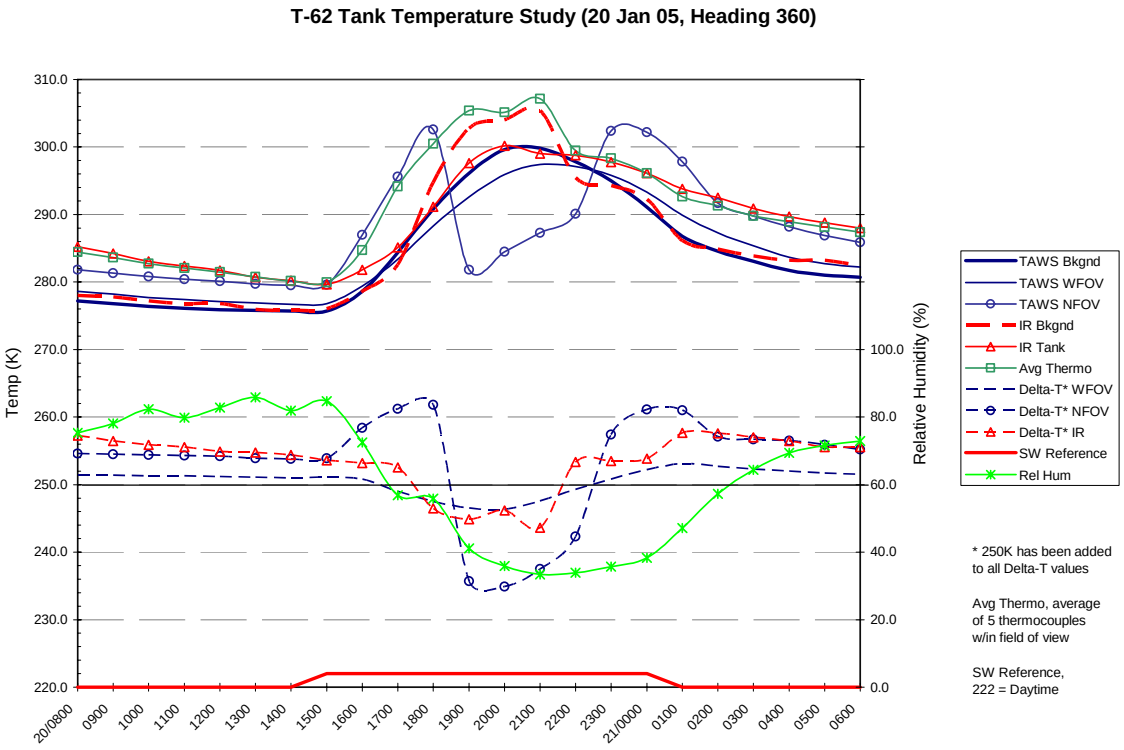

Figure 29. Same as Figure 26 for 20 Jan 05, 360.

a. Weather

Scattered to broken high-level clouds, unrestricted visibility and light variable winds. T_{min}, 7 °C, was recorded at 1157 UTC and T_{max}, 20 °C, at 2255 UTC. Relative humidity decreased and T_{dpt} varied from 4 to 8 °C.

b. Temperature Discrepancies

Table 7. Same as Table 4 for 20 Jan 05, 360.

View Dir 360	Bkgnd			WFOV			NFOV		
	AM Dark	Day	PM Dark	AM Dark	Day	PM Dark	AM Dark	Day	PM Dark
Chi-test	1.00	1.00	1.00	1.00	1.00	0.99	1.00	0.94	1.00
Correlation	0.95	0.96	0.99	1.00	0.99	0.99	1.00	**0.18**	0.96
Avg Δ T (IR)	**-0.6**	**-1.7**	**-1.0**	**-5.0**	**-2.7**	**-5.4**	**-2.0**	**-1.4**	**-0.6**
Chi-test				1.00	0.99	0.99	1.00	0.80	1.00
Correlation				0.99	0.88	0.99	1.00	**0.15**	0.97
Avg Δ T (Th)				**-4.7**	**-7.1**	**-4.5**	**-1.7**	**-5.8**	**0.4**

5. 21 Jan 2005 (View Direction 360)

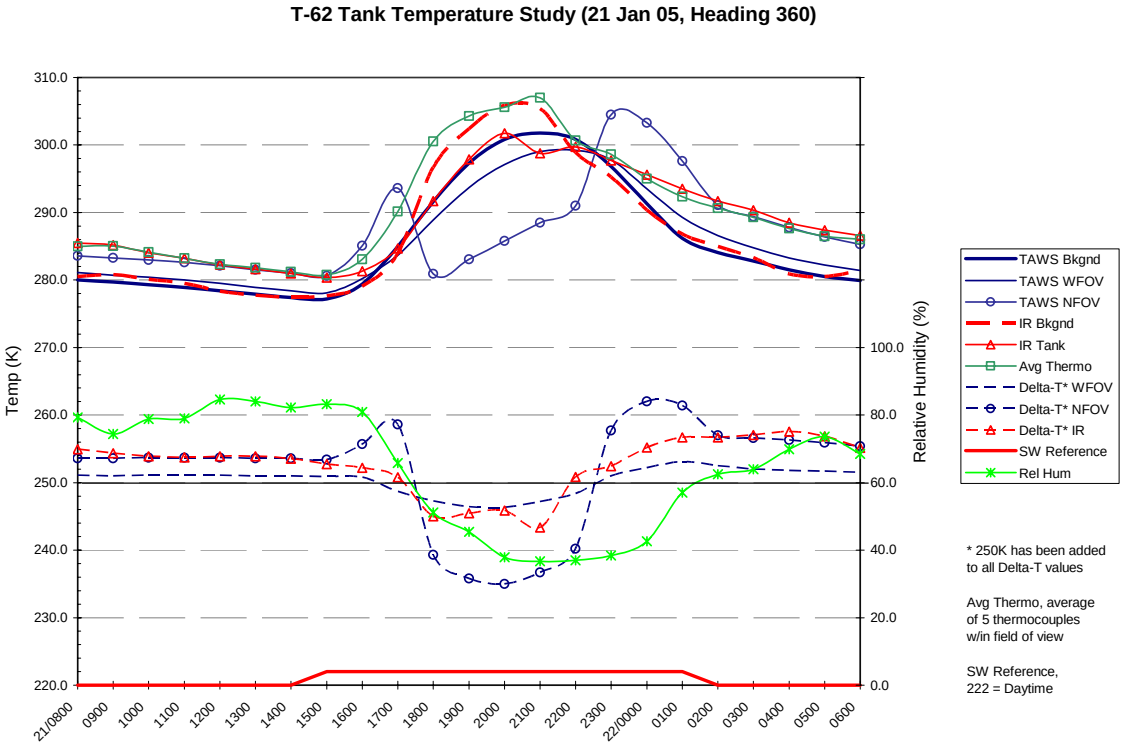

Figure 30. Same as Figure 26 for 21 Jan 05, 360.

a. Weather

Scattered high-level clouds were present with unrestricted visibility and light variable winds. T_{min}, 5 °C, was recorded at 1455 UTC and T_{max}, 20 °C, at 2255 UTC. Relative humidity decreased and T_{dpt} varied from 1 to 6 °C.

b. Temperature Discrepancies

Table 8. Same as Table 4 for 21 Jan 05, 360.

View Dir 360	Bkgnd			WFOV			NFOV		
	AM Dark	Day	PM Dark	AM Dark	Day	PM Dark	AM Dark	Day	PM Dark
Chi-test	1.00	1.00	1.00	1.00	1.00	0.99	1.00	0.95	1.00
Correlation	0.98	0.96	0.96	0.99	0.98	0.99	0.99	**0.31**	0.95
Avg Δ T (IR)	**-0.4**	**-1.4**	**-0.5**	**-3.4**	**-1.8**	**-5.1**	**-0.8**	**-3.3**	**-0.1**
Chi-test				1.00	1.00	1.00	1.00	**0.72**	1.00
Correlation				0.98	0.90	0.99	0.98	**0.09**	0.96
Avg Δ T (Th)				**-3.4**	**-5.4**	**-4.1**	**-0.8**	**-6.9**	**0.9**

6. 22 Jan 2005 (View Direction 360)

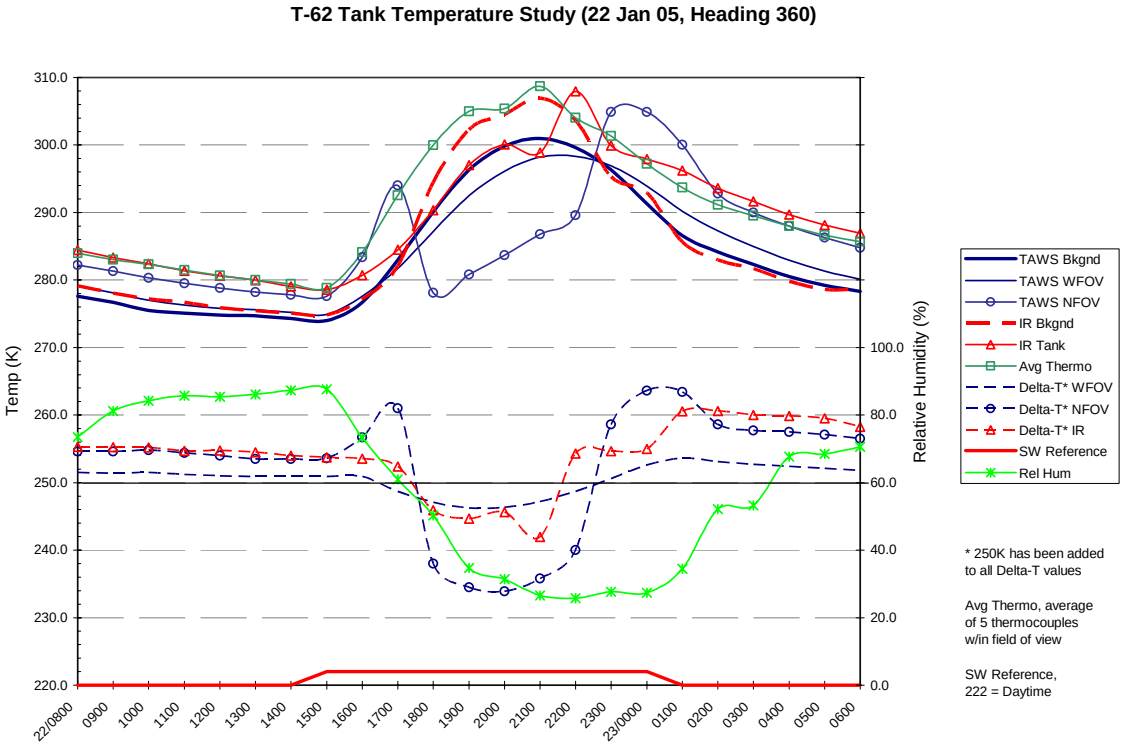

Figure 31. Same as Figure 26 for 22 Jan 05, 360.

a. Weather

Scattered to broken high-level clouds, unrestricted visibility and light variable winds. T_{min}, 6 °C, was recorded at 1456 UTC and T_{max}, 18 °C, at 2255 UTC. Relative humidity decreased and T_{dpt} varied from 2 to 7 °C.

b. Temperature Discrepancies

Table 9. Same as Table 4 for 22 Jan 05, 360.

View Dir 360	Bkgnd			WFOV			NFOV		
	AM Dark	Day	PM Dark	AM Dark	Day	PM Dark	AM Dark	Day	PM Dark
Chi-test	1.00	1.00	1.00	1.00	1.00	0.97	1.00	0.86	1.00
Correlation	0.98	0.98	0.99	0.98	0.97	1.00	1.00	**0.39**	0.97
Avg Δ T (IR)	**-1.3**	**-2.6**	**0.6**	**-4.9**	**-3.8**	**-6.6**	**-1.9**	**-5.2**	**-0.7**
Chi-test				1.00	0.98	0.99	1.00	**0.52**	1.00
Correlation				0.98	0.93	1.00	1.00	**0.19**	0.98
Avg Δ T (Th)				**-4.8**	**-8.0**	**-4.6**	**-1.8**	**-9.3**	**1.2**

7. 17 Jan 2005 (View Direction 180)

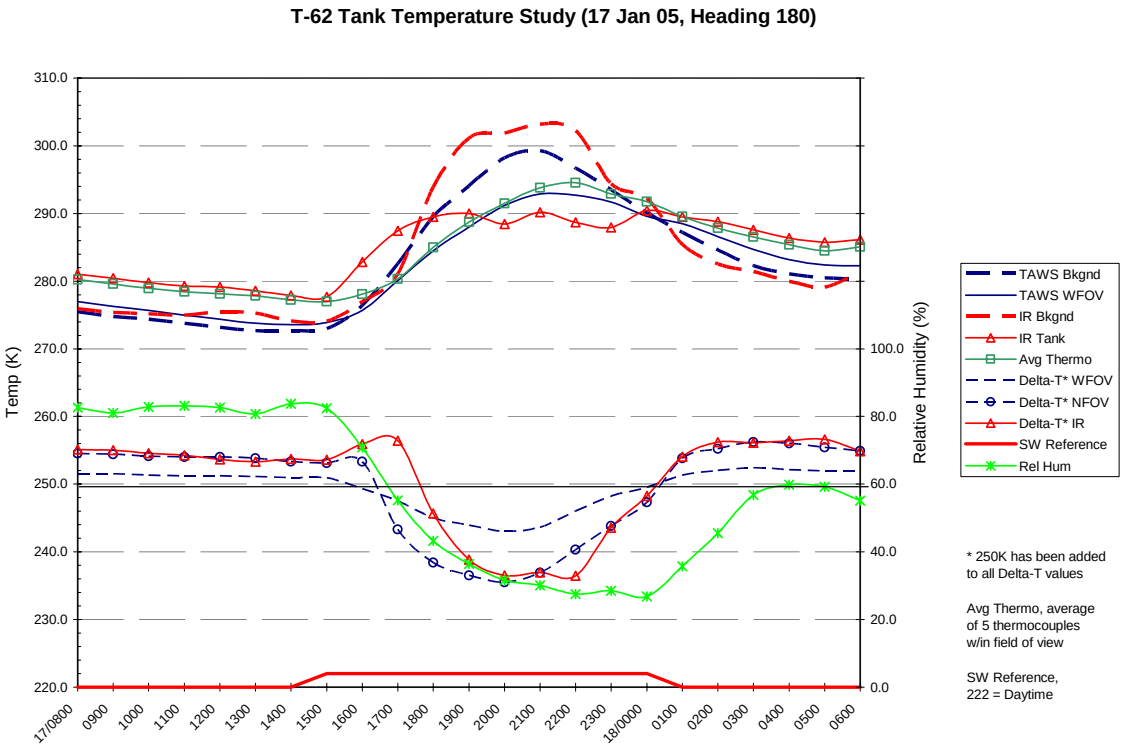

Figure 32. Same as Figure 26 for 17 Jan 05, 180.

a. Weather

Skies were predominantly clear, occasionally scattered high-clouds were present. Visibility was unrestricted and winds were light and variable. T_{min}, 4 °C, was recorded at 1155 UTC and T_{max}, 20 °C, at 2255 UTC. Relative humidity decreased and T_{dpt} varied from 1 to 5 °C.

b. Temperature Discrepancies

Table 10. Same as Table 4 for 17 Jan 05, 180.

View Dir 180	WFOV			NFOV		
	AM Dark	Day	PM Dark	AM Dark	Day	PM Dark
Chi-test	1.00	1.00	1.00	1.00	1.00	1.00
Correlation	0.98	0.82	0.99	0.99	**0.55**	0.97
Δ T (IR)	**-4.3**	**-1.3**	**-2.7**	**-1.6**	**-5.1**	**0.6**
Chi-test	1.00	1.00	1.00	1.00	1.00	1.00
Correlation	0.99	0.99	0.99	0.99	0.90	0.96
Avg Δ T (Th)	**-3.5**	**-1.3**	**-1.9**	**-0.7**	**-5.2**	**1.5**

8. 18 Jan 2005 (View Direction 180)

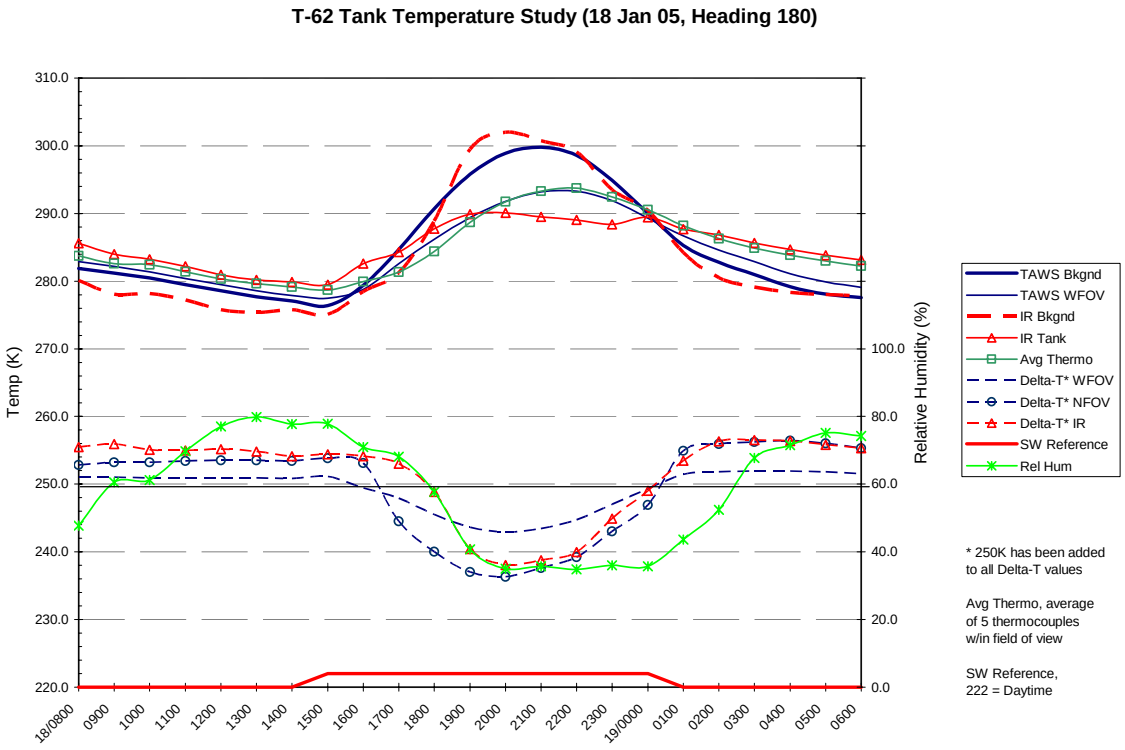

Figure 33. Same as Figure 26 for 18 Jan 05, 180.

a. Weather

Scattered to broken high-level clouds, unrestricted visibility and light variable winds. T_{min}, 6 °C, was recorded at 1456 UTC and T_{max}, 18 °C, at 2255 UTC. Relative humidity decreased and T_{dpt} varied from 2 to 7 °C.

b. Temperature Discrepancies

Table 11. Same as Table 4 for 18 Jan 05, 180.

View Dir 180	WFOV			NFOV		
	AM Dark	Day	PM Dark	AM Dark	Day	PM Dark
Chi-test	1.00	1.00	1.00	1.00	1.00	1.00
Correlation	0.99	0.94	0.99	0.97	**0.67**	1.00
Δ T (IR)	**-1.9**	**0.4**	**-2.9**	**0.5**	**-3.0**	**1.1**
Chi-test	1.00	1.00	1.00	1.00	1.00	1.00
Correlation	0.99	0.98	1.00	0.99	0.90	0.99
Avg Δ T (Th)	**-0.9**	**-0.1**	**-2.4**	**1.5**	**-3.4**	**1.7**

9. 19 Jan 2005 (View Direction 180)

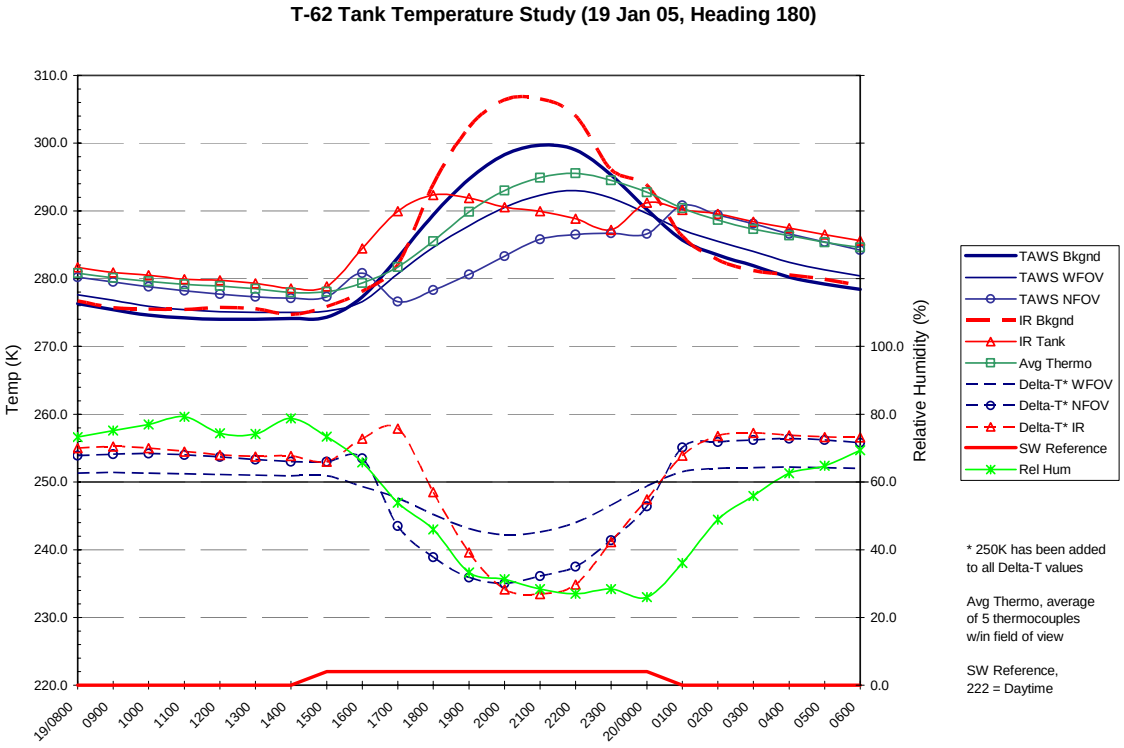

Figure 34. Same as Figure 26 for 19 Jan 05, 180.

a. Weather

High-level clouds were scattered with unrestricted visibility and light variable winds. T_{min}, 4 °C, was recorded at 1355 UTC and T_{max}, 19 °C, at 2255 UTC. Relative humidity decreased and T_{dpt} varied from 2 to 4 °C.

b. Temperature Discrepancies

Table 12. Same as Table 4 for 19 Jan 05, 180.

View Dir 180	WFOV			NFOV		
	AM Dark	Day	PM Dark	AM Dark	Day	PM Dark
Chi-test	1.00	1.00	0.99	1.00	0.99	1.00
Correlation	0.93	**0.64**	0.99	0.98	**0.26**	1.00
Δ T (IR)	**-4.3**	**-2.3**	**-4.5**	**-1.7**	**-6.3**	**-0.5**
Chi-test	1.00	1.00	1.00	1.00	0.99	1.00
Correlation	0.95	0.99	1.00	0.99	0.87	0.99
Avg Δ T (Th)	**-3.5**	**-2.3**	**-3.7**	**-0.9**	**-6.3**	**0.3**

10. 20 Jan 2005 (View Direction 180)

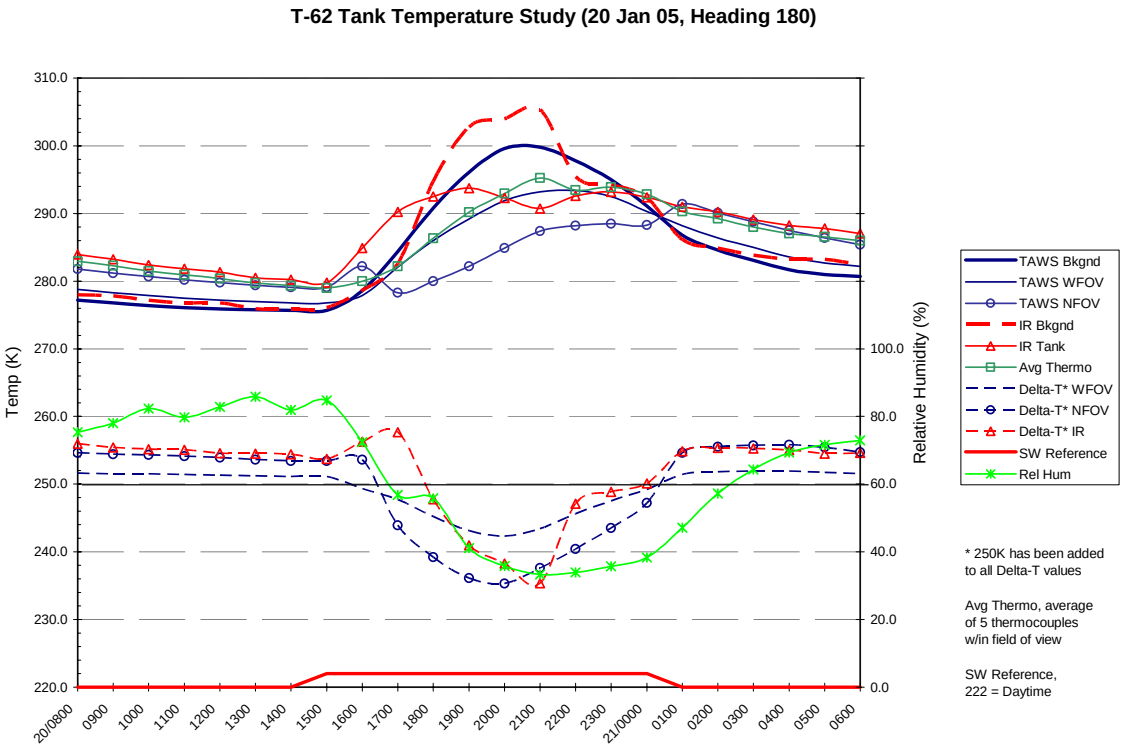

Figure 35. Same as Figure 26 for 20 Jan 05, 180.

a. Weather

Scattered to broken high-level clouds, unrestricted visibility and light variable winds. T_{min}, 7 °C, was recorded at 1157 UTC and T_{max}, 20 °C, at 2255 UTC. Relative humidity decreased and T_{dpt} varied from 4 to 8 °C.

b. Temperature Discrepancies

Table 13. Same as Table 4 for 20 Jan 05, 180.

View Dir 180	WFOV			NFOV		
	AM Dark	Day	PM Dark	AM Dark	Day	PM Dark
Chi-test	1.00	1.00	1.00	1.00	0.99	1.00
Correlation	0.99	0.84	0.99	1.00	**0.50**	1.00
Δ T (IR)	**-4.3**	**-2.9**	**-4.2**	**-1.6**	**-6.3**	**-0.6**
Chi-test	1.00	1.00	1.00	1.00	1.00	1.00
Correlation	0.99	0.99	1.00	1.00	0.86	0.99
Avg Δ T (Th)	**-3.4**	**-1.3**	**-3.2**	**-0.7**	**-4.7**	**0.4**

11. 21 Jan 2005 (View Direction 180)

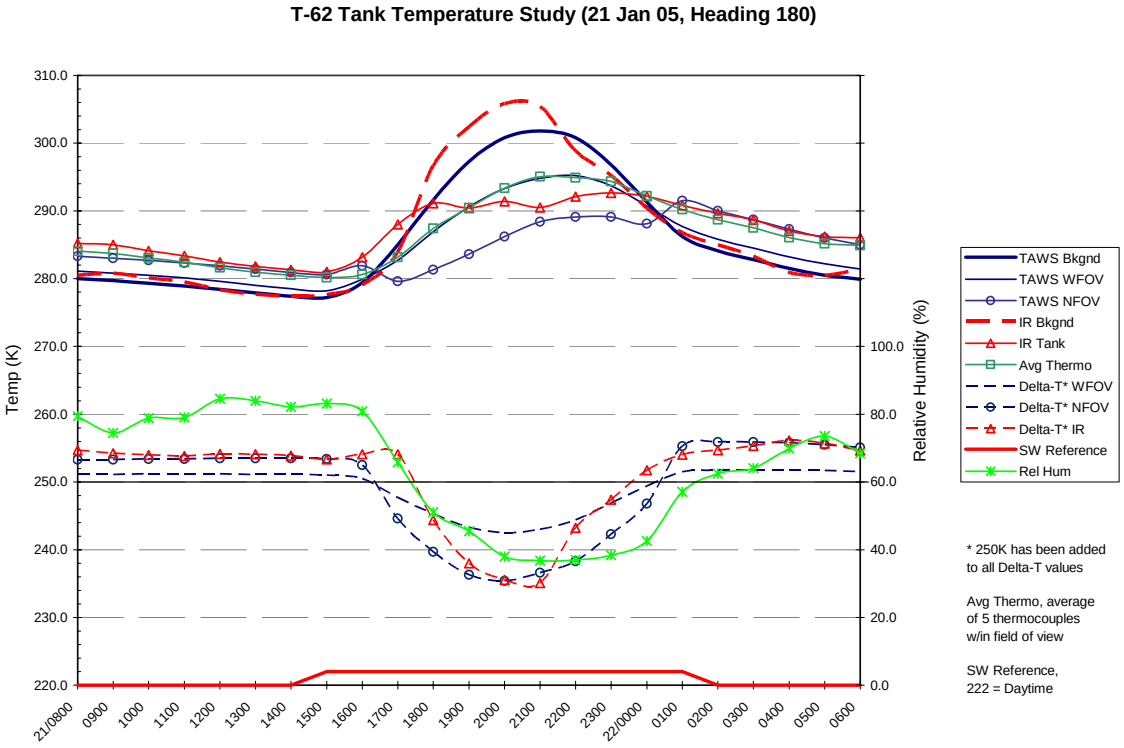

Figure 36. Same as Figure 26 for 21 Jan 05, 180.

a. Weather

Scattered high-level clouds were present with unrestricted visibility and light variable winds. T_{min}, 5 °C, was recorded at 1455 UTC and T_{max}, 20 °C, at 2255 UTC. Relative humidity decreased and T_{dpt} varied from 1 to 6 °C.

b. Temperature Discrepancies

Table 14. Same as Table 4 for 21 Jan 05, 180.

View Dir 180	WFOV			NFOV		
	AM Dark	Day	PM Dark	AM Dark	Day	PM Dark
Chi-test	1.00	1.00	1.00	1.00	1.00	1.00
Correlation	0.99	0.90	0.99	0.99	**0.69**	0.99
Δ T (IR)	**-3.4**	**-0.6**	**-3.9**	**-1.1**	**-4.5**	**0.0**
Chi-test	1.00	1.00	1.00	1.00	1.00	1.00
Correlation	0.99	1.00	1.00	0.99	0.90	0.99
Avg Δ T (Th)	**-2.4**	**-0.6**	**-3.0**	**-0.1**	**-4.4**	**1.0**

12. 22 Jan 2005 (View Direction 180)

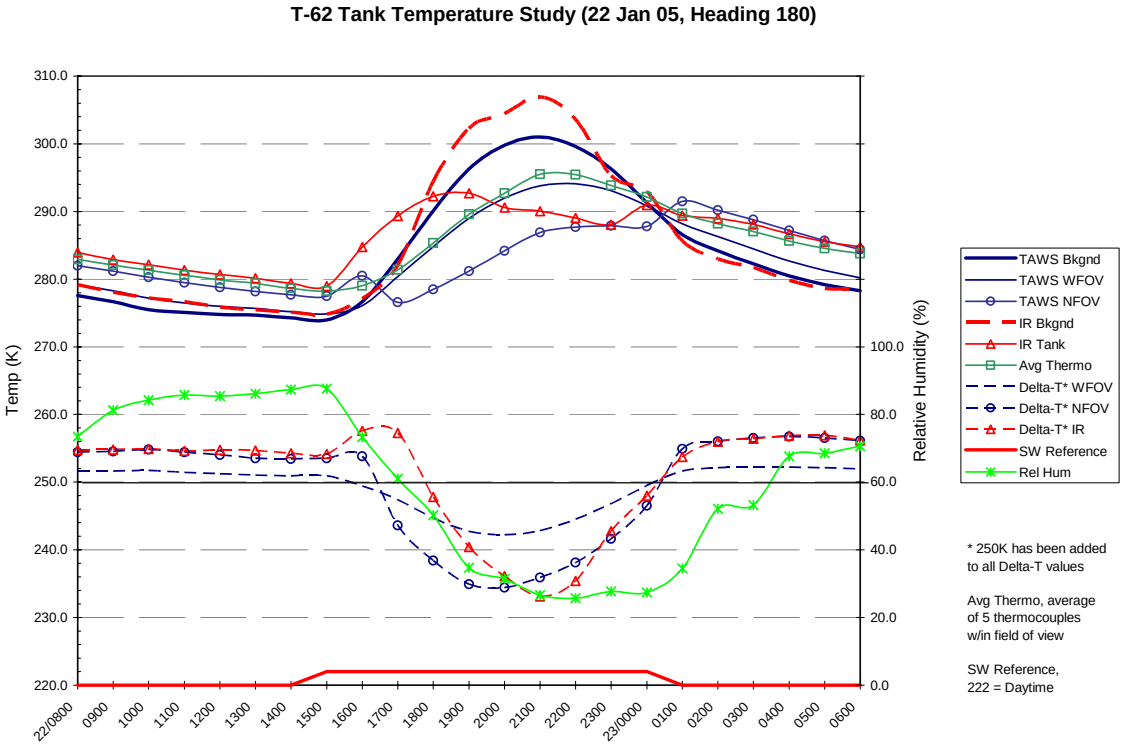

Figure 37. Same as Figure 26 for 22 Jan 05, 180.

a. Weather

Scattered to broken high-level clouds, unrestricted visibility and light variable winds. T_{min}, 6 °C, was recorded at 1456 UTC and T_{max}, 18 °C, at 2255 UTC. Relative humidity decreased and T_{dpt} varied from 2 to 7 °C.

b. Temperature Discrepancies

Table 15. Same as Table 4 for 22 Jan 05, 180

View Dir 180	WFOV			NFOV		
	AM Dark	Day	PM Dark	AM Dark	Day	PM Dark
Chi-test	1.00	1.00	1.00	1.00	0.99	1.00
Correlation	0.99	**0.67**	0.98	1.00	**0.32**	0.99
Δ T (IR)	**-4.6**	**-1.8**	**-3.4**	**-1.8**	**-5.8**	**0.7**
Chi-test	1.00	1.00	1.00	1.00	1.00	1.00
Correlation	0.99	0.99	1.00	1.00	0.89	0.99
Avg Δ T (Th)	**-3.8**	**-1.4**	**-2.6**	**-1.0**	**-5.4**	**1.5**

D. PART #2, RESULTS OF THE SCENE TEMPERATURE COLLECTIONS

1. Potential Bias

The predominance of negative ΔTs in Table 16 indicated a tendency for TAWS to predict temperature values less than measured IR and thermocouple values. TAWS average target temperatures exceeded measurements only after sunset using NFOV. These values were small and represented the best TAWS performance. The high correlation coefficients and Chi-square values for the AM dark hours of both sensor modes and view directions support the presence of a predictable negative bias for this period. Similarly, strong statistical relationships and negative biases can be found for all dark and day hours of WFOV view directions 360 and 180 and all dark hours of NFOV view direction 360 and 180. NFOV day hours for both 360 and 180 view directions displayed the weakest correlation coefficients of the study. Biases associated with this period and sensor mode are the least predictable.

Table 16. Temperature differences between observed and predicted target temperatures by period (ΔT = predicted – measured). Background temperatures considered independent of view direction, only analyzed for 360.

View Dir 360	Bkgnd			WFOV			NFOV		
	AM Dark	Day	PM Dark	AM Dark	Day	PM Dark	AM Dark	Day	PM Dark
Avg Δ T (IR)	**-0.4**	**-2.0**	**0.2**	**-4.0**	**-2.8**	**-5.8**	**-1.2**	**-3.2**	**-0.6**
Avg Δ T (Th)				**-4.0**	**-6.6**	**-4.4**	**-1.1**	**-7.1**	**0.9**

View Dir 180	WFOV			NFOV		
	AM Dark	Day	PM Dark	AM Dark	Day	PM Dark
Δ T (IR)	**-3.8**	**-1.4**	**-3.6**	**-1.2**	**-5.2**	**0.2**
Avg Δ T (Th)	**-2.9**	**-1.2**	**-2.8**	**-0.3**	**-4.9**	**1.1**

2. Discrepancies

While TAWS displayed a negative bias for most view directions, sensor modes and periods, the discrepancy was smallest (1.1° to -0.6°) during PM dark hours when the positive/negative bias tendency was less predictable. Background and WFOV temperature predictions were the best performers in this study. Both displayed a strong statistical relationship between predicted and measured and an average ΔT of -1.9°. During daytime hours, NFOV showed the least systematic discrepancy and the largest

ΔTs (-3.2° to -7.1°, average ΔT = -2.3°). Figure 38 shows the daytime NFOV ΔT and statistical analysis (solid lines) along with dark hour ΔTs (dashed lines). It was apparent the NFOV daytime error was greater than night time hours for both view directions. View direction 180, facing the shaded facets of the tank, offered a slightly greater degree of predictability with it's consistently higher correlation coefficients and Chi-square test values. View direction 360 had the greater challenge of calculating temperatures of the target facets directly exposed to the sun.

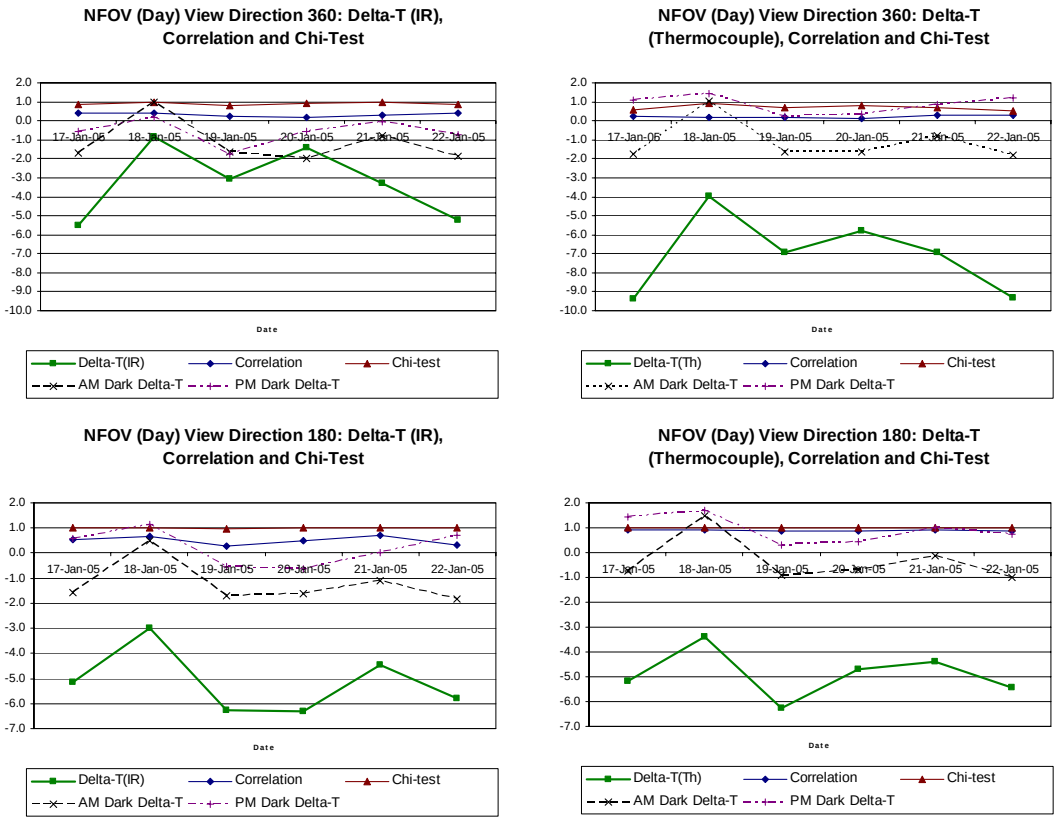

Figure 38. Graphs of Delta-T, Correlation Coefficient and Chi-square test for independence. Dashed lines are dark hour delta-Ts, all other lines are associated with day hours.

3. Part #2 Remarks

This collection occurred during a homogenous fair weather period. The least favorable performance was during daytime hours when solar loading, facet shading and target thermal response were most complicated. It should be noted, while TAWS NFOV displayed the worst performance, experimental limitations contributed to this discrepancy. Experimental limitations will be discussed in a later section. The best

performance occurred during night and early morning hours when the thermal forcing was simplified. The complete statistical worksheet can be found in Appendix F.

THIS PAGE INTENTIONALLY LEFT BLANK

IV. CONCLUSION

A. STUDY CONCLUSIONS

The results of this study support the assertion that TAWS range predictions are representative of observed ranges in an operational environment. The first part of this study indicated daytime errors in detection range predictions of -12.2% for NFOV and -21.6% for WFOV. To put these values in context, during more favorable weather conditions and from higher flight levels, 12000ft to 26000ft, Koch (Koch, 97) found NFOV MRT detection range errors of less than 13% using the TCM based Electro-Optical Tactical Decision Aid (EOTDA) program. Given the highly variable weather present during the detection portion of this study, TAWS NFOV MRT range performance was very good, if less than systematic. It should also be noted that the difference between expected and observed was often less than a mile as collected from an aircraft approaching at 200-250 knots. The WFOV MDT range discrepancy was greater, but easier to anticipate considering the strong correlation coefficient and chi squared values.

TAWS also performed well predicting thermal background temperature with an average temperature error of -1.3°. Average WFOV day time temperature discrepancies were -2.1° and did not display dramatic variation over the data set. Average NFOV daytime discrepancies were -3.8° and displayed a greater variability over the observed period. While prediction discrepancies existed, they appeared to be systematic for WFOV and background calculations. This means they can be anticipated, with the exception of NFOV, with a thorough local study to determine specific adjustments.

B. RECOMMENDATIONS

While this study was not without limitations (see Appendix G), overall TAWS performance was found to be representative. Background and WFOV assessments indicated a predictable bias for both detection range and temperature analysis. CWTs should consider replicating the detection range part of this study to develop awareness of local TAWS effectiveness. The radiometric comparison highlighted the complexity of NFOV MRT calculations of target temperatures. Additional studies using a target

specific to the MuSES model should be accomplished to determine the degree of improvement gained using the upgraded model. Unfortunately, the T-62 tank used in this study was not available as a high-resolution MuSES target.

The weak correlation of predicted and measured NFOV MRT detection range and NFOV target temperature during daytime hours for both parts of this study indicated that this should be the focus for model improvement in TAWS. Overall TAWS performance will improve with increased understanding of sensor to facet geometry and target thermal characteristics.

Combining the methods of both experiments to simultaneously collect ground radiometric target and background temperatures and target detection ranges from aircraft sensors would offer the most complete understanding of TAWS performance characteristics. Ideally, this would be done with an actual high-resolution target modeled in TAWS on a homogenous background also modeled in TAWS.

TAWS TDAs are effective in providing reliable estimates of both detection range and target scene temperatures, but as with most models it has some limitations. Understanding and anticipating these limitations are essential to providing the most accurate EM/EO mission planning guidance to the airborne war-fighter.

APPENDIX A - SCREEN CAPTURES OF TAWS INPUTS

Target

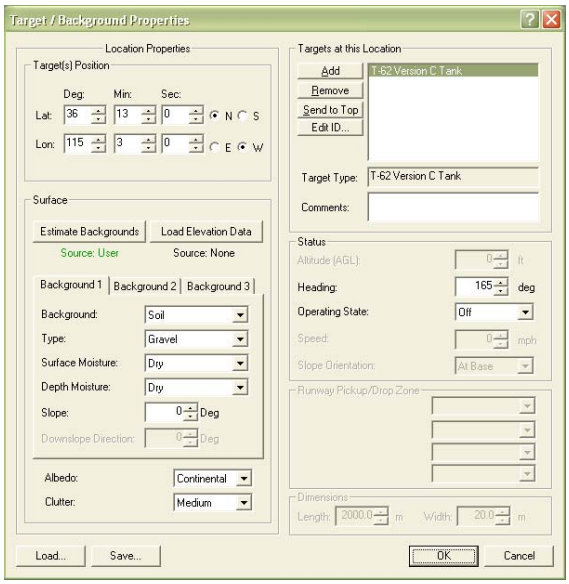

Weather

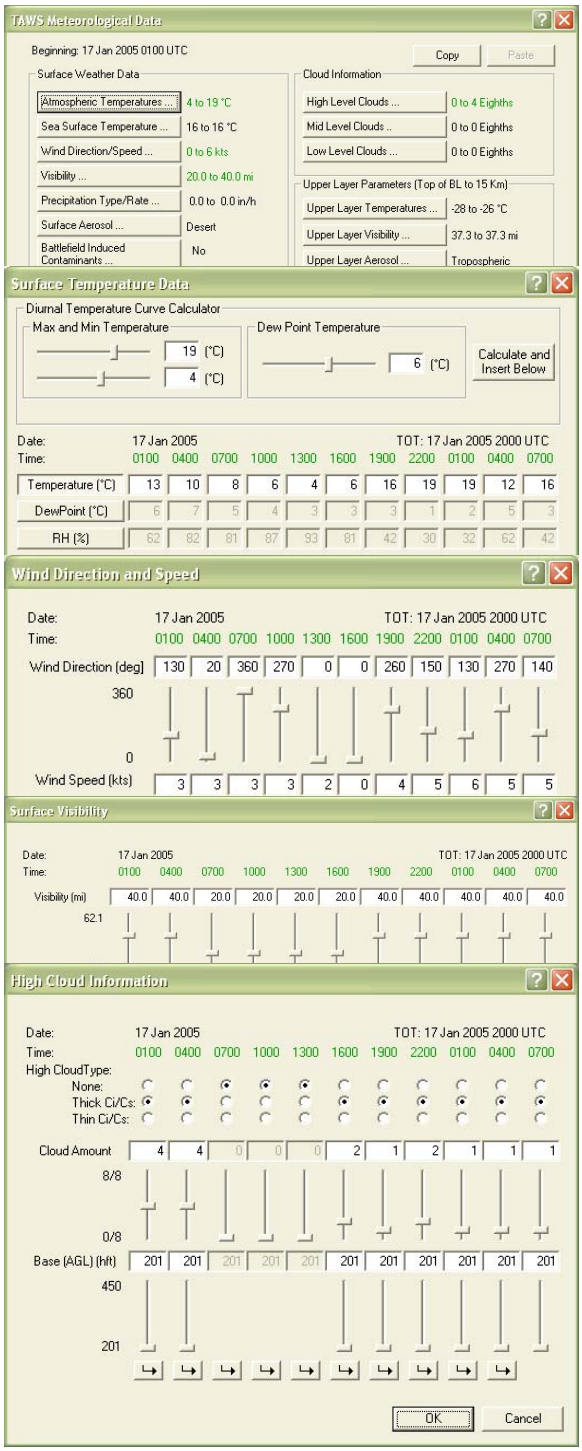

Sortie

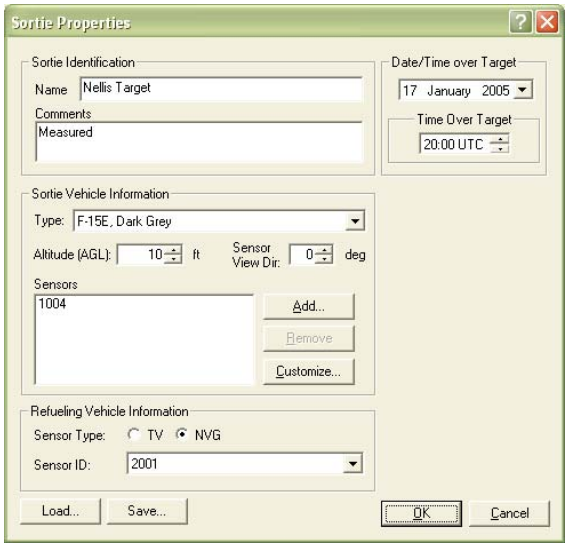

THIS PAGE INTENTIONALLY LEFT BLANK

APPENDIX B - SAMPLE TABULAR OUTPUT OF TAWS TEMPERATURE ANALYSIS

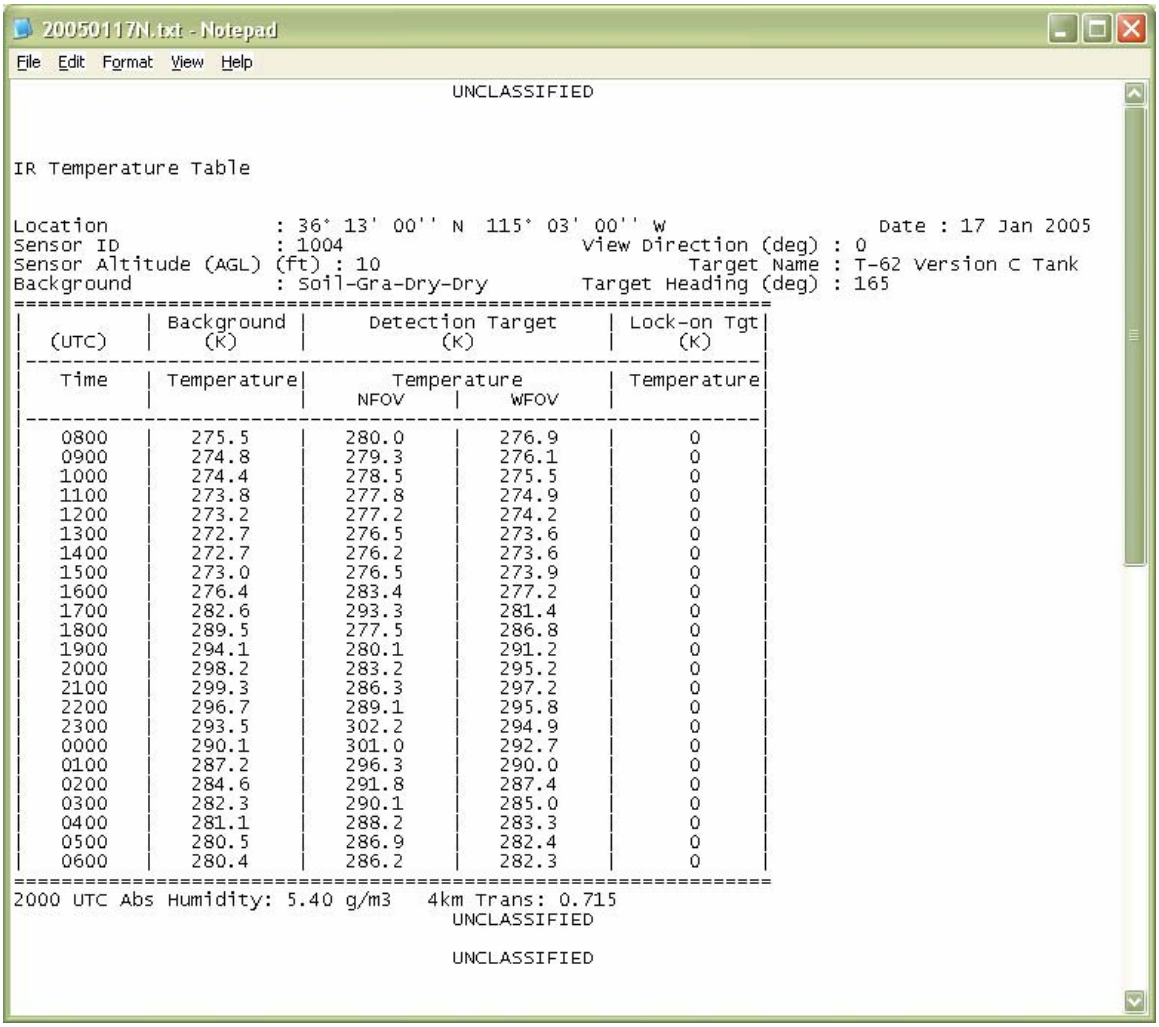

20050117N.txt - Notepad

File Edit Format View Help

UNCLASSIFIED

IR Temperature Table

Location : 36° 13' 00'' N 115° 03' 00'' W Date : 17 Jan 2005
Sensor ID : 1004 View Direction (deg) : 0
Sensor Altitude (AGL) (ft) : 10 Target Name : T-62 Version C Tank
Background : Soil-Gra-Dry-Dry Target Heading (deg) : 165

(UTC)	Background (K)	Detection Target (K)		Lock-on Tgt (K)
Time	Temperature	Temperature NFOV	Temperature WFOV	Temperature
0800	275.5	280.0	276.9	0
0900	274.8	279.3	276.1	0
1000	274.4	278.5	275.5	0
1100	273.8	277.8	274.9	0
1200	273.2	277.2	274.2	0
1300	272.7	276.5	273.6	0
1400	272.7	276.2	273.6	0
1500	273.0	276.5	273.9	0
1600	276.4	283.4	277.2	0
1700	282.6	293.3	281.4	0
1800	289.5	277.5	286.8	0
1900	294.1	280.1	291.2	0
2000	298.2	283.2	295.2	0
2100	299.3	286.3	297.2	0
2200	296.7	289.1	295.8	0
2300	293.5	302.2	294.9	0
0000	290.1	301.0	292.7	0
0100	287.2	296.3	290.0	0
0200	284.6	291.8	287.4	0
0300	282.3	290.1	285.0	0
0400	281.1	288.2	283.3	0
0500	280.5	286.9	282.4	0
0600	280.4	286.2	282.3	0

2000 UTC Abs Humidity: 5.40 g/m3 4km Trans: 0.715

UNCLASSIFIED

UNCLASSIFIED

THIS PAGE INTENTIONALLY LEFT BLANK

APPENDIX C - NELLIS APPROACH PLATE

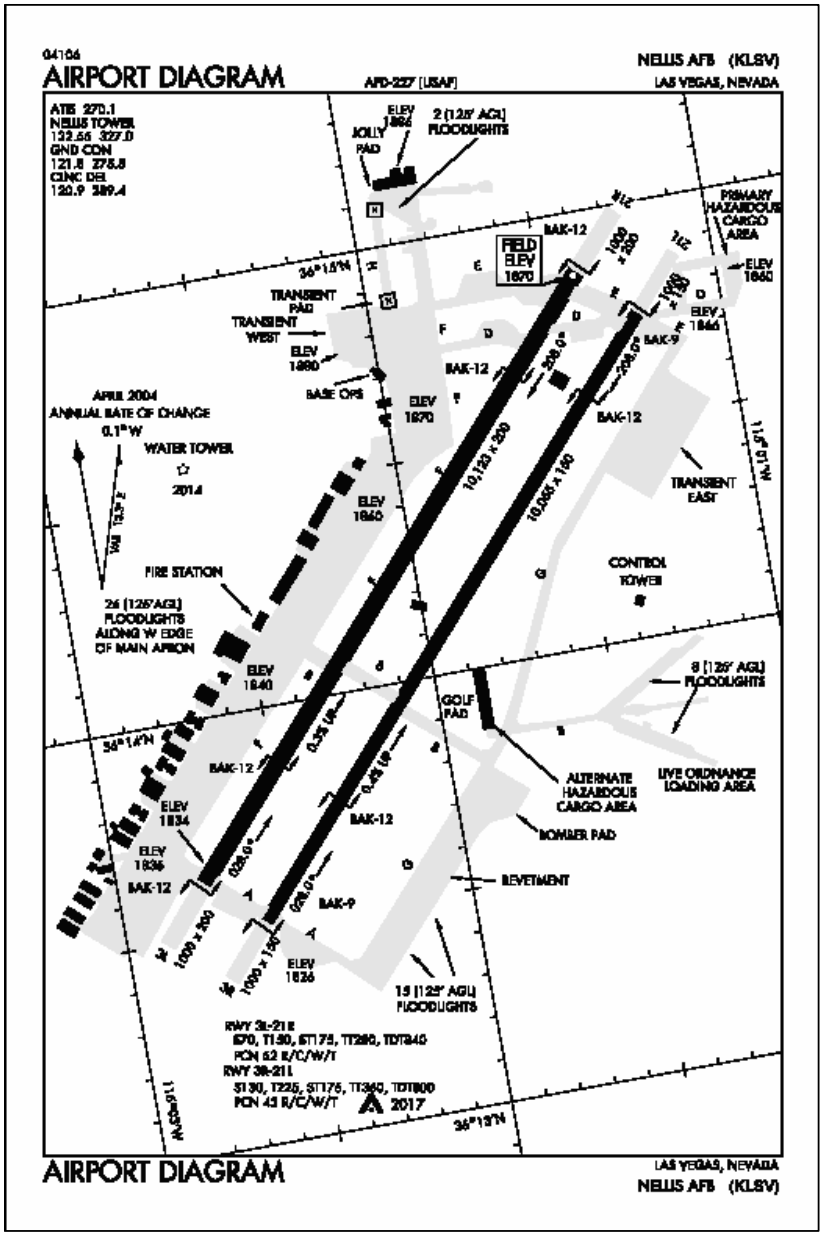

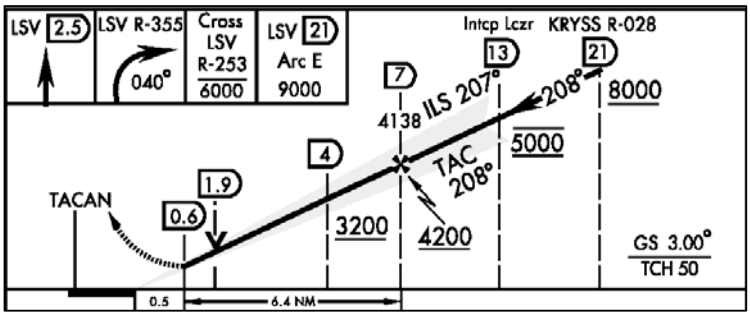

THIS PAGE INTENTIONALLY LEFT BLANK

APPENDIX D - T-62 TANK IMAGES

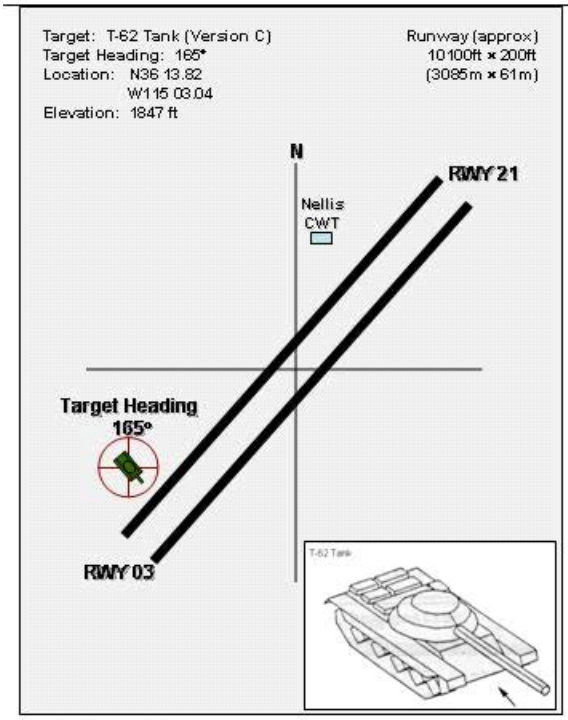

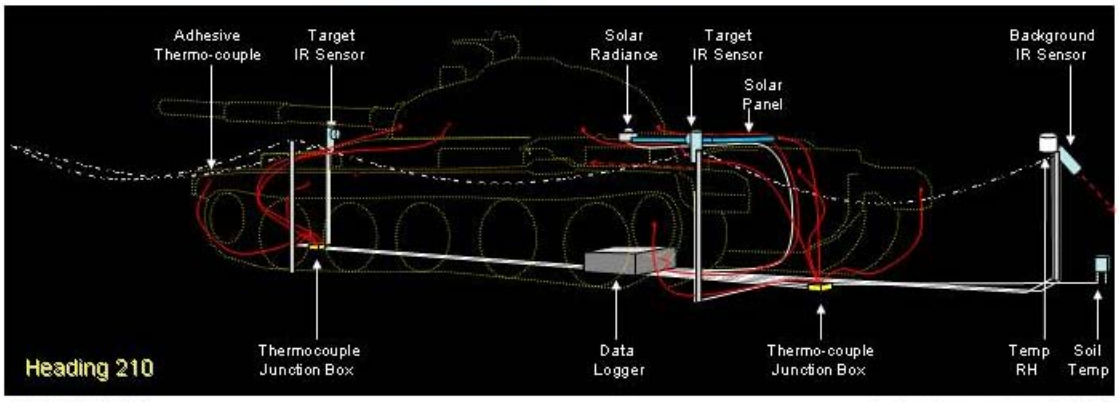

THIS PAGE INTENTIONALLY LEFT BLANK

APPENDIX E - SENSOR INSTALLATION PLAN AND SCHEMATIC

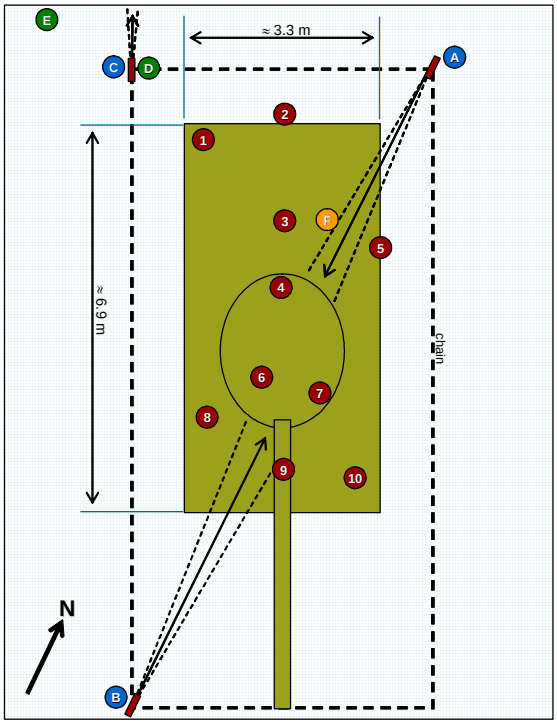

Physical Model – Sensor Configuration 01

Sensor List

A IR Temp, 8-14 μm, 4° FOV , Everest Interscience (Heading 180°, 53 cm AGL, level)

B IR Temp, 8-14 μm, 4° FOV, Everest Interscience (Heading 360°, 55 cm AGL, level)

C IR Temp, 8-14 μm, 3:1FOV, Apogee (Heading 330°, 48 cm AGL, -40°)

D Temp and Relative Humidity

E Soil Temp (≈10 cm below surface)

F Incoming Short Wave

1-10 Adhesive Thermocouples

System Limitations

Narrow IR coverage vs. TAWS sensor model

Custom sensor not configured for IR probes

Produced by Jerome H. Hernandez, Capt, USAF

THIS PAGE INTENTIONALLY LEFT BLANK

APPENDIX F - PART #2 STATISTICAL WORKSHEET, TAWS PREDICTIONS AND HOURLY MEASUREMENTS

17-Jan-05

View Dir 360	Bkgnd			WFOV			NFOV		
	AM Dark	Day	PM Dark	AM Dark	Day	PM Dark	AM Dark	Day	PM Dark
TAWS vs. Measured IR: Chi-test	1.00	1.00	1.00	1.00	1.00	0.99	1.00	0.87	1.00
Correlation	0.65	0.98	0.93	0.98	0.96	0.99	0.99	0.38	0.99
Avg D T (IR)	-1.3	-2.7	1.0	-4.6	-4.1	-5.4	-1.7	-5.5	-0.5
TAWS vs. Measured Thermo: Chi-test				1.00	0.98	1.00	1.00	0.58	1.00
Correlation				0.98	0.93	1.00	0.99	0.22	0.99
Avg D T (Th)				-4.7	-8.0	-3.8	-1.8	-9.4	1.1

View Dir 180	WFOV			NFOV		
	AM Dark	Day	PM Dark	AM Dark	Day	PM Dark
Chi-test	1.00	1.00	1.00	1.00	1.00	1.00
Correlation	0.98	0.82	0.99	0.99	0.55	0.97
Δ T (IP)	-4.3	-1.3	-2.7	-1.6	-5.1	0.6
Chi-test	1.00	1.00	1.00	1.00	1.00	1.00
Correlation	0.99	0.99	0.99	0.99	0.90	0.96
Avg D T (Th)	-3.5	-1.3	-1.9	-0.7	-5.2	1.5

18-Jan-05

View Dir 360	Bkgnd			WFOV			NFOV		
	AM Dark	Day	PM Dark	AM Dark	Day	PM Dark	AM Dark	Day	PM Dark
TAWS vs. Measured IR: Chi-test	1.00	1.00	1.00	1.00	1.00	0.99	1.00	0.99	1.00
Correlation	0.94	0.98	0.95	0.99	0.97	1.00	0.98	0.39	0.97
Avg D T (IR)	2.3	0.0	1.0	-1.8	0.2	-5.1	1.0	-0.8	0.2
TAWS vs. Measured Thermo: Chi-test				1.00	1.00	1.00	1.00	0.92	1.00
Correlation				0.98	0.97	1.00	0.98	0.18	0.99
Avg D T (Th)				-1.8	-2.9	-3.8	1.1	-4.0	1.4

View Dir 180	WFOV			NFOV		
	AM Dark	Day	PM Dark	AM Dark	Day	PM Dark
Chi-test	1.00	1.00	1.00	1.00	1.00	1.00
Correlation	0.99	0.94	0.99	0.97	0.67	1.00
Δ T (IP)	-1.9	0.4	-2.9	0.5	-3.0	1.1
Chi-test	1.00	1.00	1.00	1.00	1.00	1.00
Correlation	0.99	0.98	1.00	0.99	0.90	0.99
Avg D T (Th)	-0.9	-0.1	-2.4	1.5	-3.4	1.7

19-Jan-05

View Dir 360	Bkgnd			WFOV			NFOV		
	AM Dark	Day	PM Dark	AM Dark	Day	PM Dark	AM Dark	Day	PM Dark
TAWS vs. Measured IR: Chi-test	1.00	1.00	1.00	1.00	1.00	0.94	1.00	0.83	1.00
Correlation	0.77	0.98	0.97	0.94	0.97	1.00	0.97	0.24	0.96
Avg D T (IR)	-1.0	-3.8	-0.1	-4.4	-4.4	-7.6	-1.6	-3.1	-1.7
TAWS vs. Measured Thermo: Chi-test				1.00	0.97	0.98	1.00	0.67	1.00
Correlation				0.94	0.95	1.00	0.97	0.19	0.97
Avg D T (Th)				-4.5	-8.3	-5.6	-1.6	-6.9	0.2

View Dir 180	WFOV			NFOV		
	AM Dark	Day	PM Dark	AM Dark	Day	PM Dark
Chi-test	1.00	1.00	0.99	1.00	0.99	1.00
Correlation	0.93	0.64	0.99	0.98	0.26	1.00
Δ T (IP)	-4.3	-2.3	-4.5	-1.7	-6.3	-0.5
Chi-test	1.00	1.00	1.00	1.00	0.99	1.00
Correlation	0.95	0.99	1.00	0.99	0.87	0.99
Avg D T (Th)	-3.5	-2.3	-3.7	-0.9	-6.3	0.3

20-Jan-05

View Dir 360	Bkgnd			WFOV			NFOV		
	AM Dark	Day	PM Dark	AM Dark	Day	PM Dark	AM Dark	Day	PM Dark
TAWS vs. Measured IR: Chi-test	1.00	1.00	1.00	1.00	1.00	0.99	1.00	0.94	1.00
Correlation	0.95	0.96	0.99	1.00	0.99	0.99	1.00	0.18	0.96
Avg D T (IR)	-0.6	-1.7	-1.0	-5.0	-2.7	-5.4	-2.0	-1.4	-0.6
TAWS vs. Measured Thermo: Chi-test				1.00	0.99	0.99	1.00	0.80	1.00
Correlation				0.99	0.88	0.99	1.00	0.15	0.97
Avg D T (Th)				-4.7	-7.1	-4.5	-1.7	-5.8	0.4

View Dir 180	WFOV			NFOV		
	AM Dark	Day	PM Dark	AM Dark	Day	PM Dark
Chi-test	1.00	1.00	1.00	1.00	0.99	1.00
Correlation	0.99	0.84	0.99	1.00	0.50	1.00
Δ T (IP)	-4.3	-2.9	-4.2	-1.6	-6.3	-0.6
Chi-test	1.00	1.00	1.00	1.00	1.00	1.00
Correlation	0.99	0.99	1.00	1.00	0.86	0.99
Avg D T (Th)	-3.4	-1.3	-3.2	-0.7	-4.7	0.4

21-Jan-05

View Dir 360	Bkgnd			WFOV			NFOV		
	AM Dark	Day	PM Dark	AM Dark	Day	PM Dark	AM Dark	Day	PM Dark
TAWS vs. Measured IR: Chi-test	1.00	1.00	1.00	1.00	1.00	0.99	1.00	0.95	1.00
Correlation	0.98	0.96	0.96	0.99	0.98	0.99	0.99	0.31	0.95
Avg D T (IR)	-0.4	-1.4	-0.5	-3.4	-1.8	-5.1	-0.8	-3.3	-0.1
TAWS vs. Measured Thermo: Chi-test				1.00	1.00	1.00	1.00	0.72	1.00
Correlation				0.98	0.90	0.99	0.98	0.09	0.96
Avg D T (Th)				-3.4	-5.4	-4.1	-0.8	-6.9	0.9

View Dir 180	WFOV			NFOV		
	AM Dark	Day	PM Dark	AM Dark	Day	PM Dark
Chi-test	1.00	1.00	1.00	1.00	1.00	1.00
Correlation	0.99	0.90	0.99	0.99	0.69	0.99
Δ T (IP)	-3.4	-0.6	-3.9	-1.1	-4.5	0.0
Chi-test	1.00	1.00	1.00	1.00	1.00	1.00
Correlation	0.99	1.00	1.00	0.99	0.90	0.99
Avg D T (Th)	-2.4	-0.6	-3.0	-0.1	-4.4	1.0

22-Jan-05

View Dir 360	Bkgnd			WFOV			NFOV		
	AM Dark	Day	PM Dark	AM Dark	Day	PM Dark	AM Dark	Day	PM Dark
TAWS vs. Measured IR: Chi-test	1.00	1.00	1.00	1.00	1.00	0.97	1.00	0.86	1.00
Correlation	0.98	0.98	0.99	0.98	0.97	1.00	1.00	0.39	0.97
Avg D T (IR)	-1.3	-2.6	0.6	-4.9	-3.8	-6.6	-1.9	-5.2	-0.7
TAWS vs. Measured Thermo: Chi-test				1.00	0.98	0.99	1.00	0.52	1.00
Correlation				0.98	0.93	1.00	1.00	0.19	0.98
Avg D T (Th)				-4.8	-8.0	-4.6	-1.8	-9.3	1.2

View Dir 180	WFOV			NFOV		
	AM Dark	Day	PM Dark	AM Dark	Day	PM Dark
Chi-test	1.00	1.00	1.00	1.00	0.99	1.00
Correlation	0.99	0.67	0.98	1.00	0.32	0.99
Δ T (IP)	-4.6	-1.8	-3.4	-1.8	-5.8	0.7
Chi-test	1.00	1.00	1.00	1.00	1.00	1.00
Correlation	0.99	0.99	1.00	1.00	0.89	0.99
Avg D T (Th)	-3.8	-1.4	-2.6	-1.0	-5.4	1.5

View Dir 360	Bkgnd			WFOV			NFOV		
	AM Dark	Day	PM Dark	AM Dark	Day	PM Dark	AM Dark	Day	PM Dark
Avg D T (IR)	-0.4	-2.0	0.2	-4.0	-2.8	-5.8	-1.2	-3.2	-0.6
Avg D T (Th)				-4.0	-6.6	-4.4	-1.1	-7.1	0.9

View Dir 180	WFOV			NFOV		
	AM Dark	Day	PM Dark	AM Dark	Day	PM Dark
Δ T (IP)	-3.8	-1.4	-3.6	-1.2	-5.2	0.2
Avg D T (Th)	-2.9	-1.2	-2.8	-0.3	-4.9	1.1

January 2005 TIME	TAWS Heading 360 BKGND	TAWS Heading 360 NFOV	TAWS Heading 360 WFOV	TAWS Heading 180 NFOV	TAWS Heading 180 WFOV	IR Bkgnd TargetCorr 3:1	IR Tank (36 ThumbT_Av 4deg(5707)	IR Tank (18 ThumbT_Av 4deg (5708	Set B (360) thermocoup heading(B)	Set A (180) thermocoup heading(A)	CR5000 RelHum_Av 180	sun	1.9	Background	WFOV 360 IR	WFOV 360 Therm	NFOV 360 IR	NFOV 360 Therm	WFOV 180 IR	WFOV 180 Therm	NFOV 180 IR	NFOV 180 Therm	January 2005 TIME
17/0800	275.5	280.0	276.9	280.0	277.0	275.9	281.9	281.1	281.6	280.2	82.6	220.0		-0.4	-5.0	-4.7	-1.9	-1.6	-4.1	-3.2	-1.1	-0.2	17/0800
0900	274.8	279.3	276.1	279.2	276.3	275.4	281.0	280.4	280.9	279.6	81.0	220.0		-0.6	-4.9	-4.8	-1.7	-1.6	-4.1	-3.3	-1.2	-0.4	0900
1000	274.4	278.5	275.5	278.5	275.7	275.2	280.1	279.8	280.1	278.9	82.8	220.0		-0.8	-4.6	-4.6	-1.6	-1.6	-4.1	-3.2	-1.3	-0.4	1000
1100	273.8	277.8	274.9	277.8	275.0	275.0	279.4	279.3	279.5	278.4	83.1	220.0		-1.2	-4.5	-4.6	-1.6	-1.7	-4.3	-3.4	-1.5	-0.6	1100
1200	273.2	277.2	274.2	277.2	274.4	275.5	279.0	279.2	279.1	278.1	82.6	220.0		-2.3	-4.8	-4.9	-1.8	-1.9	-4.8	-3.7	-2.0	-0.9	1200
1300	272.7	276.5	273.6	276.5	273.8	275.3	278.3	278.6	278.7	277.8	80.7	220.0		-2.6	-4.7	-5.1	-1.8	-2.2	-4.8	-4.0	-2.1	-1.3	1300
1400	272.7	276.2	273.6	276.0	273.6	274.1	277.5	277.9	277.9	277.2	83.7	220.0		-1.4	-3.9	-4.3	-1.3	-1.7	-4.3	-3.6	-1.9	-1.2	1400
1500	273.0	276.5	273.9	276.1	273.9	274.1	277.2	277.7	277.5	277.0	82.4	222.0		-1.1	-3.3	-3.6	-0.7	-1.0	-3.8	-3.1	-1.6	-0.9	1500
1600	276.4	283.4	277.2	279.7	275.7	276.9	279.4	282.8	282.8	278.1	70.8	222.0		-0.5	-2.2	-5.6	4.0	0.6	-7.1	-2.4	-3.1	1.6	1600
1700	282.6	293.3	281.4	275.9	280.1	281.1	283.5	287.5	292.1	280.3	55.3	222.0		1.5	-2.1	-10.7	9.8	1.2	-7.4	-0.2	-11.6	-4.4	1700
1800	289.5	277.5	286.8	277.9	284.5	293.8	290.6	289.5	299.7	285.0	43.2	222.0		-4.3	-3.8	-12.9	-13.1	-22.2	-5.0	-0.5	-11.6	-7.1	1800
1900	294.1	280.1	291.2	280.6	288.0	301.1	297.0	290.0	304.8	288.8	36.4	222.0		-7.0	-5.8	-13.6	-16.9	-24.7	-2.0	-0.8	-9.4	-8.2	1900
2000	298.2	283.2	295.2	283.7	291.2	301.9	300.3	288.4	302.5	291.5	31.6	222.0		-3.7	-5.1	-7.3	-17.1	-19.3	2.8	-0.3	-4.7	-7.8	2000
2100	299.3	286.3	297.2	286.2	292.9	303.2	296.9	290.2	307.1	293.8	30.1	222.0		-3.9	0.3	-9.9	-10.6	-20.8	2.7	-0.9	-4.0	-7.6	2100
2200	296.7	289.1	295.8	287.0	292.7	302.2	306.4	288.7	302.7	294.5	27.5	222.0		-5.5	-10.6	-6.9	-17.3	-13.6	4.0	-1.8	-1.7	-7.5	2200
2300	293.5	302.2	294.9	287.3	291.7	294.4	299.4	287.9	300.5	292.9	28.6	222.0		-0.9	-4.5	-5.6	2.8	1.7	3.8	-1.2	-0.6	-5.6	2300
18/0000	290.1	301.0	292.7	287.4	289.6	292.2	297.1	290.4	296.4	291.7	26.8	222.0		-2.1	-4.4	-3.7	3.9	4.6	-0.8	-2.1	-3.0	-4.3	18/0000
0100	287.2	296.3	290.0	291.0	288.5	285.4	295.5	289.5	293.1	289.5	35.7	220.0		1.8	-5.4	-3.1	0.9	3.2	-1.0	-1.0	1.5	1.5	0100
0200	284.6	291.8	287.4	289.8	286.6	282.5	292.9	288.8	290.6	287.8	45.5	220.0		2.1	-5.5	-3.2	-1.1	1.2	-2.2	-1.2	1.0	2.0	0200
0300	282.3	290.1	285.0	288.5	284.7	281.5	290.8	287.6	289.0	286.5	56.9	220.0		0.9	-5.8	-4.0	-0.7	1.1	-2.9	-1.8	0.9	2.0	0300
0400	281.1	288.2	283.3	287.1	283.2	280.0	289.1	286.4	287.4	285.4	59.8	220.0		1.1	-5.8	-4.1	-0.9	0.8	-3.2	-2.2	0.7	1.7	0400
0500	280.5	286.9	282.4	285.9	282.4	279.1	287.8	285.7	286.3	284.5	59.2	220.0		1.4	-5.4	-3.9	-0.9	0.6	-3.3	-2.1	0.2	1.4	0500
0600	280.4	286.2	282.3	285.3	282.3	281.3	286.8	286.2	286.6	285.1	55.2	220.0		-0.9	-4.5	-4.3	-0.6	-0.4	-3.9	-2.8	-0.9	0.2	0600
18/0800	281.9	285.8	282.9	284.7	282.9	280.1	285.7	285.6	285.4	283.8	47.7	220.0		1.8	-2.8	-2.5	0.1	0.4	-2.7	-0.9	-0.9	0.9	18/0800
0900	281.2	285.3	282.2	284.4	282.2	278.1	284.1	284.0	283.6	282.6	60.6	220.0		3.1	-1.9	-1.4	1.2	1.7	-1.8	-0.4	0.4	1.8	0900
1000	280.5	284.3	281.3	283.7	281.4	278.2	283.1	283.3	283.1	282.4	61.2	220.0		2.3	-1.8	-1.8	1.2	1.2	-1.9	-1.0	0.4	1.3	1000
1100	279.5	283.2	280.4	282.9	280.4	277.2	282.0	282.2	281.9	281.4	69.7	220.0		2.3	-1.6	-1.5	1.2	1.3	-1.8	-1.0	0.7	1.5	1100
1200	278.6	282.2	279.5	282.1	279.5	275.8	280.9	280.9	280.9	280.3	77.1	220.0		2.8	-1.4	-1.4	1.3	1.3	-1.4	-0.8	1.2	1.8	1200
1300	277.7	281.2	278.5	281.2	278.6	275.4	280.1	280.2	280.3	279.6	79.8	220.0		2.3	-1.6	-1.8	1.1	0.9	-1.6	-1.0	1.0	1.6	1300
1400	277.1	280.5	277.9	280.5	277.9	275.8	279.6	279.9	279.9	279.1	77.8	220.0		1.3	-1.7	-2.0	0.9	0.6	-2.0	-1.2	0.6	1.4	1400
1500	276.4	280.2	277.4	280.2	277.5	275.1	279.0	279.5	279.3	278.7	77.9	222.0		1.3	-1.6	-1.9	1.2	0.9	-2.0	-1.2	0.7	1.5	1500
1600	279.4	286.2	280.3	282.5	278.8	278.4	280.4	282.6	282.3	279.9	71.0	222.0		1.0	-0.1	-2.0	5.8	3.9	-3.8	-1.1	-0.1	2.6	1600
1700	284.7	293.8	283.6	279.2	282.6	281.2	281.9	284.3	285.5	281.3	68.1	222.0		3.5	1.7	-1.8	11.9	8.4	-1.7	1.3	-5.1	-2.1	1700
1800	290.7	280.4	288.3	280.7	286.2	288.9	285.6	287.8	291.2	284.4	57.7	222.0		1.8	2.7	-2.9	-5.2	-10.8	-1.6	1.8	-7.1	-3.7	1800
1900	295.8	282.5	292.5	282.8	289.4	299.5	292.8	289.9	299.8	288.7	40.7	222.0		-3.7	-0.3	-7.3	-10.3	-17.3	-0.5	0.7	-7.1	-5.9	1900
2000	298.9	284.9	295.5	285.2	291.8	302.0	296.1	290.1	300.4	291.7	35.0	222.0		-3.1	-0.6	-4.9	-11.2	-15.5	1.7	0.1	-4.9	-6.5	2000
2100	299.8	287.4	297.1	287.4	293.2	300.7	293.9	289.5	301.3	293.3	35.7	222.0		-0.9	3.3	-4.2	-6.4	-13.9	3.7	-0.1	-2.1	-5.9	2100
2200	298.6	289.6	297.1	287.8	293.3	299.1	298.4	289.0	298.9	293.7	34.8	222.0		-0.5	-1.3	-1.8	-8.8	-9.3	4.3	-0.4	-1.2	-5.9	2200
2300	294.9	302.6	295.9	287.9	291.9	293.5	295.7	288.4	296.8	292.4	36.1	222.0		1.4	0.2	-0.9	6.9	5.8	3.5	-0.5	-0.5	-4.5	2300
19/0000	290.0	301.6	292.1	286.9	289.3	290.4	293.9	289.4	293.7	290.5	35.7	222.0		-0.4	-1.8	-1.6	7.7	7.9	-0.1	-1.2	-2.5	-3.6	19/0000
0100	285.3	296.5	288.3	290.2	286.7	284.2	292.3	287.7	290.7	288.2	43.7	220.0		1.1	-4.0	-2.4	4.2	5.8	-1.0	-1.5	2.5	2.0	0100
0200	282.8	289.9	285.4	288.7	284.6	280.5	290.2	286.9	288.4	286.3	52.4	220.0		2.3	-4.8	-3.0	-0.3	1.5	-2.2	-1.7	1.9	2.4	0200
0300	281.0	288.0	283.2	287.2	282.9	279.1	288.3	285.7	286.7	284.9	67.7	220.0		1.9	-5.1	-3.5	-0.3	1.3	-2.8	-2.0	1.6	2.3	0300
0400	279.2	286.1	281.1	285.6	281.1	278.3	286.7	284.7	285.5	283.8	71.5	220.0		0.9	-5.6	-4.4	-0.6	0.6	-3.6	-2.7	0.9	1.8	0400
0500	278.1	284.5	279.8	284.1	279.9	278.0	285.5	283.9	284.6	283.0	75.1	220.0		0.1	-5.7	-4.8	-1.0	-0.1	-3.9	-3.1	0.3	1.1	0500
0600	277.6	283.2	279.0	282.9	279.1	277.8	284.3	283.1	283.7	282.2	74.2	220.0		-0.2	-5.3	-4.7	-1.1	-0.5	-4.0	-3.1	-0.2	0.7	0600
19/0800	276.3	280.4	277.5	280.2	277.6	276.7	282.3	281.7	282.0	280.8	73.2	220.0		-0.4	-4.8	-4.5	-1.9	-1.6	-4.1	-3.2	-1.5	-0.6	19/0800
0900	275.4	279.6	276.6	279.5	276.8	275.7	281.3	280.9	281.2	280.1	75.2	220.0		-0.3	-4.7	-4.6	-1.7	-1.6	-4.1	-3.3	-1.4	-0.6	0900
1000	274.6	278.8	275.8	278.8	275.9	275.5	280.8	280.5	280.6	279.6	77.0	220.0		-0.9	-5.0	-4.8	-2.0	-1.8	-4.6	-3.7	-1.7	-0.8	1000
1100	274.2	278.2	275.3	278.2	275.4	275.5	279.9	279.9	280.1	279.2	79.3	220.0		-1.3	-4.6	-4.8	-1.7	-1.9	-4.5	-3.8	-1.7	-1.0	1100
1200	274.0	277.8	275.0	277.7	275.1	275.8	279.6	279.8	279.6	278.9	74.4	220.0		-1.8	-4.6	-4.6	-1.8	-1.8	-4.7	-3.8	-2.1	-1.2	1200
1300	274.0	277.6	274.9	277.3	275.0	275.6	279.0	279.3	279.1	278.5	74.2	220.0		-1.6	-4.1	-4.2	-1.4	-1.5	-4.3	-3.5	-2.0	-1.2	1300
1400	274.1	277.5	275.0	277.1	275.0	274.7	278.3	278.6	278.6	278.0	78.7	220.0		-0.6	-3.3	-3.6	-0.8	-1.1	-3.6	-3.0	-1.5	-0.9	1400
1500	274.3	277.9	275.2	277.3	275.2	275.9	278.3	278.8	278.6	278.1	73.3	222.0		-1.6	-3.1	-3.4	-0.4	-0.7	-3.6	-2.9	-1.5	-0.8	1500
1600	277.3	285.2	278.4	280.8	276.6	278.1	280.7	284.5	283.7	279.4	65.8	222.0		-0.8	-2.3	-5.3	4.5	1.5	-7.9	-2.8	-3.7	1.4	1600
1700	283.1	294.4	282.1	276.6	280.7	282.1	284.3	290.0	292.5	281.7	53.9	222.0		1.0	-2.2	-10.4	10.1	1.9	-9.3	-1.0	-13.4	-5.1	1700
1800	289.4	301.5	287.0	278.3	284.6	293.9	289.6	292.4	297.9	285.5	45.9	222.0		-4.5	-2.6	-10.9	11.9	3.6	-7.7	-0.9	-14.1	-7.2	1800
1900	294.7	280.2	291.3	280.6	287.8	302.3	296.3	291.9	304.5	289.8	33.3	222.0		-7.6	-5.0	-13.2	-16.1	-24.3	-4.1	-2.0	-11.3	-9.2	1900
2000	298.3	282.9	294.7	283.3	290.5	306.4	301.5	290.5	305.6	293.0	31.3	222.0		-8.1	-6.8	-10.9	-18.6	-22.7	0.0	-2.5	-7.2	-9.7	2000
2100	299.7	285.9	296.8	285.8	292.3	306.5	298.4	290.0	308.2	294.9	28.4	222.0		-6.8	-1.6	-11.4	-12.5	-22.3	2.3	-2.6	-4.2	-9.1	2100
2200	299.0	288.7	297.5	286.5	293.0	304.0	307.8	288.8	304.0	295.6	27.0	222.0		-5.0	-10.3	-6.5	-19.1	-15.3	4.2	-2.6	-2.3	-9.1	2200
2300	295.3	304.4	296.0	286.7	291.9	296.1	300.8	287.2	301.9	294.5	28.4	222.0		-0.8	-4.8	-5.9	3.6	2.5	4.7	-2.6	-0.5	-7.8	2300
20/0000	290.2	304.5	292.9	286.6	289.6	293.7	298.6	291.2	297.9	292.8	26.0	222.0		-3.5	-5.6	-5.0	6.0	6.6	-1.6	-3.2	-4.6	-6.2	20/0000
0100	285.7	299.7	289.3	290.8	287.2	286.3	296.8	290.2	294.2	290.4	36.1	220.0		-0.6	-7.5	-4.9	2.9	5.5	-3.0	-3.2	0.6	0.4	0100
0200	283.5	292.3	286.6	289.4	285.5	282.8	294.2	289.5	291.6	288.6	48.8	220.0		0.7	-7.6	-5.0	-1.9	0.7	-4.0	-3.1	-0.1	0.8	0200
0300	281.9	289.3	284.6	288.1	284.0	281.2	292.3	288.4	290.2	287.3	55.8	220.0		0.7	-7.7	-5.6	-3.0	-0.9	-4.4	-3.3	-0.3	0.8	0300
0400	280.2	287.7	282.7	286.6	282.4	280.6	290.5	287.5	288.8	286.4	62.6	220.0		-0.4	-7.8	-6.1	-2.8	-1.1	-5.1	-4.0	-0.9	0.2	0400
0500	279.2	286.2	281.3	285.4	281.3	279.9	288.9	286.5	287.5	285.4	64.8	220.0		-0.7	-7.6	-6.2	-2.7	-1.3	-5.2	-4.1	-1.1	0.0	0500
0600	278.4	284.9	280.4	284.2	280.4	279.0	287.6	285.6	286.4	284.6	69.4	220.0		-0.6	-7.2	-6.0	-2.7	-1.5	-5.2	-4.2	-1.4	-0.4	0600

20/0800	277.2	281.8	278.6	281.8	278.8	278.0	285.2	283.9	284.4	283.0	75.3	220.0	-0.8	-6.6	-5.8	-3.4	-2.6	-5.1	-4.2	-2.1	-1.2	20/0800
0900	276.8	281.3	278.2	281.2	278.3	277.8	284.3	283.2	283.6	282.3	78.1	220.0	-1.0	-6.1	-5.4	-2.9	-2.3	-4.9	-4.0	-2.0	-1.1	0900
1000	276.4	280.8	277.7	280.7	277.9	277.2	283.1	282.4	282.7	281.5	82.3	220.0	-0.8	-5.4	-5.0	-2.3	-1.9	-4.5	-3.6	-1.7	-0.8	1000
1100	276.1	280.4	277.4	280.2	277.5	276.8	282.4	281.8	282.1	280.9	79.8	220.0	-0.7	-4.9	-4.7	-1.9	-1.7	-4.3	-3.4	-1.6	-0.7	1100
1200	275.9	280.1	277.1	279.8	277.2	276.8	281.7	281.4	281.5	280.4	82.8	220.0	-0.9	-4.6	-4.4	-1.6	-1.4	-4.1	-3.2	-1.5	-0.6	1200
1300	275.8	279.7	276.9	279.4	277.0	276.0	280.7	280.5	280.8	279.8	85.8	220.0	-0.2	-3.8	-3.9	-1.0	-1.1	-3.5	-2.8	-1.1	-0.4	1300
1400	275.7	279.5	276.7	279.1	276.8	275.8	280.2	280.2	280.2	279.3	81.9	220.0	-0.1	-3.5	-3.5	-0.7	-0.7	-3.4	-2.5	-1.1	-0.2	1400
1500	275.7	279.6	276.8	279.1	276.8	276.1	279.7	279.8	280.0	279.0	84.7	222.0	-0.4	-2.9	-3.2	-0.1	-0.4	-3.0	-2.2	-0.7	0.1	1500
1600	278.6	287.0	279.4	282.2	277.9	278.6	281.8	284.9	284.7	280.0	72.5	222.0	0.0	-2.4	-5.3	5.2	2.3	-7.0	-2.1	-2.7	2.2	1600
1700	284.4	295.6	283.4	278.3	282.1	282.6	285.1	290.2	294.2	282.2	56.8	222.0	1.8	-1.7	-10.8	10.5	1.4	-8.1	-0.1	-11.9	-3.9	1700
1800	290.8	302.6	288.3	280.0	286.0	294.7	291.2	292.5	300.5	286.4	55.8	222.0	-3.9	-2.9	-12.2	11.4	2.1	-6.5	-0.3	-12.5	-6.3	1800
1900	296.1	281.8	292.6	282.2	289.2	302.8	297.6	293.8	305.4	290.2	41.2	222.0	-6.7	-5.0	-12.8	-15.8	-23.6	-4.6	-1.0	-11.6	-8.0	1900
2000	299.6	284.5	295.9	284.9	291.9	304.0	300.2	292.3	305.1	292.9	35.9	222.0	-4.4	-4.3	-9.2	-15.7	-20.6	-0.4	-1.0	-7.4	-8.0	2000
2100	299.8	287.3	297.4	287.4	293.2	305.4	299.0	290.7	307.1	295.2	33.4	222.0	-5.6	-1.6	-9.7	-11.7	-19.8	2.5	-2.0	-3.3	-7.8	2100
2200	297.8	290.1	297.1	288.2	293.4	295.5	298.8	292.6	299.5	293.4	33.9	222.0	2.4	-1.7	-2.4	-8.7	-9.4	0.8	0.0	-4.4	-5.2	2200
2300	295.0	302.4	295.8	288.5	292.5	294.3	297.8	293.2	298.3	293.9	35.7	222.0	0.7	-2.0	-2.5	4.6	4.1	-0.7	-1.4	-4.7	-5.4	2300
21/0000	291.1	302.2	293.3	288.3	290.3	292.3	296.1	292.4	296.1	292.9	38.3	222.0	-1.2	-2.8	-2.8	6.1	6.1	-2.1	-2.6	-4.1	-4.6	21/0000
0100	286.8	297.8	289.9	291.4	288.2	286.1	293.8	291.0	292.7	290.3	47.2	220.0	0.7	-3.9	-2.8	4.0	5.1	-2.8	-2.1	0.4	1.1	0100
0200	284.6	291.7	287.3	290.1	286.4	284.9	292.5	290.3	291.3	289.2	57.3	220.0	-0.3	-5.2	-4.0	-0.8	0.4	-3.9	-2.8	-0.1	0.9	0200
0300	283.1	289.8	285.4	288.8	285.0	283.9	290.9	289.1	289.8	288.0	64.4	220.0	-0.8	-5.5	-4.4	-1.1	0.0	-4.1	-3.0	-0.3	0.8	0300
0400	281.7	288.2	283.7	287.5	283.6	283.2	289.7	288.2	288.9	287.1	69.4	220.0	-1.5	-6.0	-5.2	-1.5	-0.7	-4.6	-3.5	-0.7	0.4	0400
0500	281.0	286.9	282.7	286.4	282.7	283.2	288.8	287.8	288.1	286.6	71.6	220.0	-2.2	-6.1	-5.4	-1.9	-1.2	-5.1	-3.9	-1.4	-0.2	0500
0600	280.7	285.9	282.2	285.4	282.2	282.4	288.0	287.1	287.4	286.0	72.9	220.0	-1.7	-5.8	-5.2	-2.1	-1.5	-4.8	-3.8	-1.6	-0.6	0600
21/0800	280.0	283.6	281.1	283.3	281.1	280.5	285.5	285.2	285.0	284.1	79.4	220.0	-0.5	-4.4	-3.9	-1.9	-1.4	-4.1	-2.9	-1.9	-0.7	21/0800
0900	279.7	283.3	280.7	283.0	280.8	280.8	285.2	285.0	285.0	283.7	74.5	220.0	-1.1	-4.5	-4.3	-1.9	-1.7	-4.2	-2.9	-2.0	-0.7	0900
1000	279.3	283.0	280.4	282.7	280.5	280.1	284.0	284.1	284.1	283.1	78.8	220.0	-0.8	-3.6	-3.7	-1.0	-1.1	-3.6	-2.6	-1.4	-0.4	1000
1100	278.9	282.6	280.0	282.3	280.1	279.5	283.3	283.3	283.2	282.4	79.0	220.0	-0.6	-3.3	-3.2	-0.6	-0.6	-3.2	-2.3	-1.0	-0.1	1100
1200	278.4	282.1	279.5	281.9	279.6	278.4	282.3	282.5	282.3	281.6	84.6	220.0	0.0	-2.8	-2.8	-0.2	-0.2	-2.9	-2.0	-0.6	0.3	1200
1300	277.9	281.5	278.9	281.4	279.0	277.7	281.6	281.8	281.8	281.0	84.0	220.0	0.2	-2.7	-2.9	-0.1	-0.3	-2.8	-2.0	-0.4	0.4	1300
1400	277.4	281.0	278.4	280.9	278.5	277.4	281.0	281.3	281.2	280.5	82.2	220.0	0.0	-2.6	-2.8	0.0	-0.2	-2.8	-2.0	-0.4	0.4	1400
1500	277.2	280.6	278.1	280.6	278.2	277.7	280.4	281.0	280.8	280.2	83.2	222.0	-0.5	-2.3	-2.7	0.2	-0.2	-2.8	-2.0	-0.4	0.4	1500
1600	279.4	285.1	280.2	281.9	279.9	279.1	281.3	283.2	283.1	280.6	80.9	222.0	0.3	-1.1	-2.9	3.8	2.0	-3.3	-0.7	-1.3	1.3	1600
1700	285.0	293.6	283.7	279.6	282.7	283.9	284.7	288.0	290.2	283.2	65.8	222.0	1.1	-1.0	-6.5	8.9	3.4	-5.3	-0.5	-8.4	-3.6	1700
1800	291.6	280.9	288.9	281.3	286.9	296.7	291.7	291.1	300.5	287.4	51.1	222.0	-5.1	-2.8	-11.6	-10.8	-19.6	-4.2	-0.5	-9.8	-6.1	1800
1900	297.3	283.1	293.7	283.6	290.6	302.4	297.9	290.4	304.3	290.5	45.5	222.0	-5.1	-4.2	-10.6	-14.8	-21.2	0.2	0.1	-6.8	-6.9	1900
2000	300.8	285.8	297.1	286.2	293.3	305.9	301.7	291.4	305.6	293.4	38.0	222.0	-5.1	-4.6	-8.5	-15.9	-19.8	1.9	-0.1	-5.2	-7.2	2000
2100	301.8	288.5	299.0	288.4	294.8	305.4	298.8	290.5	307.0	295.0	36.8	222.0	-3.6	0.3	-8.0	-10.3	-18.5	4.3	-0.2	-2.1	-6.6	2100
2200	300.8	291.0	299.2	289.1	295.2	298.9	299.7	292.1	300.7	294.9	37.0	222.0	2.0	-0.5	-1.5	-8.7	-9.7	3.1	0.3	-3.0	-5.8	2200
2300	296.8	304.5	297.8	289.1	293.7	295.3	297.7	292.7	298.6	294.4	38.4	222.0	1.5	0.1	-0.8	6.8	5.9	1.0	-0.7	-3.6	-5.3	2300
22/0000	291.3	303.3	293.5	288.1	290.7	290.4	295.6	292.1	295.0	292.2	42.6	222.0	0.9	-2.1	-1.5	7.7	8.3	-1.4	-1.5	-4.0	-4.1	22/0000
0100	286.2	297.6	289.3	291.5	287.7	286.8	293.5	290.8	292.3	290.2	57.1	222.0	-0.6	-4.2	-3.0	4.1	5.3	-3.1	-2.5	0.7	1.3	0100
0200	284.1	291.1	286.6	290.0	285.8	285.0	291.7	289.7	290.6	288.7	62.4	220.0	-0.9	-5.1	-4.0	-0.6	0.5	-3.8	-2.9	0.4	1.3	0200
0300	282.8	289.4	284.8	288.7	284.5	283.3	290.4	288.7	289.3	287.5	64.0	220.0	-0.5	-5.6	-4.5	-1.0	0.1	-4.1	-3.0	0.1	1.2	0300
0400	281.5	287.8	283.3	287.3	283.2	280.9	288.5	287.1	287.6	286.1	69.9	220.0	0.6	-5.2	-4.3	-0.7	0.2	-3.9	-2.9	0.2	1.2	0400
0500	280.5	286.4	282.2	286.0	282.2	280.5	287.4	286.2	286.5	285.2	73.6	220.0	0.0	-5.2	-4.3	-1.0	-0.1	-4.0	-3.0	-0.2	0.8	0500
0600	279.9	285.3	281.4	285.0	281.4	281.4	286.6	286.0	286.0	284.9	68.5	220.0	-1.5	-5.2	-4.6	-1.3	-0.7	-4.6	-3.5	-1.0	0.1	0600
22/0800	277.6	282.2	279.1	282.0	279.2	279.2	284.4	283.9	284.0	282.9	73.5	220.0	-1.6	-5.3	-4.9	-2.2	-1.8	-4.7	-3.7	-1.9	-0.9	22/0800
0900	276.7	281.3	278.1	281.2	278.3	278.1	283.3	282.9	283.0	282.1	81.2	220.0	-1.4	-5.2	-4.9	-2.0	-1.7	-4.6	-3.8	-1.7	-0.9	0900
1000	275.5	280.3	277.0	280.3	277.2	277.2	282.4	282.1	282.3	281.3	84.2	220.0	-1.7	-5.4	-5.3	-2.1	-2.0	-4.9	-4.1	-1.8	-1.0	1000
1100	275.1	279.5	276.3	279.5	276.5	276.7	281.4	281.3	281.5	280.6	85.7	220.0	-1.6	-5.1	-5.2	-1.9	-2.0	-4.8	-4.1	-1.8	-1.1	1100
1200	274.8	278.8	275.8	278.8	276.0	275.9	280.6	280.7	280.7	279.9	85.4	220.0	-1.1	-4.8	-4.9	-1.8	-1.9	-4.7	-3.9	-1.9	-1.1	1200
1300	274.7	278.2	275.6	278.2	275.7	275.5	280.0	280.1	280.0	279.4	86.1	220.0	-0.8	-4.4	-4.4	-1.8	-1.8	-4.4	-3.7	-1.9	-1.2	1300
1400	274.3	277.8	275.2	277.7	275.2	275.1	279.1	279.4	279.4	278.6	87.3	220.0	-0.8	-3.9	-4.2	-1.3	-1.6	-4.2	-3.4	-1.7	-0.9	1400
1500	274.0	277.6	274.9	277.5	274.9	274.8	278.6	279.0	278.8	278.2	87.6	222.0	-0.8	-3.7	-3.9	-1.0	-1.2	-4.1	-3.3	-1.5	-0.7	1500
1600	276.7	283.4	277.6	280.5	276.1	277.2	280.7	284.7	284.1	279.0	73.3	222.0	-0.5	-3.1	-6.5	2.7	-0.7	-8.6	-2.9	-4.2	1.5	1600
1700	283.0	294.0	281.7	276.6	280.4	282.1	284.5	289.3	292.5	281.4	61.0	222.0	1.0	-2.8	-10.8	9.5	1.5	-8.9	-1.0	-12.7	-4.8	1700
1800	290.1	278.1	287.2	278.5	284.8	294.4	290.3	292.2	300.0	285.3	50.2	222.0	-4.3	-3.1	-12.8	-12.2	-21.9	-7.4	-0.5	-13.7	-6.8	1800
1900	296.3	280.8	292.5	281.2	289.0	302.3	297.0	292.7	305.0	289.6	34.7	222.0	-6.0	-4.5	-12.5	-16.2	-24.2	-3.7	-0.6	-11.5	-8.4	1900
2000	299.8	283.7	296.1	284.2	292.0	304.5	300.1	290.6	305.4	292.7	31.4	222.0	-4.7	-4.0	-9.3	-16.4	-21.7	1.4	-0.7	-6.4	-8.5	2000
2100	301.0	286.8	298.2	286.9	293.8	306.9	298.9	290.1	308.7	295.5	26.6	222.0	-5.9	-0.7	-10.5	-12.1	-21.9	3.7	-1.7	-3.2	-8.6	2100
2200	299.6	289.6	298.3	287.7	294.1	303.6	307.9	289.0	304.0	295.5	25.7	222.0	-4.0	-9.6	-5.7	-18.3	-14.4	5.1	-1.4	-1.3	-7.8	2200
2300	296.3	304.9	296.9	287.9	293.1	295.3	299.9	288.1	301.3	293.9	27.7	222.0	1.0	-3.0	-4.4	5.0	3.6	5.1	-0.8	-0.1	-6.0	2300
23/0000	291.3	304.9	293.9	287.8	290.8	292.9	297.9	290.9	297.2	292.1	27.4	222.0	-1.6	-4.0	-3.3	7.0	7.7	-0.1	-1.3	-3.1	-4.3	23/0000
0100	286.6	300.0	290.2	291.5	288.2	285.7	296.2	289.4	293.7	289.7	34.5	220.0	1.0	-6.0	-3.5	3.8	6.3	-1.2	-1.5	2.1	1.8	0100
0200	284.2	292.8	287.3	290.2	286.3	283.0	293.6	289.0	291.2	288.2	52.1	220.0	1.2	-6.3	-3.9	-0.8	1.6	-2.7	-1.9	1.2	2.0	0200
0300	282.3	290.0	285.0	288.8	284.5	281.7	291.7	288.1	289.5	287.0	53.3	220.0	0.6	-6.7	-4.5	-1.7	0.5	-3.6	-2.5	0.7	1.8	0300
0400	280.5	288.0	282.9	287.2	282.7	279.8	289.7	286.7	288.0	285.6	67.7	220.0	0.7	-6.8	-5.1	-1.7	0.0	-4.0	-2.9	0.5	1.6	0400
0500	279.2	286.3	281.3	285.7	281.3	278.6	288.1	285.6	286.6	284.5	68.5	220.0	0.6	-6.8	-5.3	-1.8	-0.3	-4.2	-3.2	0.2	1.2	0500
0600	278.3	284.8	280.1	284.4	280.2	278.6	286.9	284.8	285.7	283.8	70.6	220.0	-0.3	-6.8	-5.6	-2.1	-0.9	-4.6	-3.6	-0.4	0.6	0600

THIS PAGE INTENTIONALLY LEFT BLANK

APPENDIX G – STUDY LIMITATIONS

Limiting factors (limfac) in this field study consist of those inherent in the experiment design and those particular to the systems and location used in the collection. The following list is a full disclosure of considered study assumptions, mitigating factors and study limitations.

A. PART #1 DETECTION RANGE COLLECTION

1. Assumption A: Aircraft Targeting System Ranges are "Truth"

Aircraft targeting and navigation systems have varying levels of wear to the protective windscreen of their sensor optical casing. Presumably, an optical wind screen exposed to sand scouring can reduce IR energy transmission to the sensor. Varying degrees of WSO experience could also impact detection ranges. These potential limfacs were mitigated by using a single aircraft targeting system and WSO for the duration of the study.

2. Assumption B: KLSV Weather Most Representative of Target Conditions

KLSV wind sensors are located on each end of the runway. The temperature sensor is located at the mid point of the runway length. When 210 is the active runway, the active wind recorder is approximately 2 nm from the target location. The nearest upper air sounding came from Desert Rock NV (elevation 3314ft), approximately 60 nm from KLSV. Careful interrogation of KLSV and KLAS METAR observations helped ensure target weather was the most representative for the TOT. Similarly, KDRA and Eta upper air analysis products were compared to determine best SLH value. Flight levels below the SLH also mitigated the impact of the spatially separated upper air site.

3. Limfac A: Trees in Target Scene

Most likely, tree spacing and foliage separation allowed for complete transmission of the IR signature of the tank. However, the foliage could impact the background temperature as determined by an incoming aircraft. Depending on the time of the day, the leaves could cool or warm the background. As a result, the thermal contrast could be impacted. Neighboring asphalt and concrete backgrounds included in the periphery of the target scene could mitigate the impact of the smaller area of leaves.

4. Limfac B: Background not Specifically Modeled in TAWS

The thick pumice stone top layer of the target background is not modeled in TAWS. The sandy loam foundation layer was available in TAWS, but was too far below the top layer to be the dominant background. The rocky field in TAWS was not appropriate as it describes a scene with high quartz content. The soil-gravel background was used in all TAWS analysis for this study.

5. Limfac C: Descending Aircraft Flight Level

TAWS calculations are determined for a single flight level. The final approach to KLSV requires a descending flight path to the active end of the runway. The average descent between WFOV MDT detection and NFOV MRT detection was approximately 700 ft. The impact of this limfac was minimized since the flight level difference was small and both levels were below the SLH.

6 Limfac D: Sample Size and Weather Variability

Weather conditions were highly variable for the sample period and 16 samples were collected. Considering the lack of homogeneity in weather, more collections would have provided more reliable statistics. CWTs replicating this experiment should strive to collect more samples.

7. Limfac E: Range Determination from Graphical Product

The detection range part of this study focused on WFOV MDT and NFOV MRT. TAWS tabular provided alphanumeric values of only the greater of MDT or MRT. TAWS detection ranges used for comparison in this study had to be obtained from graphic plots. This method can include small errors as a result of inconsistent range interpretation.

B. PART #2 TARGET SCENE TEMPERATURE COLLECTIONS

1. Limfac A: Scientific Sensor not Specifically Modeled in TAWS

TAWS provided a means of customizing IR sensors, but did not facilitate the modeling of scientific sensors used in this portion of the study. This limfac was minimized by considering only the radiometric temperatures of the scene and not detection/lock-on ranges specific to tactical systems.

2. Limfac B: Scientific Sensor to Target Geometry

The horizontal footprint viewed by the Interscience IR sensor from 144 cm was approximately 0.10 m. This was smaller than the TAWS modeled IFOV (≈ 0.56 m) and NOFV ((≈ 161.10 m) from 3 nm and IFOV (≈ 1.30 m) and NOFV ((≈ 372.98 m) from 7 nm. This spatial difference was mitigated by positioning the IR sensors to view portions of the largest target facets. Recall TAWS target temperatures for this study are area weighted averages.

3. Limfac C: Two Types of Scientific Sensors Used

Two types of scientific IR sensors were used in this study, Everest Interscience and Apogee. This sensor inconsistency had minimal impact sense technical specifications were similar in all regards but field of view. The widest FOV was used for background measurements.

4. Limfac D: Background not Specifically Modeled in TAWS

See discussion for part #1. Trees were not a factor in this part of the study.

THIS PAGE INTENTIONALLY LEFT BLANK

LIST OF REFERENCES

AFRL, 2004: Target Acquisition Weapons Software Version 3.4. Northrup Gruman

Goroch A. K., 2005: Personal Correspondence

Brase, C.H. and Brase, C.P., 1987: Understandable Statistics. D.C. Heath and Company, p. 519.

Elrick, J.R. and Meade, A.C., 1987: Weather Sensitivities of Electro-optical Weapons Systems. Air Weather Service Tech. Note AWS/TN-87/003, p. 46.

Howe, J.D., 1993: Electro-Optical Imaging System Performance Prediction. The Infrared and Electro-Optical Systems Handbook. Volume 4: Electro-Optical Systems Design, Analysis, and Testing, J.S. Accetta and D.L. Schumaker (Editors), pp. 57-106.

Kneizys, F.X. et al., 1988: Users Guide to LOWTRAN 7. AFGL-TR-88-0177, p. 146.

Koch, C.A., 1997: Operational Evaluation of the Electro-Optic Tactical Decision Aid, Version 3.1. Master's Meteorology Thesis, Naval Postgraduate School, p. 91.

Machado, D., 1998: Comparison of FLIR Tactical Decision Aids for Interservice Use. Master's System Engineering Thesis, Naval Postgraduate School, p. 134.

Microsoft, 1997: Microsoft Excel: Regression Analysis and Best-fit Lines. 5/97-XE0124, p. 11.

SBIR,cited 2003: Radiometric Temperature: Concepts and Solutions.[Available online at http://www.sbir.com/pdf/RdeltaT.pdf] last date accessed, Mar 06

Thomas, M.E. and Duncan, D.D., 1993: Atmospheric Transmission. The Infrared and Electro-Optical Systems Handbook. Volume 2: Atmospheric Propagation of Radiation, F.G. Smith (Editor), pp. 3-127.

Utts, J.M., 1999: Seeing Through Statistics. Duxbury Press, p. 156.

Lloyd, J.M., 1975: Thermal Imaging Systems, Plenum Press, p. 456.

Wolfe, W.L. and Zissis, G.J., 1985: The Infrared Handbook. Environmental Research Institute of Michigan, p. 1700.

THIS PAGE INTENTIONALLY LEFT BLANK

INITIAL DISTRIBUTION LIST

1. Defense Technical Information Center
   Ft. Belvoir, Virginia

2. Dudley Knox Library
   Naval Postgraduate School
   Monterey, California

3. Dr. Philip A. Durkee
   Department of Meteorology
   Naval Postgraduate School
   Monterey, California

4. Dr. Kenneth L. Davidson
   Department of Meteorology
   Naval Postgraduate School
   Monterey, California

5. Dr. Andreas K. Goroch
   Marine Meteorology Division
   Naval Research Laboratory
   Monterey, California